ADDIS ABABA UNIVERSITY

ADDIS ABABA INSTITUTE OF TECHNOLOGY

PERFORMANCE OPTIMIZATION OF GENERATING POWER ON A FLOATING SOLAR POWER PLANT IN LAKE TANA

A Graduate Thesis Submitted to School of Electrical and Computer Engineering,
Addis Ababa Institute of Technology (AAiT)
In partial fulfillment of the requirements for the degree of masters of Science in Electrical and computer engineering (control engineering)

By

Habtamu Adera

Advisor: Dereje Shiferaw (Ph.D.)

Addis Ababa, Ethiopia

Year, 2021

ADDIS ABABA UNIVERSITY

ADDIS ABABA INSTITUTE OF TECHNOLOGY

PERFORMANCE OPTIMIZATION OF GENERATING POWER ON A FLOATING SOLAR POWER PLANT IN LAKE TANA

BY

Habtamu Adera

Approved by Board of Examiners

_____	_____
Chairman, Department of Graduate committee	Signature
Dr.Dereje Shiferaw	_____
Advisor	Signature
Ato Mesefine Tilahun	_____
Internal Examiner	Signature
Dr Chala Merga Abdissa	_____
External Examiner	Signature

DECLARATION

I, the undersigned pronounce that this proposition is my original work, and has not been displayed for a degree in this or any other university, and all sources of materials utilized for the thesis have been fully acknowledged.

Habtamu Adera _____

Name Signature

Addis Ababa, Ethiopia August, 2021

Place Date of submission

This thesis has been submitted with my approval as a university advisor

Dr.Dereje Shiferaw _____

Advisor Signature

ACKNOWLEDGMENTS

To begin with of all, I am profoundly thankful to my advisor, Dr. Dereje Shiferaw for his support, guidance, and proficient skill. My uncommon much obliged go to all teaches who thought me during graduate study. Thanks my family for their unwavering support and offered throughout the thesis work.

ABSTRACT

Today, the renewable energy is used to long-term growth and to reduce the green house gas emission. Floating Sun oriented boards are a type of renewable energy that converts sun light into electricity and give a solution for the problem of power generation and land scarcity. Single axis solar tracking (SAST) needs to optimize the solar panel power throughout the day. The tracking device is accurately track the sun using one freedom of rotational axis. Light Dependent Resistor (LDR) is commonly applied in sun tracking system. The two LDRs can be used in sun tracking depend on the intensity of light. The floating sun based control system produces more power due to solar tracking with cooling impact of water than fixed land sun oriented system. It can be introduced in any water bodies which is able be diminish the cost of land. The model of single axis solar tracking is modeled. The fuzzy PID controller has been designed and simulated using MATLAB/SIMULINK. Its performance has been compared with Ziegler Nichols PID controller tuned method. Amid the era of vitality, the rising of the temperature on the boards has been noteworthy issue on the surface of solar PV framework. Since, it has been specifically impacts on the vitality era; the higher working temperatures of sun oriented PV framework diminish its vitality capacity. As the temperature increase the voltage output decreases. The overall efficiency and performance decrease due to the excessive heat is occur on the solar panels and solar tracking system changes, the inclination angle variation is occurred. The daylight point "θ" increment, the control of the sun based board is diminishing. Fuzzy logic controller which are vibration balance and the actuator (DC servo motor) able to controls the development of sun powered panels. Thus, The simulation result is observed that the Ziegler-Nichols closed loop PID controller tuning simulation results that the overshoot is 46.8%, rising time is 0.842seconds, choosing time is 2.13seconds and the settling time is 11.2seconds with the proposed fuzzy-PID controller while overshoot is 3.646%, rising time is 0.0527seconds; pick time is 0.112second and the sampling time is taken as 0.4seconds. The fuzzy PID simulation result indicated that has better performance than Ziegler Nichols PID controller tuned method.

Key Words: Floating Solar Plant; Fuzzy – PID controller; Fuzzy logic control; Single Axis Solar Tracking (SAST); DC servo motor and LDR sensor.

Contents

LIST OF ABBREVIATION

AAiT	Addis Ababa institute of technology
B	Friction Coefficient
CE	Change of error
CCW	Anticlockwise
CW	Clockwise
COG	Center of gravity
DAST	Dual axis solar tracking
D	Duty cycle
DC	Direct current
E	Error
Eb	Back emf constant
ECL	Change of error low
ECH	Change of error high
Eg	Band-gab energy
Emf	Electromotive force
FF	Fill factor
FB	Buoyancy force
FLC	Fuzzy-logic controller
FIS	Fuzzy interface system
FPI	Fuzzy proportional integral
FPD	Fuzzy proportional derivative
FPID	Fuzzy proportional integral derivative
FPV	Floating photovoltaic
Fs	Sample time
FSPV	Floating solar
G	Actual Radiation
Gn	Nominal Irradiation
HDPE	High Density Polyethylene
HSAT	Horizontal Single Axis Tracking
HM	The Height Method
Ia	Armature Current

IEC	International Electro Technical Commission
I	Current
Imp	Maximum Point Current
Ipv	Photo Current
Isc	Short Circuit Current
Isc,n	Nominal Short Circuit Current
Io	Reverse Saturation Current
Io,n	Nominal Saturation Current
J	Inertia of Motor Rotor
K	Boltzmann's Constant
Kb	Back Emf Constant
Kt	Torque Constant
Kd	Derivative Constant
Kp	Proportional Constant
Kcr	Critical Point Gain
Ku	Ultimate Gain
L	Delay Time
La	Armature Inductance
LDR	Light Dependent Resistor
M	Mass of Element
MATLAM	Matrix Laboratory
MF	Membership Function
MPP	Maximum Power Point
Mp	Maximum Overshoot
MOM	Mean of Maximum
NN	Neural Network
Np	Number of Pararallel Connection
Ns	Number of Series Connection
Pcr	Critical Period
PI	Proportional Integral
PID	Proportional Integral Derivative
PV	Photovoltai

LIST of Tables

LIST OF FIGURES

CHAPTER ONE
INTRODUCTION

1.1 Background

The consumption of energy is increasing with related to human living standard. These days, the world populace is raising limitations of natural alter that occur on soil after the time of globalization. The fossil fuel, sunlight, wind, tides, and rain are the source of the renewable electrical energy. The Vitality utilization and generation exercises are responsible for the greenhouse emission. The electricity demand has greatly increased in current years due to economy and population growth in creating nations, a gradual rise in comfort levels in well-developed countries [1]. There are two ways to take in solar energy, along solar heat and solar photovoltaic(PV). A photovoltaic cell is an electric control generator, comprising of semiconductor layers that change over sun oriented vitality into power, panel characteristics depending on environmental condition. In PV generation, a device called a solar cell is used to turn light directly into electricity. The direct current (DC) generated by a cluster of sun powered module (solar cells grouped and packaged together) then goes into an inverter, where it is converted to substituting current. To measure photovoltaic board voltage or current, agreeing to the control sort utilized for control inverter, current controlled or voltage controlled [2]. FPV plant consists of solar PV panels mounted on a floating structure, composed of several floats connected together. The floating platform is made of primary floats, supporting PV panels, and secondary floats used for maintenance, maintaining distance together by reinforced connection pins. The tilt angle and orientation can be depending of the use and the location of solar plant. The platform installation will be installed in Lake Tana. Lake Tana is located at the Northwest of Ethiopia adjacent to Bahir dare Town with coordinates of $11°36'N, 37°23'E$ and it is largest freshwater body with a surface area of $3150km^2, (36\%\ of\ total\ inland\ water\ of\ ethiopia)$ with length of 78kms and width of 68kms[3]. A solar tracker is used to track the orientation of the sun. In case of the trackers the panel is situated to track the greatest sun light all through the day by altering the tracker points (both rise and azimuth points).

A photovoltaic (PV) gadget changes over daylight into power. In this paper, development and evaluation of PID based device solar tracking and control system of maintaining in peak position of a PV array for maximum efficiency. The position of array is changing relative to the irradiance of sun direction [4].

In recent years, renewable energy sources are growing rapidly all over the world. Solar energy is considered to be one of the most promising energy alternatives due to its ubiquity and sustain-ability. The sun oriented vitality is free and hugely accessible all through the world. The most perfect way to utilize sun powered vitality is PV framework. Photovoltaic (PV) modules are one of the foremost successful, economical, and eco inviting items within the field of renewable vitality. The main burden of land mounted solar system is availability of land. There is expansive water bodies accessible in different parts of the nation which can decrease the sparing fetched of arrive and working fetched for control era costs. So, the sun oriented PV frameworks can gotten to be a really consistent elective for saddling sun powered vitality by utilizing obtainable water bodies and offer assistance to extend the financial reasonability of sun based ventures. Vitality from photovoltaics through a renewable source, keeps up a moo effectiveness of less than 15% in its long-life utilize. Coasting sun powered create more power than ground mount and housetop (sun powered) frameworks since of the cooling impact of water.

It too decreases store dissipation and green growth development by shading the water. The coasting stages are 100% recyclable, utilizing high-density polyethylene which can withstand ultraviolet's beams and erosion [5].

Table 1.1: The country studies on the floating solar PV system (FSPV) [6]; [7]

Country	FPV System	Location	Benefits
Brazil	PVT:3°&10°(fixed)	Sao Francisco River basin &	10.55GWh/year &
	250 Wp & 245Wp	Gaviao reservoir in Northeast Brazil	835.82GWh/year
China		water surface in eastern region	160Gwh/year
USA	PVT:11° (fixed),	Man-mad water bodies in contagious	786000GWh/year
Korea	PVT:40°,215.25Wp	In limestone Mine pit lake	0.9716GWh/year
	PV: 20°, 210Wp	1134 reservoirs	2931.94GWh/year
India	PVT: 12° ,300Wp	Karasur Village's lake	2.658GWh/year
	320Wp	Neel-Nirjan Dam in Bakreswarr	14.97GWh/year
		Lake in kota	25.74GWh/year
		Large reservoirs	909.05GWh/year
Portugal	PVT:20°,260Wp	Alqueva Dam	0.4557GWh/year
Japan		Yamakura Dam, east of Toky	13.5MW

1.2 Statement of the problem

Solar energy is currently one of the foremost encouraging renewable technologies. Solar energy is the most generous resource on the world, thus encouraging the development of technological solutions to transform this energy in an efficient way. Large-scale PV plant requires high land availability, while dressing land scarcity, where as in sustainable economy, lands take portion in a main role for irrigation.

Like that, usage of sun oriented PV plant continuously faces arrive cases such as arrive sun powered PV plant has arranged expansive farther area, investments cost increases. On the other way, Solar PV plant performance is affected by temperature. As, the temperature rises then the power output of solar PV plant decreases due to high absorption of PV modules. The rising of the temperature on the panels has been significant problem on the surface of FPV during the generation of energy. Since, it has been directly impacts on the energy generation; the higher operating temperatures of solar PV system decrease its energy capacity. As the temperature increase the voltage output decreases. The overall efficiency and performance decrease due to the excessive heat is occur on the solar panels and solar tracking system changes, the inclination angle variation is occurred. The daylight point "θ" increment, the control of the sun powered board is diminish Hence, to reduce this effect can be used an adaptive control strategy for the PV system. Solar tracking technology should be developed and utilization efficiency improved. As the angles of sunlight change with different seasons and times of the day, a solar tracking system can adjust the angle of photovoltaic panels to gain the highest utilization efficiency by maximizing exposure to the rays of the sun that beat down vertically on the earth. With solar tracking technology [7], the annual solar irradiation intensity of regions with average solar resources can be improved by using artificial intelligence mathematical algorithm, DC motor derive and adaptive control mechanism.

Therefore, it is proposed to use adaptive control PID is implemented and fuzzy logic mathematical algorism/technique can be a better option due to increasing performance, optimizing energy and maintain the system.

1.3 General Objective

The goal of this research is to enhance the performance optimization of floating solar panel using an adaptive control system. The main objective of this research is that introducing versatile optimization control procedure in arrange to improve the performance and assurance a robust nonlinear and optimal on solar tracking technique in a floating solar system can increase its performance and optimize the system. The general objective of the thesis is to show that impact of performance optimization of generating power on a floating solar plant.

1.3.1 Specific Objectives

The specific objectives of the research work are:

- To model and analyze solar floating PV system.
- To design fuzzy based adaptive tracking controller.
- To investigate the performance of the control system.

1.4 Contribution of the thesis

The outcome of this research contributes to improve the renewable energy using nonlinear control by employing an advanced optimization. The FPV had optimization problem due to the highly uncertain conditions. Hence, such as adaptive control and nonlinear optimization methods, capable of treating uncertainties are needed to achieve optimal performance and to overcome the difficulty in the presence of uncertainties.

In addition, it benefits lower costs, higher reliability, and system performance; As well as local environmental benefits to reduce evaporation of water.

1.5 **Scope of the research**

On this thesis, the execution and optimization vitality of the Floating Solar Panels will be introduced theoretically as well as mathematical modeled and it will be compared to using traditional control and adaptive control strategy. The theoretical explanation will be validated using a digital simulation like MATLAB/SIMULINK and PVSYST software. The practical implementation of the system is not under the scope of this research.

CHAPTER TWO

LITERATURE REVIEW

2. Introduction Floating Solar Power Plant System

This chapter will review the fundamentals of floating solar plant system, basics of thermal treated solar panels focusing on the control system. The performance of solar PV systems will be also reviewed.

Mohsen Taherbaneh , 2010 [8] had proposed that the two fuzzy controllers created in order to maximize the generated yield power of solar panel in photovoltaic system, a fuzzy- based sun tracking and maximum power point tracking. Three methods used to maximize the output power of a solar panel, thus are; fuzzy. Based maximum power point tracking was the first method. It is watched that approximately 23W was obtained during the measurement time, which is about 51% of nominal output power. In the second method, fuzzy-based sun tracking was applied and it is observed that approximately 11w was obtained during the measurement period, which is about 24.5% of the nominal output power. Finally, the combination of fuzzy-based most extreme control tracking and fuzzy- based sun tracking was used to maximize the output power.

A. Zeroual et al. [9] had proposed an automatic sun-tracker system for optimum solar energy collection in 1997. They used electro-optical sensors for sun finding and microprocessor controller units for data processing and for control of the mechanical derive system. This system allowed solar energy collectors to take after the sun position for optimum efficiency. Numerous parameters are controlled for framework security such as temperature, weight and wind speed. The framework had been tried for a long period in variable brightening. The result appeared that it worked legitimately with tall exactness.

Brito et al., 2013 [10] proposed INC with proportional integral regulator to find the modified INC MPPT method with proportional integral (PI) regulator in arrange to improve the response of the MPPT, minimizing the error between the actual conductance and INC. The parameter of such a PI compensator can be adjusted/tuned as per system necessity. Also, this PI controller can reduce the ripple oscillations in steady state. The tracking efficiency (%) is 86.41–88.00, little overshoot (%), voltage, current sensors used and circuit is complex and complex, power calculation is required.

Algazar, Monier, Halimand Salem 2012[11] proposed MPPT methods based on artificial intelligence have become prevalent in later a long time as compared to conventional methods because of very good and fast response with no overshoot and less fluctuations under rapid variations in temperature and solar radiation. The fuzzy logic-based MPPT method does not

require the precise show of PV system for its design. In most of the literature, a fuzzy logic-based MPPT has been proposed with two inputs and one output. The two input factors are error *E(k)* and change in error *E(k)*. The fuzzy inference can be carried out by one of the various available methods (Mamdani's method has been mostly used) and defuzzification can be done using the center of gravity strategy to compute the yield (duty cycle). The tracking efficiency (%) is 87.46–90.38, voltage, current sensors used and circuit is complex and complex, power calculation is required.

Young- Kwan Choi et al [12] has compared and analyzed the generation efficiency of floating and land photovoltaic systems. It has appeared more prominent era proficiency by over 10% compared with the common PV frameworks introduced overland. His paper compares and analyzes the experimental information of the drifting PV framework, which K-water has installed with that of the existing overland PV and has verified that the generating efficiency of floating PV system is superior by 11% and more.

Minor M. Arturo, 2010 [13] had demonstrated as the system for following the sun which is based on the utilizing of a commercial webcam as the sensor component. A test electro-mechanism was planned and created to assess its exactness and proficiency in following the sun beneath distinctive climate conditions.

The utilization of a sensor element allowed avoiding most of the common problems usually seen with the solar trackers currently under use. One is the high sensitivity of the discrete element such as photodiodes or phototransistor to weather conditions, particularly to temperature and humidity. The system showed an accuracy of $0.1^{\circ}$and high resistance to temperature varieties. It illustrated its capacity to move the sun, as well as extrapolate its position when it is undetectable for a period of time.

Tonui and Tripanagnostopoulos , 2007 [14] had highlighted that the PV cells endure a drop in effectiveness as their working temperature increments; lessening working temperature by cooling the cells will progress their execution.

They utilized a suspended lean level metallic sheet at center or blades at the back divider of an discuss channel as warm exchange enlargements in an air-cooled PV/thermal (PV/T) sun based collector to make strides its by and large execution.

2.1 History Floating Solar Power System

Swimsol was founded by Martin Putschek in 2012. Two years later, in cooperation with the Vienna University of Technology and the Fraunhofer Institute in Germany, they launched the world's first floating solar power plant for the marine environment –Solar Sea. Moreover, they succeeded in making it less expensive than diesel-generated electricity, a precondition

for a gradual replacement of diesel generators through clean solar power solutions in those regions. By using the free space on the water, the technology makes large solar systems possible even for islands that do not have enough roofs or land for solar panels. Their floating systems are currently operating in the Maldives and demonstrate great potential for other marine regions [15].

Floating PV system is a newly development technology. There are many places around the world that do not have enough land for PV installations, mainly islands such as Japan, Korea, Singapore, Philippines and many others [15].

The Aichi, Japan project was developed by a research team from the National Institute of Advanced Industrial Science and Technology in Japan developed their own floating PV prototype. The aim of their research was to compare the electricity output from an array that was water cooled and another that was air cooled. The panels in this case were installed as an array lying at a slight tilt (1.3° south facing) on top of foam polystyrene board floating on top of the water body. The major variance in experimental results between the two systems was mainly due to the accumulation of bird dropping over the air-cooled PV system (where the water-cooled system was kept clean because of the 10-min regular water coverage) [16].

2.2 Floating Solar PV System

A floating solar PV system consists of four components that are the floaters, the floating PV system, and mooring system and under water cables. PV generation equipment that is FPV modules installed on surface of the floating system, power converters, power inverters; controller, and distribution line.

2.2.1 Anchoring system in FPV

The floating system PV systems needed to be anchored to the waterbed, and this system should be able to withstand the simple water variations as well flood water levels with minimum sage. The floating bed cannot be sinking or sag towards the shore excessively which it will cause damage to the PV system and power cables. Therefore, the anchoring system should be designed considering these situations and also it should be designed with less mechanical controlling strategies to simplify the problems cause by mechanical system. Fig.2.1 explains the anchoring phenomena in FPV system. Fig 2.2 shows the anchoring design which needs to consider a distance D between the anchor and the island. To make sure that the anchoring is well designed, the angle α between the ground and the mooring line should not be over $45°$, and ideally is calculated regarding floatability issues. This angle is linked to distance between the solar island and the anchor, as well as on the depth the anchoring point [17].

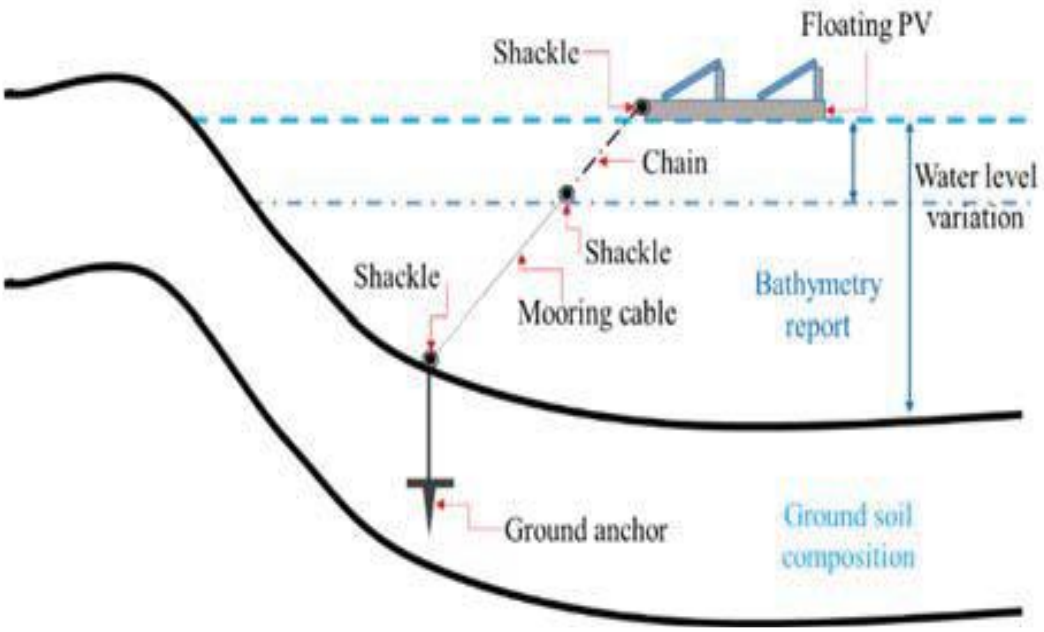

Figure 2.1: Detailed FPV anchoring system design

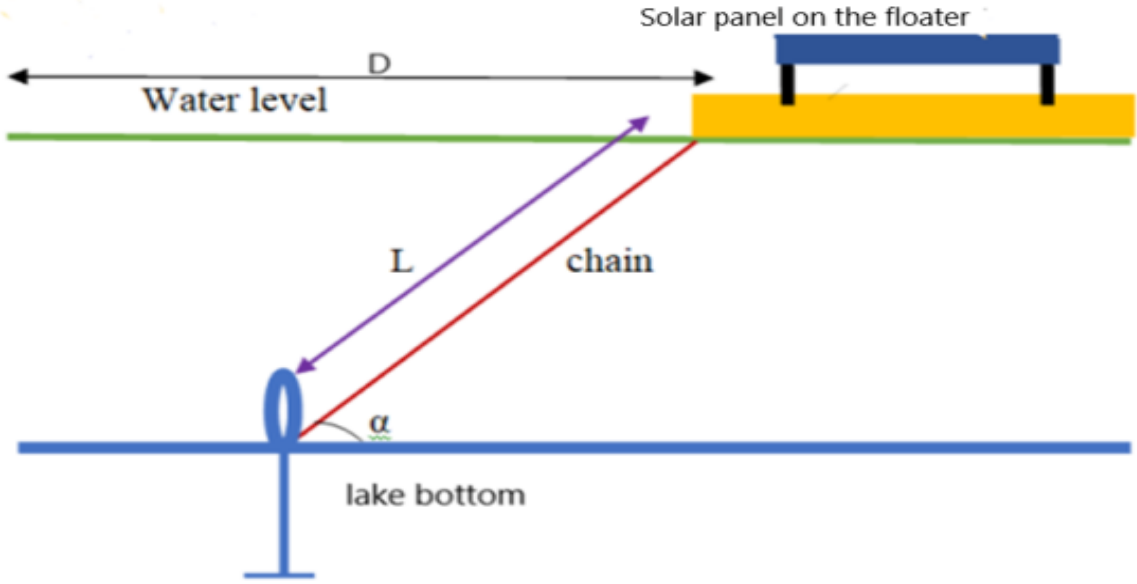

Figure 2.2: anchoring cable design of FPV

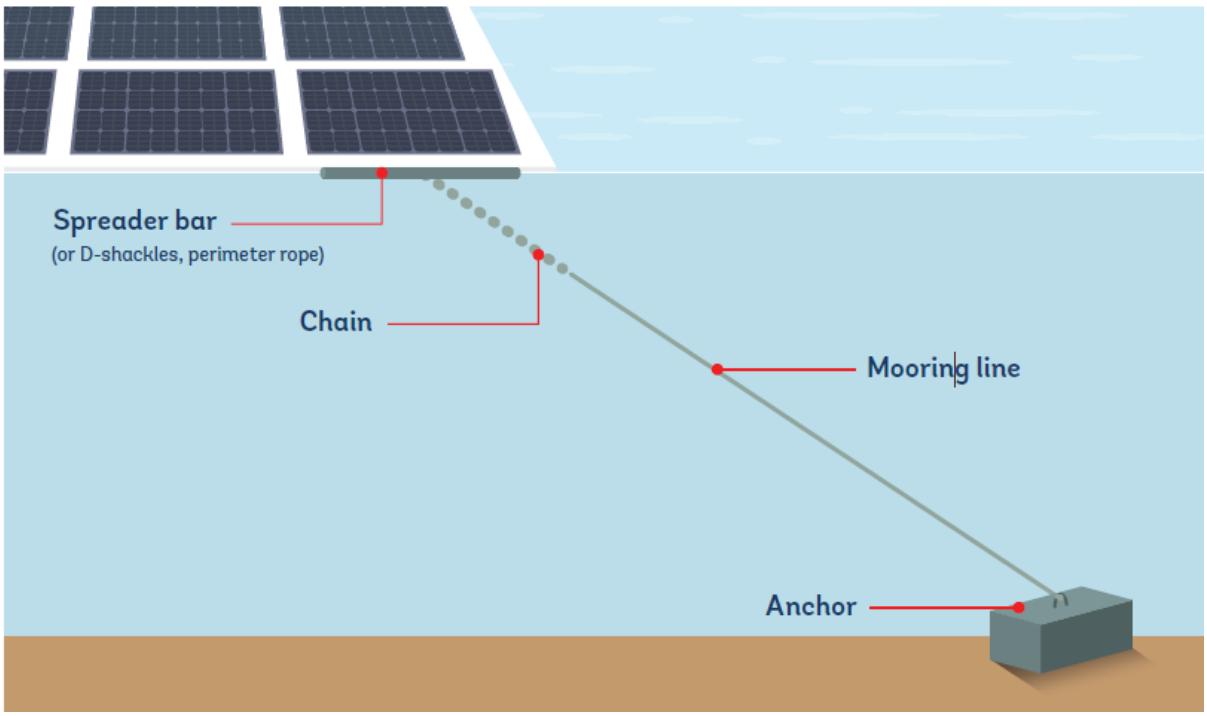

Figure 2.3: Installing floating PV solar panels (Ceil et Terre)

Components of floating solar PV system [11]

Pontoon/Floating structure

A pontoon is floatation structure and has buoyancy enough to float on water and support a heavy load. The structure is designed such as it can hold number of panels.

Mooring system

A mooring alludes to any changeless structure to which a coasting structure may be secured. A coasting structure is secured to mooring hinder free development of the drifting structure on the water. A grapple mooring fixes a drifting structure's position relative to a point on the foot of conduit without interfacing the coasting structure to shore.

Solar module

A single solar module can produce only a limit amount of power; most installations contain multiple modules. A photovoltaic system typically includes a panel or an array of solar modules, solar inverter, and sometimes a battery, solar tracker and interconnection wiring. Mostly crystalline solar PV modules have been used for the floating solar systems.

Cabling

Due to their outdoor usage, solar cables are specifically designed to be resistant against UV radiation and extremely high temperature fluctuations and are generally unaffected by the weather.

Solar PV panel cooling methods

The main advantage of FPV systems is their capability to utilize the water body as a source to cool the PV panels appropriately. Proper cooling is important to solar systems and it can significantly increase performance and the energy harvested from the sun. The increase the efficiency by cooling results from two different sources [18]. (1) The water refraction index of 1.3 which helps reduce the reflection effects of solar radiation when water flows over the solar panel. This effect gives a gain of about 2% if radiation is perpendicular to the panel. (2) The loss of efficiency as the temperature increases. For every $1℃$ increase in surface temperature on the PV module will cause a reduction in efficiency of 0.5%.

The maximum power generated by the solar PV panels is highly affected by the temperature. The temperature growth has negative influence on the electrical energy produced by photovoltaic cells. The solar PV panels temperature value to be raised in percentage which leads the lifetime reduction. This condition to be improved by using the techniques to cool PV panels, the main cooling methods of the solar PV panels are shown in figure 2.4 [1].

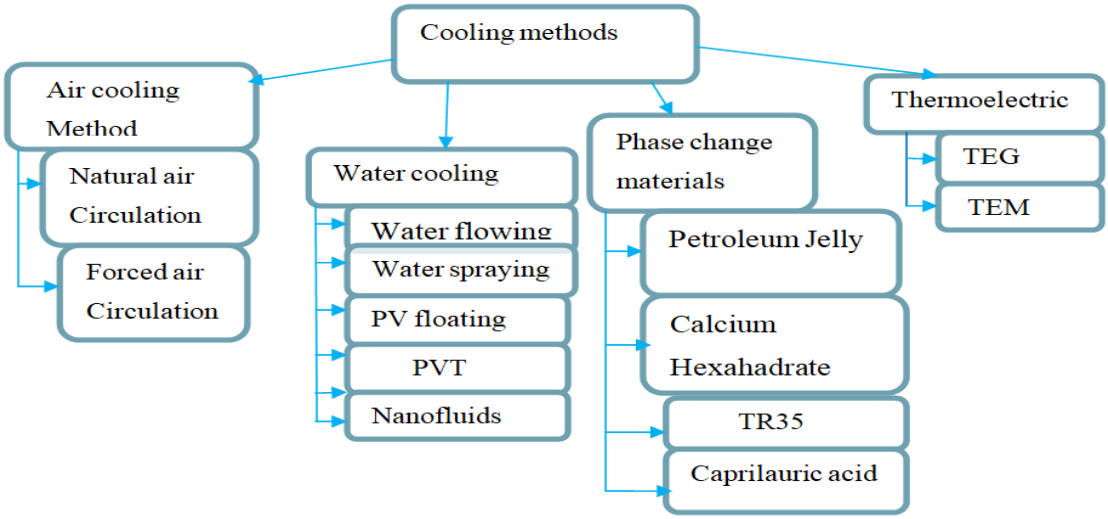

Figure 2.4: The main cooling techniques

2.3.1 Air cooling

The natural air flow is the most effective technique for cooling the solar PV panels. The cost being low due to no extra materials being needed, the cooling of solar PV panels can be improved if on the back of PV panels metallic materials with fins are mounted to ensure a very good air circulation. By using nature air flow between the building vertical walls and PV system mounted on them, the temperature of the solar PV panels can be maintained at less

than $40℃$. The forced air circulation is an active techniques' to cool the PV panels. There are more Techniques to force the air circulation, such as open channel beneath, steel plate with an air channel underneath, and array of ducts underneath the PV panel's optimum fins.

2.3.2 Water cooling

Water veil cooling system consists of pump and an irrigation system made of polyethylene pipe positioned on the top of each solar panel. This technique includes a temperature control system that switches on when the solar panel temperature exceeds a fixed threshold; typically the maximum temperature for solar panel is $30℃$. WVC system is estimated to increase the efficiency of a solar panel by 10% on an annual basis to 15% output at peak radiation conditions. There is also potential for panel surface cleaning caused from the irrigation system water flow. The main disadvantages of WVC system need a large power requirement to circulate the cooling water [19].

Figure 2.5: Diagram of WVC

Water sprinkler cooling system

It is a simple alternative to a WCV system. Instead of irrigation pipes, the system utilizes high-pressure sprinklers that operate at a pressure of 2 to 3 bar. The cost of cooling is much less than WVC system while still increasing the power output by 10% on an annual basis. The disadvantage of this cooling system is water and heat wastage.

Figure2.6: Visual of high- pressure sprinkler head for solar panel cooling system

2.4 Solar Tracking PV System

A solar tracking system is a system used for orienting a solar photovoltaic panel toward the sun beam direction, especially in solar cell applications require a high degree of accuracy to ensure that the concentrated sunlight is directed precisely to the powered device. This system can be electrical or mechanical system, the main objective of the system is to find the maximum solar power output.

Components of Solar Tracking Systems

The most components of a sun based following framework are the following gadget, the following calculation and warm or electro-optical for non-algorithm, the control unit, the situating framework, the driving instrument, and the detecting devices [20]. (I) the algorithm is a tracking control scheme that calculates the points that are utilized to decide the position of the sun oriented tracker. There are two types of algorithms: astronomical algorithms and real-time light intensity algorithms. The astronomical algorithm is a purely mathematical algorithm based on astronomical references to calculate the solar angles. The non-algorithm thermal control scheme uses differential thermal expansion of a working fluid to exert torque to move the tracker. The non-algorithm electro-optical control scheme uses differential optical signal to exert torque on the tracking device to follow the sun. (II) The positioning system is the system that moves the tracking device to face the sun at the calculated angles. The positioning system can be electrical or hydraulic. (III) The driving mechanism is the mechanism that is responsible for moving the tracking device to the position determined by the positioning system. (IV) The sensing devices comprise a group of

sensors that measure the ambient conditions (such as ambient temperature, relative humidity, amount of rain, and other ambient measurements), the light intensity (in the case of real-time light intensity algorithms), and the tilt angle of the tracker. The latter is accomplished by means of an inclinometer or a combination of limit switches and motor encoder counts.

2.4.2 Sun position

The position of the sun relative to an observer on the surface of the Earth is an important input needed to model PV system performance. The convention used to describe solar position includes:

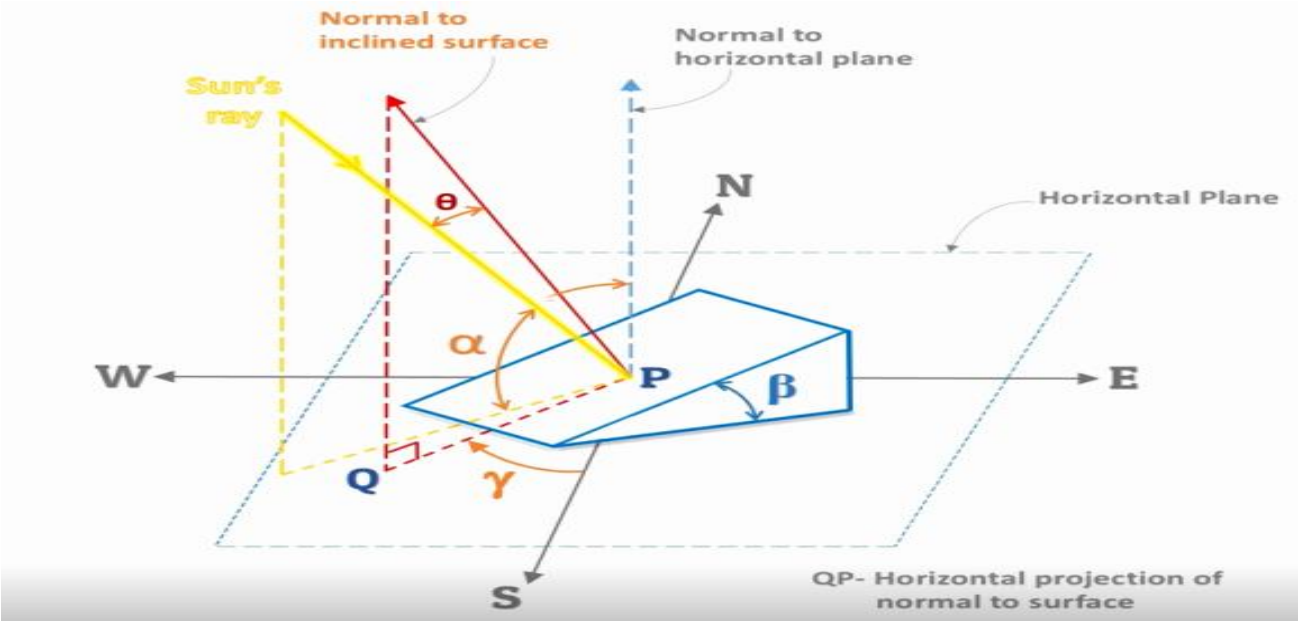

Figure2.7: the sun angles of solar tracking

Angles of the sun are defined as the following ways:

Angle of latitude ($\emptyset$) : it is the vertical angle between the line joining that point of location to the center of the earth and its projection on an equatorial plane. When the point is north of equator the angle is positive and when south it is negative. Angles are represented as $\emptyset^{\circ}N$ *or* $\emptyset^{\circ}S$ of equator. Also $\emptyset = 0^{\circ}$ for the point on the equator, $\emptyset = \pm 90^{\circ}$ for appoint at the poles.

Inclination angle (α): the angle between sun's ray and its projection on horizontal surface is known as inclination angle (α). $\alpha = 0^{\circ}$ at sunrise and sunset.

Zenith angle (θ_z): the angle between the sun's ray and the perpendicular (normal) to horizontal plane is known as the zenith angle (θ_Z). The zenith angle is compliment of

inclination (altitude) angle. i.e.,$\alpha + \theta_Z = 90^{\circ}$, hence at sunrise zenith angle is $+90^{\circ}\ whereas - 90^{\circ}$ at sunset.

Solar azimuth angle (γ_s): the angle on a horizontal plane between the line due south and the projection of sun's ray on the horizontal plane is known as solar azimuth angle. It is considered as positive when it is measured from south towards to west.

Tilt angle or slope (β): it is an angle between the inclined surface and the horizontal plane.

Angle of incidence (θ): it is an angle between sun's ray incident on plane surface and normal to that surface. For horizontal surface; slope, $\beta = 0^{\circ}$; Zenith angle θ_z = angle of incidence θ. It is the angle in the horizontal plane, between the line due south and the horizontal projection of the normal to the inclined plane surface.

2.4.3 Solar Position and Local Time

The second point to consider is the calculation of the solar position and its relation to an oriented panel. The two basic variables for the solar position are the solar altitude angle, α_S, and the solar azimuth angle γ_S. The solar altitude angle, α_S, is the angle between the horizontal and the line to the sun. It is the complement of the zenith angle θ_Z .The solar azimuth angle, γ_S is the angular displacement from south of the projection of beam radiation on the horizontal plane; displacements east of south are negative and west of south are positive [21]. In Fig.2.8 the two angles related to the sun position and the angles β and γ that define the PV module position. β is the tilt angle and γ is the surface azimuth angle. Further, the angle θ between the normal to the PV surface and the incident beam radiation is indicated.

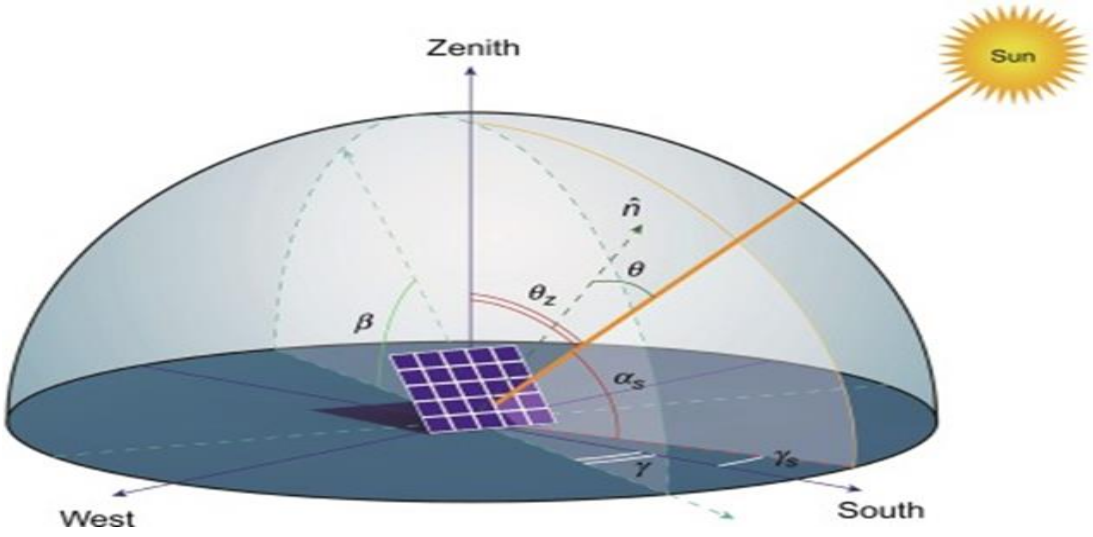

Figure2.8: Solar and PV module characteristic angles

The angle θ is given by the trigonometric relation,

$cos\theta = cos\theta z\, cos\beta + sin\theta_Z sin\beta cos(\gamma_S - \gamma)$

To define the solar ray angles, we need further information about the declination angle δ which is the angular position of the sun at solar noon with respect to the plane of the equator (north positive), and given by the following equation:

Declination angle (δ): It is the angle between the sun's positions in relation to the earth's equator. The earth's axis is typically tilted 23.34° from the plane of the earth's orbit around the sun and the earth is in its annual path around the sun causes the declination angle to vary from 23.45° north on December 22 to 23.45° south on June 22 [22].

Declination is calculated using the following formula:

$$\delta = 23.45 * \sin\left(2\pi.\frac{284+N}{365}\right) \quad (2.1)$$

N=day number, with January 1, being day 1

With the declination δ, the latitude ϕ, and the hour angle ω, the solar zenith angle θ can then be found from the following equation:

$$\sin(\alpha_s) = \sin(\phi)\sin(\delta) + \cos(\phi)\cos(\delta)\cos(\omega), \quad (2.2)$$

$$\omega = \frac{15^{\circ}}{hour}(ST\ in\ before\ solar\ noon), \quad (2.3)$$

$$sin\gamma_s = [\frac{\cos(\delta).\sin(\omega)}{cos\alpha_s}] \quad (2.4$$

2.4.4 Advantage of Solar Tracking

- Increase solar panel output
- Maximum efficiency of the panel
- Able to grasp the energy throughout the day
- Maximum power Per unit area

Types of Solar Trackers

The types of solar tracker which can be grouped into single axis and dual axis solar trackers. Those are: (1) Single axis solar tracker and (2) Dual axis solar tracker.

1. Single axis solar tracker

These trackers have one degree of freedom that acts as the axis of rotation. The axis of rotation of rotation of single axis trackers is aligned along the meridian of the true North. With advanced tracking algorithm, it is possible to align them in any cardinal direction. Common implementations of single axis trackers include horizontal single axis tracker (HSAT), horizontal tilted single axis trackers (TSAT) and polar aligned single axis trackers

(PST) [23]. The horizontal type is used in tropical regions where the sun gets very high at noon. But the days are short. The vertical type is used in high latitudes (such as in UK) where the sun does not get very high, but summer days can be very long. These have a manually adjustable tilt angle of $0 - 45°$ and automatically tracking of the sun from East to West. They use the PV modules themselves as light sensors to avoid unnecessary tracking movement and for reliability. At night the trackers take up a horizontal position.

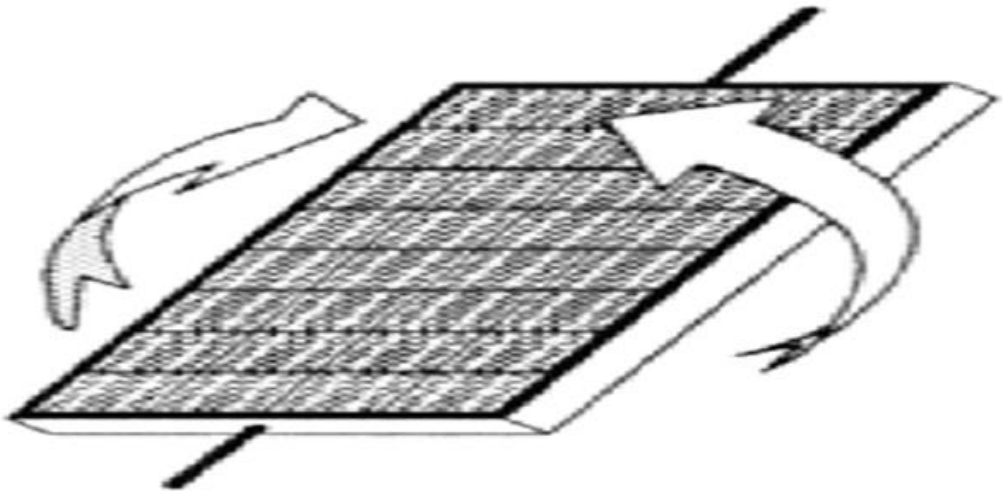

Figure2. 9: single axis solar tracking system [24]

Advantages of Single-Axis Solar Tracking System

The main advantages of single-axis trackers includes as follows: Single-axis trackers are more reliable; Single-axis trackers have a longer lifespan than Dual-axis trackers because they have a simple mechanism and operate at low cost; Single – axis trackers are nearly 32.17% efficient compared to a fixed solar tracker mount panel; These trackers follow the sun from East to West, providing consistent power output all day long; The trackers generate 15-16% higher annual power as compared to a static of the installed capacity;

Single axis trackers provide the highest density of PV panel placement per square.

Figure 2.10: The position of the solar panel [25]

2. Dual axis solar tracker

A dual axis sun tracker (DAST) has two degree of freedom that acts axe of rotation. The first axis is a vertically pivoted shaft that allows the device to move to a compass point. The second one is a horizontal elevation pivot implanted upon the platform. The Azimuth motor rotates along the vertical axis to adjust azimuth position of the sun. A second motor will operate the panel elevation acting on the horizontal axis to altercate the sun altitude. Using a combination of the two axes, any location in the upward hemisphere could be pointed. Four LDR (Light Detecting Resistor) sensors are used in the four sides of the panel, which can sense the position of the sun. LDR can detect the voltage across them. If any voltage difference occurs in LDR on the two opposite sides, the panel can move and make a voltage difference zero. This means the light can equally distribute to the whole panel. Two sensors are responsible for east to west direction that is for the whole day and the other two sensors are used for north to south movement that is the whole year [26].

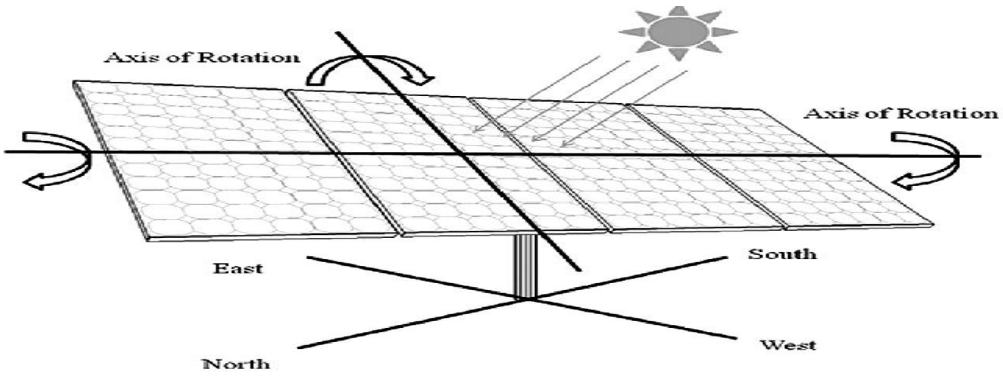

Figure 2.11: Dual axis solar tracking system [27]

2.1 Advantages of the Dual-Axis Solar Tracking System

Dual –axis trackers follow the Sun continually and provide constant throughout the day;

These solar trackers provide a reasonable solution in case of the limited power capacity of the connection to the grid; dual –axis tracker need smaller space; these trackers generate 45-50% higher output per year, as compared to a static station of the same installed capacity.

2.2 Disadvantage of dual-axis solar tracker system

Dual-axis trackers have higher technical complexity, which makes it potentially vulnerable to glitches; these trackers have a shorter lifespan and lesser reliability; low performance in cloudy or overcast weather.

2.4.6 Derivation of the Tracker Angles

Due to sun's development, its position changes both in day and with the seasons. The sun powered vitality capturing by the settled position sun based boards amid the course of the

day isn't adequate due to its position continuously being inactive; this diminishes the scope of the board towards the sun. The position of the sun changes throughout the day as well as seasons. Depending upon cost, character and performance there are many varieties of solar trackers. The usage of the solar tracker decides the position of the panel [4]. The Sun oriented radiation information is ordinarily within the shape of circular radiation falling on a even plane. For this reason, the solar panels are positioned at a certain angle with the horizontal plane. The sun moves in the sky during the day. For a solar collector and / or panel in the steady state shown in Fig.2.12, the projection of the respective receiver region onto the plane is determined as the cosine of the incoming light. As the sunshine angle "θ" increases, the power received from the panel decreases. Solar tracking systems aim to maximize the energy to be obtained by trying to keep the solar panels according to the sun in the perpendicular position to get the best possible radiation from the sun.

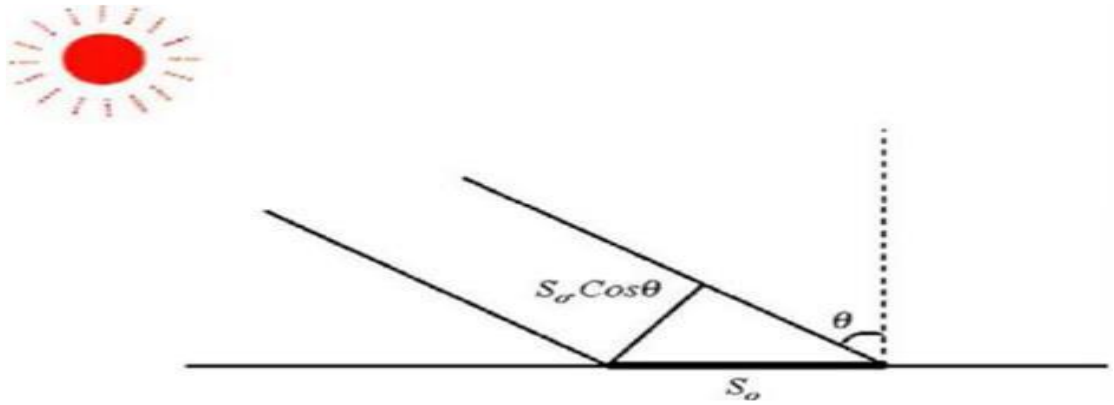

Figure 2.12: Sun shine angle, θ [28]

2.5 Photovoltaic Panels

The floating PV panel output current I_{Pv} depends on the following parameters such as; the type of materials that the PV panel is made (ideality factor n); shunt and series resistance and number of parallel and solar series cells(N_s & N_p).

The photovoltaic (PV) panels used in this research are manufactured by sunrise which produce junction with Intrinsic Thin Layer solar cells. These modules are made from poly crystalline silicon wafers that are surrounded by incredibly thin amorphous silicon layers. This form of hybrid panel is made from the purest form of silicon, and thus delivers an incredibly high level of efficiency. The solar cells are a unique product on the market and

only available from sunrise. The combination of cells in series or are parallel forms a module. A typical module may have 36, 54, 60, 72 and 96 cells in series as the required. When photovoltaic are wired in series, they all carry the same current and their voltages add.

The overall voltage in module is given as:

$V_{module} = N_s(V_d - IR)$

Where; N_s is number of cells in series

SR-P660260 model have 260Wp poly crystalline solar modules that contain 60 cells connected in series with the following dimensions: 1640 X 992 mm and thickness 35mm [PV SYST].

2.5.1 Temperature and Irradiance impact on PV System

The floating solar panel performance is depending on: The designing location; The PV characters; the seasonal condition; the local environmental factors; Global horizontal and horizontal diffuse irradiation.

Lake Tana geographical data had been taken from NASA-SSE Satellite data (1983-2005); thus, data are seasonal ambient temperature, Global horizontal irradiation and horizontal diffuse irradiation etc. due to the seasonal change of solar path at Lake Tana the tilt angle had been affected. The inputs of typical PV module model are the data commonly provided by manufactures on their published datasheets. Those are shown below:

- Open circuit- voltage,V_{OC}
- Short circuit current, I_{Sc}
- Current at maximum power point,I_{mp}
- Voltage at maximum power point, V_{mp}
- Power at maximum power point, P_{mp}
- k_IThermal coefficient of I_{sc}, % C^0,
- K_vThermal coefficient of V_{oc}, % , C^0,
- $maximum\ voltage\ at\ IEC$

Figure 2.13: selected PV panel SR-P660260/60, 260 watts poly crystalline with 60 cells

The factors that affect the performance and efficiency of the PV panels are; Limitation of the manufacturing and material specifications; Lose occurs the power conversion for PV panels systems, where the conversion from the generated DC-AC causes loses in efficiency; Local environmental factors (temperature, wind speed, wave force); Character of PV panels (orientation, tilting)

Advantage of floating solar power plant:

Preserving land resources; Higher efficiency/performance; Easy cleaning and dust removal from the panel; Conserving water due to reducing evaporation; Decreasing algae formation due to less sunlight entering the water body.

2.6 PID controller

The PID controller is the foremost common shape of criticism. It was an essential element of early governors, it got to be the standard instrument when prepare control developed within the 1940s. In handle control nowadays, more than 95% of the control circles are of PID sort, most circles are really PI controller. PID controllers are these days found in all districts where control is utilized. The controllers come in numerous diverse shapes.

There are standalone Frameworks in boxes for one or a couple of circles, which are made by the hundred thousand annually. PID control is an important ingredient of a distributed control system. The controllers are also embedded in many special purpose control systems.

PID control is regularly combined with logic, consecutive capacities, selectors, and straightforward work pieces to construct thecomplicated computerization frameworks util ized for vitality generation, transportation, and manufacturing. Many sophisticated control strategies, such as model predictive control, are also organized hierarchically. PID control is utilized at the most reduced level; the multivariable controller gives the set focuses to the controllers at the lower level [29]. PID controllers have survived numerous changes in innovation, from mechanics and pneumatics to chip through electronic tubes, transistors, and coordinates circuits. The chip has had a sensational impact on the PID controller. For all intents and purposes all PID controllers made nowadays are based on chip. It has given openings to supply extra highlights like programmed tuning, pick up planning, and persistent adjustment [29].

2.6.1 PID controller Algorithms

A PID controller calculates an error value as the difference between a measured process variable and a desired set point. The controller attempts to minimize the error by adjusting the process through use of a manipulated variable.

Proportional Term: The proportional term produces an output value that is proportional to the current *error* value. The relative reaction can be balanced by duplicating the blunder by a steady K_p called the corresponding pick up steady. The relative term is given by:

$$P_{out} = K_p e(t) \quad (2.5)$$

A high proportional gain results in a large change in the output for a given change in the error. If the proportional gain is too high, the system can become unstable. In differentiate; a little pick up comes about in a little yield reaction to a expansive input blunder, and a less responsive or less touchy controller. In the event that the corresponding pick up is as well low, the control activity may be as well little when reacting to framework unsettling influences. Tuning hypothesis and mechanical hone show that the corresponding term ought to contribute the bulk of the yield alter.

Integral Term: The contribution from the integral term is proportional to both the magnitude of the error and the duration of the error. The integral in a PID controller is the sum of the instantaneous error over time and gives the accumulated offset that should have been corrected previously. The accumulated error is then multiplied by the integral gain k_i and added to the controller output.

$$I_{out} = K_i \int_0^t e(\tau) d\tau \quad (2.6)$$

The integral term accelerates the movement of the process towards set-point and eliminates the residual steady-state error that occurs with a pure proportional controller. However, since the integral term responds to accumulated errors from the past, it can cause the present value to overshoot the set-point value.

Derivative Term: The derivative of the process error is calculated by determining the slope of the error over time and multiplying this rate of change by the derivative gain Kd. The magnitude of the contribution of the derivative term to the overall control action is termed the derivative gain, Kd. The derivative term is given by:

$$D_{out} = K_d \frac{d}{dt} e(t) \quad (2.7)$$

2.7 Fundamental Fuzzy Controller

Fuzzy logic which was first introduced by Zadeh in 1995 is a theory that uses mathematical formulas to explain human reasoning. The computational formula in fuzzy logic is not complex. Fuzzy logic interprets qualitative information to mathematical relations. That makes it suitable to explain unpredictable system behavior that cannot be easily modeled. Fuzzy theory shares the same general concept with the traditional set theory, except that there are no crisp transitions between values. Variables are expressed by functions or curves between two

digits, mainly 0 and 1 or any other digits. A series of weights describe the degree of belonging of a variable to a certain value within assigned range. While, traditional set theory defines a variable by its equality or non equality to certain value [30]. To define a fuzzy set, both the members of the set (value) and degree of membership (weight of each value) are needed. Fuzzy logic operations or fuzzy concepts are used to relate fuzzy sets [31], [32].

The main operations of fuzzy sets are:

Union of two sets: A and B: $\mathrm{M(x)} + \mathrm{B(X)} = \max(\mathrm{MA(x)}, \mathrm{MB(x)})$ (2.8)

Intersection of A and B: $\min(\mathrm{MA(x)}, \mathrm{MB(x)})$ (2.9)

Negation of A $\mathrm{M(A(x))} = (1 - \mathrm{MA(x)})$ (2.10)

2.7.1 Membership functions

Fuzzy input and output variables are represented by membership functions (MF). Membership functions related each input and output to weighted variable depending on the shape of curve [33]. The membership function is usually chosen by the designer of the controller [34]. The most common membership functions are [35]:- Triangular (when using triangular functions oscillations with generally reduced and fast convergence was achieved); trapezoidal (results in more oscillatory output); Gaussian; Bell; π shaped MF; S shaped MF; The main factors that should be considered when selecting a membership functions are [36] [37]:- (1) Sufficient width of the membership function to allow for noise detection; (2) Sufficient overlapping to correctly identify the controller; (3) Gaps between function curves should be prevented, because they result in ill-defined controller; (4) Coordination between the number and the width of a set should be achieved. A fuzzy logic controller has four main parts as shown in figure 1.14. (I) Fuzzification, (II) Interface engine, (III) Rule base, (IV) Defuzzification.

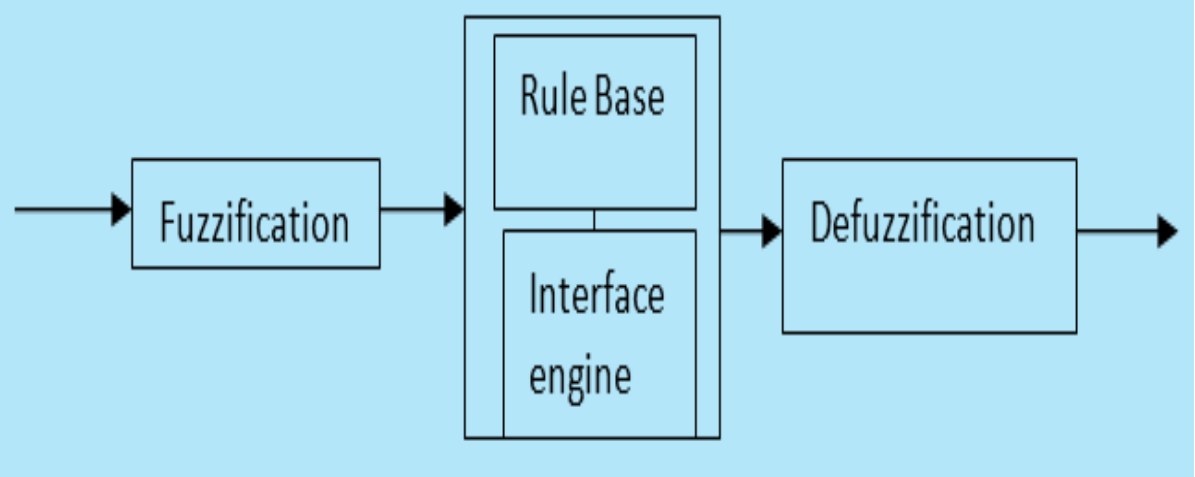

Figure 2.14: Fuzzy logic controller structure

Fuzzification: the primary step in planning a fuzzy controller is to decide which state variables represent the system dynamic performance must be taken as the input signals to the controller.Fuzzy rationale employments etymological factors rather than numerical factors. The handle of changing over a numerical variable (real number or crisp variables into linguistic variable (fuzzy number) is called fuzzification.

Interface engine: interface engine is define as the software code which processes the rule, cases, objects or other type of knowledge and expertise based on the facts of a given situation. When there's a issue to be illuminated that includes logic rather than fencing skills, we take a arrangement of deduction steps that may include deduction, association, recognition, and decision making. A deduction motor is a data preparing system (such as a computer program) that systematically employs inference steps similar to human brain.

Rule base: Mamdani fuzzy is the most used fuzzy membership rule set. It was introduced by E.H.Mamdani. It uses simple methods in designing the membership function and fuzzy rules, and is especially compatible with single input single output systems. Mamdani strategy is based on more intuitions and human knowledge and it works well with systems that are unpredictable and have high uncertainties [38]; [39]; [40]. A choice making rationale which is recreating a human choice handle, inters fluffy activity from the information of the control rules and etymological definitions. The run the show in "If Then" organize and formally the in case side is called conditions and the At that point side is called the conclusion. The computer is able to execute the rules and compute a control signal depending on the measured inputs error (e) and change in error (de). In run the show based controller the control procedure is put away in a more or less normal dialect. A run the show base controller is simple to get it and simple to preserve for a non-specialist conclusion client and an equivalent controller may well be executed utilizing customary procedures.

2.8 The Fundamental Theory of Fuzzy PID Control

The routine fuzzy control uses three of controllers, The Fuzzy-Proportional-integral (FPI) control, the fuzzy-proportional –derivative (FPD) control and the Fuzzy-Proportional-Integral-Derivative (Fuzzy-PID) control. The Fuzzy –PI control has good performance in steady states as it minimizes the permanent error but less performance at transient states, while the fuzzy-PD comes with good performance at the transient state but fails to eliminate the lasting mistake at unfaltering states [37]. The ordinary Fuzzy-PID control has both the Fuzzy-PI and Fuzzy-PD control but has three inputs (blunder, alter of mistake and speeding up of mistake) which increment revile of dimensionality. The PID sort Fluffy control (Fuzzy-PID) has as it were two inputs (error and alter of error). It composed by a Fuzzy-PI and a

Fuzzy-PD working in parallel. The rule-based is two dimensional and it is just like the Fuzzy-PI type control rule base. Due to the reality that the inputs of the Fuzzy-PID are limited to two, complexity is decreased while the advantages of the conventional Fuzzy-PID with the two inputs [41].

2.9 Light Sensor

Light dependent resistors (LDRs) are exceptionally valuable particularly in dark/light sensor circuits. The LDR resistance is exceptionally high in some cases come up to 1,000,000 ohms, but when LDRS are lit up with light, the resistance drops drastically. Light dependent resistor (LDR) is a variable resistor whose resistance is contrarily relative to the intensity of the incident light. As it is a passive transducer, a potential divider circuit is used to get the comparing voltage esteem from the LDRs. The higher the intensity of light, the lower the LDR resistance and hence lower the output voltage (V_{out}) and vice versa. Thus in the thesis, LDR plays the main role in controlling DC servo motor based on the intensity of light. The light dependent resistor (LDR) is represented in figure 2.15 [42].

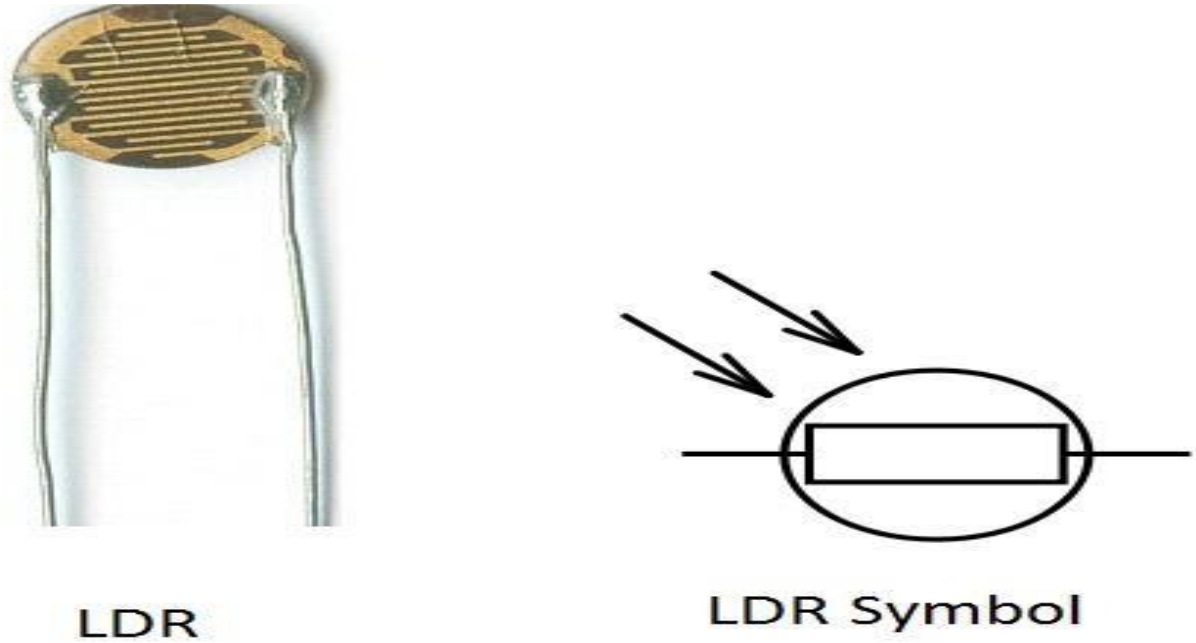

Figure 2.15: Light Dependent Resistor

.

CHAPTER THREE

MATERIAL AND METHODOLOGY

This chapter deals with the materials and the methods used in accomplishing the thesis. The materials used are digital computer and MATLAB/SIMULINK software. Modeling, designing and analyzing are the methods used. The takings after areas present each of these in detail.

3.1 Modeling of solar tracking floating PV system

The primary step in the analysis and design of the control framework is mathematical modeling of the different components. The transfer function is broadly utilized in designing control systems. After assumptions and approximations are made to mathematical equations describing the components, transfer functions are expressed. Thus, these transfer function, the sun based following framework is modeled. The block diagram in Figure 3.1 shows the most components of coasting sun powered panel system for SAST. The design the control system, the appropriate model for each component should be obtained.

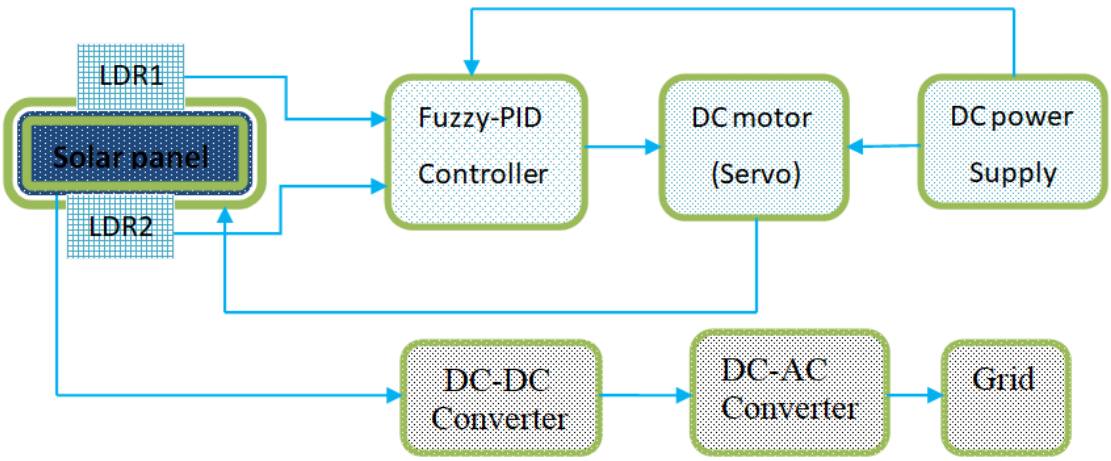

Figure 3.1: General block diagram of single axis solar tracking for floating solar panel

3.2 Modeling of sun based PV board

The PV board specification of the SR-P660260 modeling is appeared in the table 3.

The utilize of equivalent electric circuit Figure 3.2 and Figure 3.3 makes it possible to model characteristics of a PV cell. The model includes the following components (1) Current source (2) A diode (3) A series resistance

A parallel resistance, it is the leakage resistance of the cell is very small in a single module. The photons are generating the current source and the output of the model is constant with

constant temperature and constant intensity of light. The sun based PV cell can be planned by utilizing current source and modified diode associated in parallel to it as appeared figure 3.2. The series resistance because of the obstacle within the way to flow electrons from n to p intersection and parallel resistance is since of spillage current. A solar PV module has several PV cells connected in series\parallel. Series connections are utilized to increasing the voltage of the PV module, whereas the parallel connection is used to increase the current. Several solar PV modules can be interconnected in series and parallel configuration to form PV array. At a fixed ambient temperature and solar radiation, the current – voltage (I-V) and power – voltage (P-V) characteristics of a typical PV solar cell are non-linear in nature [43].

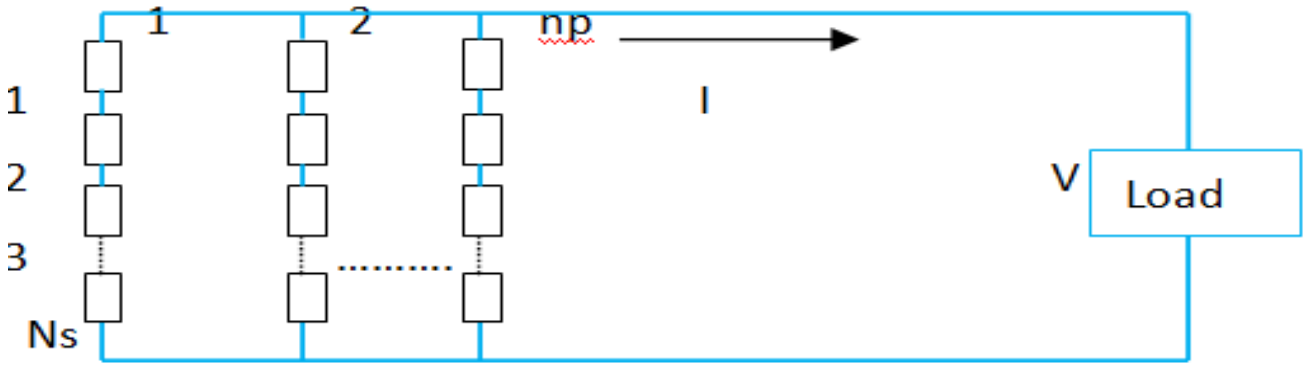

Figure 3.2: Equivalent circuit of a PV module with series and parallel connected PV cells

The character of I – V curve range from short-circuit (I_{sc}) to open-circuit current and open-circuit voltage (V_{oc}). At the node of a normal I − V curve is the M_{pp} (I_{mp}, V_{mp}), the point at which the PV cell generates maximum electrical power [44].

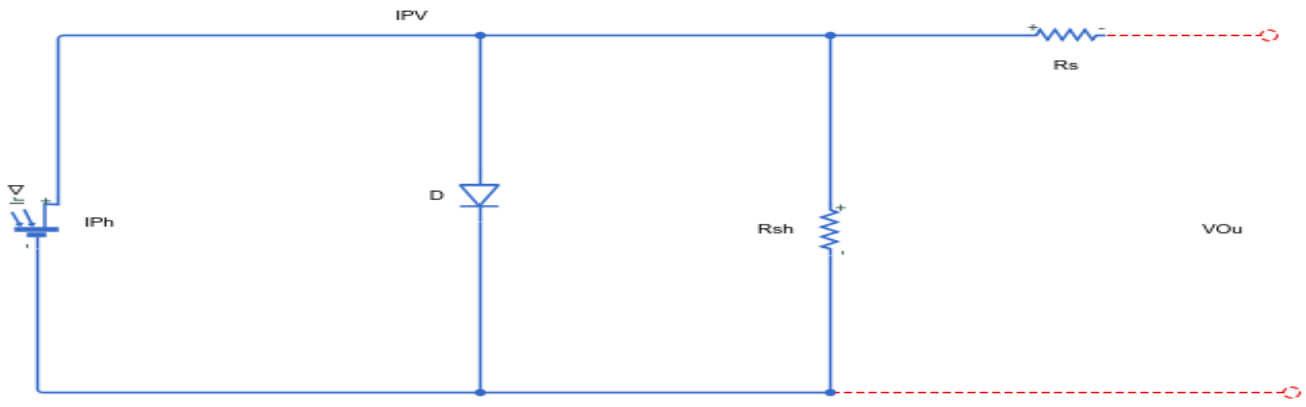

Figure 3.3: Ideal and practical single diode model of a PV cell

The basic mathematical expression of the output current of the PV module (Figure 3.3) can be expressed as

$$I = n_p I_{pv} - n_p I_o \left[\exp\left(\frac{qV}{KT\alpha n_s}\right) - 1\right] \quad (3.1)$$

Where;

I: The current,

V: Voltage of the PV module,

I_{pv} : The photo-current,

I_o : Reverse saturation current,

n_p : The number of cells connected in parallel,

n_s : The number of cells connected in series,

K: Boltzmann's constant $\left(1.38 * 10^{-23}\frac{J}{k}\right)$, and

T: The PV module temperature.

A practical PV module composed of several PV cells requires the additional parameters to the basic equation [45].

$$I = n_p I_{pv} - n_p I_O \left[\exp\left(\frac{V+R_S I}{V_t \alpha}\right) - 1\right] - \frac{V+R_S I}{R_p} \quad (3.2)$$

Where, $Vt = \frac{N_S KT}{q}$

It is the thermal voltage of the module with N_s cells connected in series, $R_s \; and \; R_p$ are equivalent series and parallel resistances. The PV current of the solar cells depends on the series and parallel resistances. Datasheets only provide the nominal short-circuit current (I_{sc}, n), which is the maximum current available at the terminals of the practical device. The assumption $I_{sc} \approx I_{pv}$ has mostly been used in photovoltaic models because in practical devices the series resistance is low and the parallel resistance is of high value. The PV current depends on the solar irradiation and is influenced by the temperature according to the following equation:

$$\mathrm{I_{pv}} = (\mathrm{I_{pv}}, \mathrm{n} + \mathrm{Ki}(\mathrm{T} - \mathrm{T_n}) * \frac{\mathrm{G}}{\mathrm{G_n}} \quad (3.3)$$

Where, $\mathrm{I_{pv,n}}$ is the PV current at the nominal condition (at 25 ◦C and 1000W/m2), T and T_n are the actual and nominal temperatures, G and $\mathrm{G_n}$ are the actual and nominal radiation and Ki is the short-circuit current/temperature coefficient. Diode saturation current depend on the solar radiation and the temperature as

$$I_O = I_{O,n}\left[\frac{T_n}{T}\right]^3 \exp\left(\frac{qE_g}{k\alpha}\left[\frac{1}{T_n} - \frac{1}{T}\right]\right) \quad (3.4)$$

Where E_g is the band-gab energy of the semiconductor and $I_{o,n}\ is$ the nominal saturation current can be expressed as

$$I_{o,n} = \frac{I_{sc,n}}{\exp\left(\frac{V_{oc,n}}{\alpha V_{t,n}}\right)-1} \quad , I_{o,n} = I_{rs} \tag{3.5}$$

Where; $V_{t,n}$ being the thermal voltage at the nominal temperature T_n. At normal value of irradiance, the short-circuit current can be assumed to be equal to the photo current I_{pv}. Short-circuit current $I_{sc} \approx I_{Pv}$ of the PV module is not strongly temperature dependent; it tends to increase slightly with an increase in the module temperature. For the comparison of various MPPT algorithms, variation in short-circuit current with change in temperature can be considered negligible. The short-circuit current can then be determined by [45]

$$I_{sc} = I_{sc,n}\left(\frac{G}{G_n}\right)^{\alpha} \tag{3.6}$$

Where; $I_{sc,n}$is the short-circuit current under the nominal irradiance (G_n) while I_{sc} is the short-circuit current of the PV module under the irradiance *G* and α is the exponent responsible for all the non-linear effects that the photocurrent depends on. Under different irradiance levels, short-circuit current is different, so that the parameter α can be determined by

$$\alpha = \frac{\ln\left(\frac{I_{sc,n}}{I_{sc,1}}\right)}{\ln\left(G_n/G1\right.} \tag{3.7}$$

Where $I_{sc,n}$and $I_{sc,l}$ are the short-circuit currents of the PV module under radiation G_n and G_l. Other important characteristics of the PV module versus open-circuit voltage V_{oc}; fill factor FF and the maximum power output P_{max} are the function of radiation and panel temperature. The relationship between the open-circuit voltage and radiation follows a logarithmic function based on the ideal diode equation and due to the effect of temperature. There is an exponential increase in the diode saturation current with an increase in temperature. The open-circuit voltage at any given condition can be expressed by

$$V_{oc} = \frac{V_{oc,n}}{1+\beta \ln\left(\frac{G_n}{G}\right)}\left(\frac{T_n}{T}\right)^{\gamma} \tag{3.8}$$

Where $V_{oc}$and $V_{oc,n}$are the open-circuit voltage of the PV module under the normal radiation *G* and the nominal radiation G_n, β is a PV module technology-specific coefficient and γ is the exponent considering all the nonlinear effects. The values of α, β and γ can be referred from the datasheet of the solar module.

Fill factor is a dimensionless term and is a measure of the deviation of the actual $I-V$ characteristic from the ideal one. The series and shunt resistance associated with PV modules

reduce the fill factor. The expression for determination of the fill factor is [45], [46], [47], [48].

$$FF = FF_o\left(1 - \frac{R_S}{\frac{V_{OC}}{I_{SC}}}\right) \tag{3.9}$$

Where;

$$FF_o = (V_{OC} - \ln(V_{oc} + 0.72))/1 + v_{oc} \tag{3.10}$$

Where, FF_o is the fill factor of the ideal PV module without resistance effects, R_s is the series resistance and $V_{oc}$is the normalized value of the open-circuit voltage to the thermal voltage, i.e.

$$v_{oc} = \frac{V_{oc}}{nKT/q}, \tag{3.11}$$

The maximum power output P_{max}can be given by [46],

$P_{max} = FF * V_{oc} * I_{sc}$;

$$P_{max} = \frac{v_{oc} - \ln(v_{oc}+0.72)}{1+v_{oc}}\left(1 - \frac{R_S}{\frac{V_{OC}}{I_{SC}}}\right) * \frac{V_{oc,n}}{1+\beta\ln\left(\frac{G_n}{G}\right)}\left(\frac{T_n}{T}\right)^{\gamma} I_{sc,n}\left(\frac{G}{G_n}\right)^{\alpha} \tag{3.12}$$

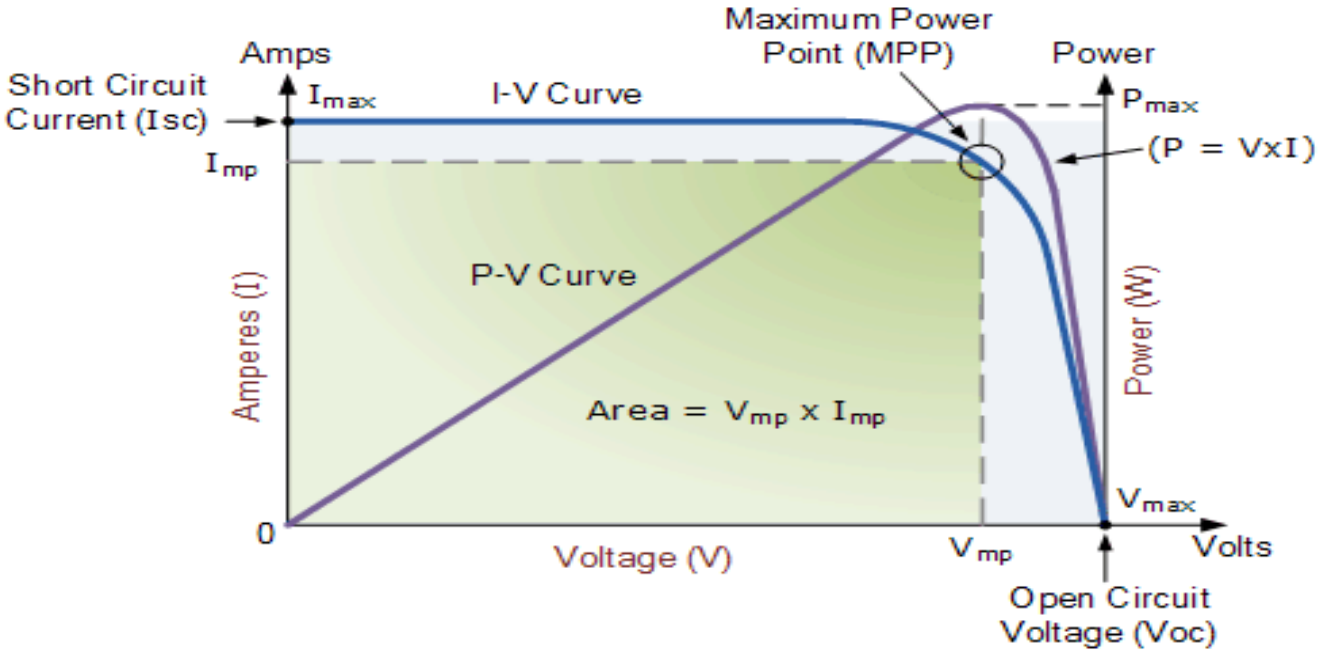

Figure 3.4: I − V and P − V characteristics of a solar cell

The PV Electrical specification of the FPV model is SR-P660260 used in this research. Adapted from sunrise model at standard test condition, the data is generated from PVSYST software.

Table 3.1: SR-P660260 PV panel Electrical specification for the FPV model

Open circuit- voltage (V_{OV})	37.89V
Short circuit current (I_{SC})	9.08A
Current at maximum power point (I_{mpp})	8.5A
Voltage at maximum power point (V_{mpp})	30.61V
Number of cells in series Ns	60
Power at maximum power point(Mpp)	260W
K_IThermal coefficient of I_{sc}%℃	4.5mA/℃
K_vThermal coefficient of V_{ov}% ℃	-139mV/℃
K_p max	-0.45℃

3.3 Mathematical modeling of MATLAB SIMULINK

The solar cell model is shown in figure 3.3. The mathematical modeling of the solar cell for single diode is given as;

$$I_{ph} = (I_{sc} + K_I * (T - 298) * \frac{G}{1000} \quad (3.13)$$

$$I_o = I_{rs} \left(\frac{T}{T_n}\right)^3 \exp\left[q * \frac{Eg\left(\frac{1}{T_n} - \frac{1}{T}\right)}{\alpha K}\right] \quad (3.14)$$

$$I_{rs} = \frac{I_{sc}}{e^{q*\frac{V_{voc}}{\alpha N_S KT}} - 1} \quad (3.15)$$

$$I_{sh} = \frac{V + I * R_s}{R_{sh}} \quad (3.16)$$

$$I = I_{ph} - I_o * \left[\frac{e^{q*V+IR_s}}{\alpha.k.N_s.T}\right] - 1 - I_{sh} \quad (3.17)$$

Where;

Photo current of solar cell (I_{ph});

Saturation current (I_o);

Reverse saturation current (I_{rs});

Current through shunt resistor(I_{sh}),

Output current (I)

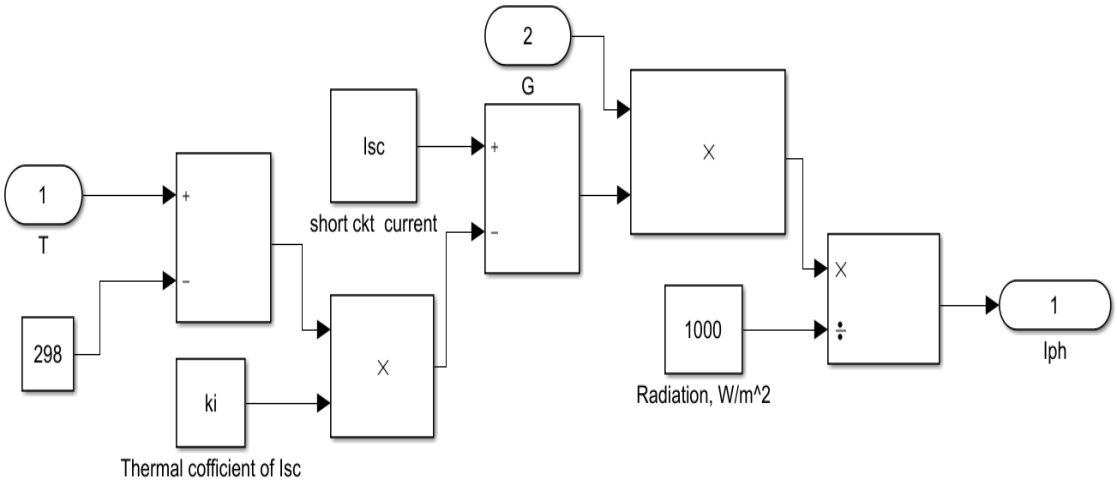
2
G
Isc
short ckt current
1
T
298
ki
Thermal cofficient of Isc
1000
Radiation, W/m^2
1
Iph

(1)

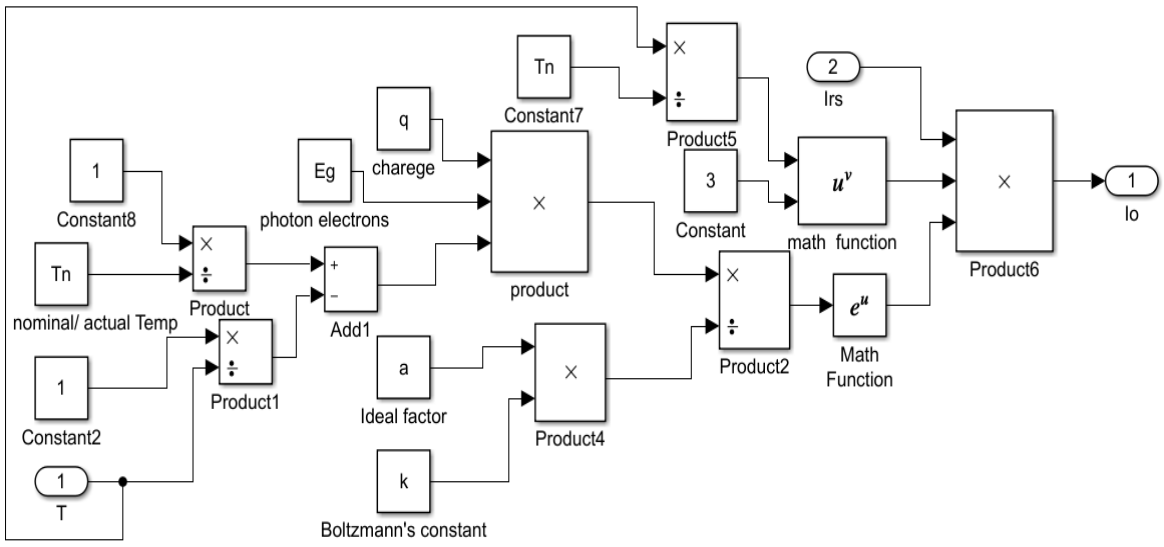
Tn
Constant7
Product5
2
Irs
q
charege
Eg
photon electrons
1
Constant8
3
Constant
math function
Product6
1
Io
product
Tn
nominal/ actual Temp
Product
Add1
Product2
Math Function
1
Constant2
Product1
a
Ideal factor
Product4
1
T
k
Boltzmann's constant

(2)

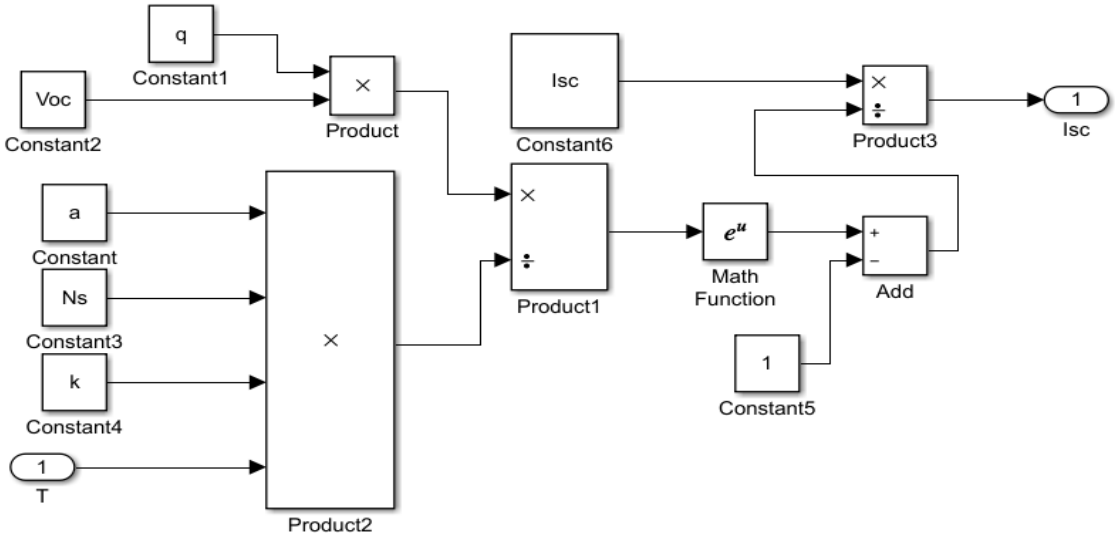
q
Constant1
Voc
Constant2
Product
Isc
Constant6
Product3
1
Isc
a
Constant
Ns
Constant3
k
Constant4
1
T
Product2
Product1
Math
Function
Add
1
Constant5

(3)

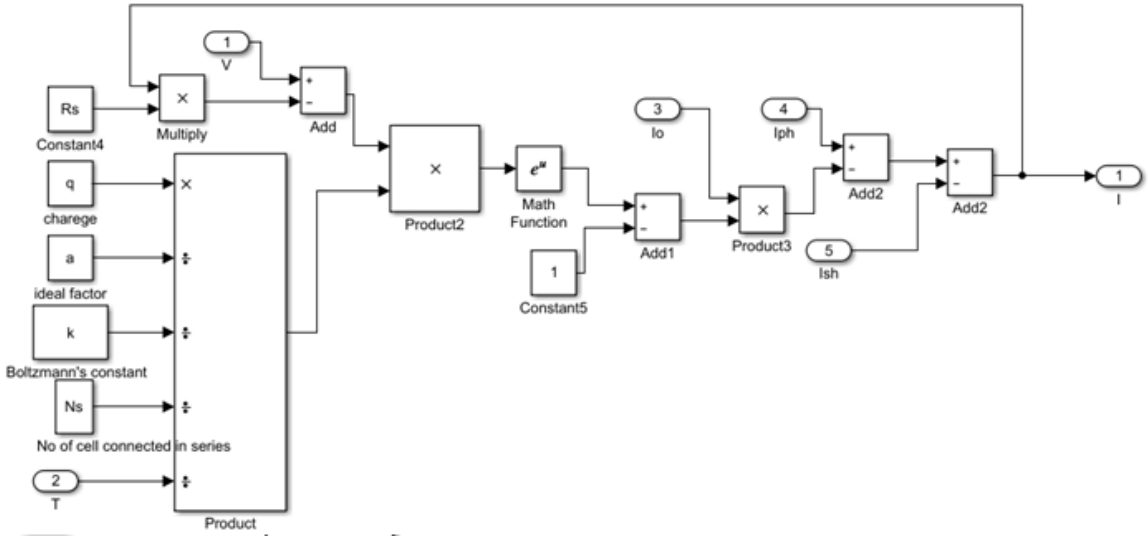
1
V
Rs
Constant4
Multiply
Add
Product2
Math
Function
3
Io
4
Iph
Add2
Add2
1
I
q
charege
a
ideal factor
k
Boltzmann's constant
Ns
No of cell connected in series
2
T
Product
1
Constant5
Add1
Product3
5
Ish

(4)

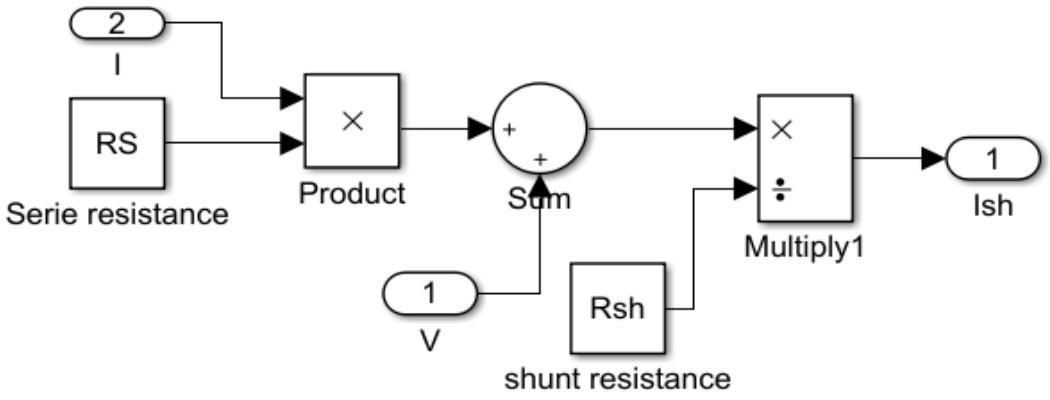

(5)

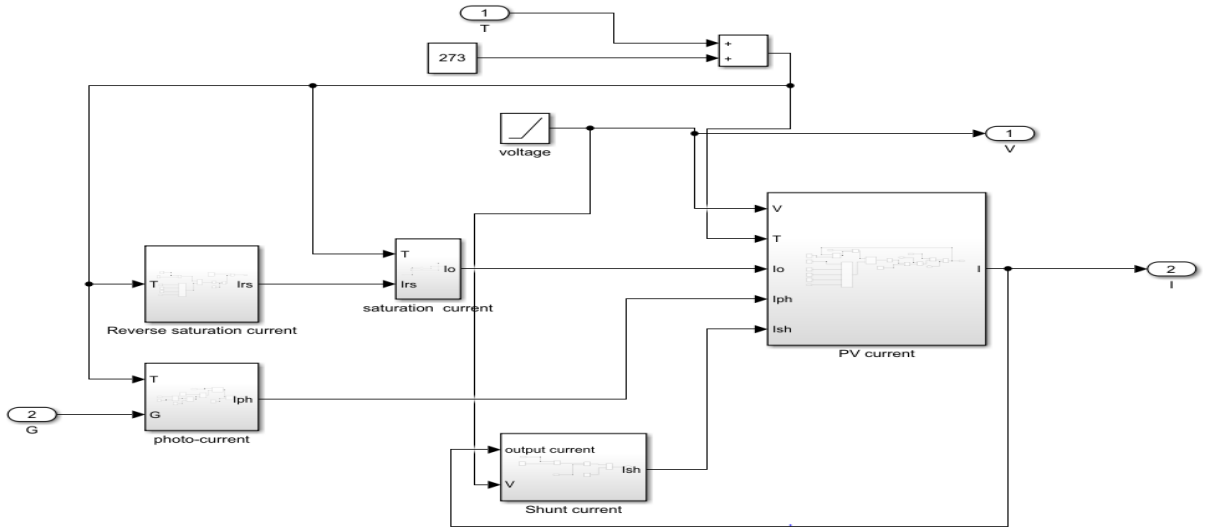

Figure 3.5: Subsystem of solar parameters in MATLAB SIMULINK (1), (2),(3),(4),(5)

Table 3.2: Constant parameters and variables for modeling

No	Parameter	Constant values	Units
1	Photo-current ((I_{ph}))	-	A
2	Short circuit current at SCT (I_{SC})	9.08	A
3	Operating temperature(T)	25	$℃$
4	Nominal temperature (K)	298	K
5	Solar irradiance (G)	1000	W/m^2
6	Electron charge (q)	$1.6 * e - 19$	C
7	Open circuit voltage (V_{OV})	37.89	V
8	Ideality factor of diode (a)	1.3	-
9	Boltzmann constant (k)	$1.38 * e - 23$	J/K
10	Band gap energy of semiconductor (E_g)	1.1	eV
11	Number of cells connected in series (Ns)	6	-

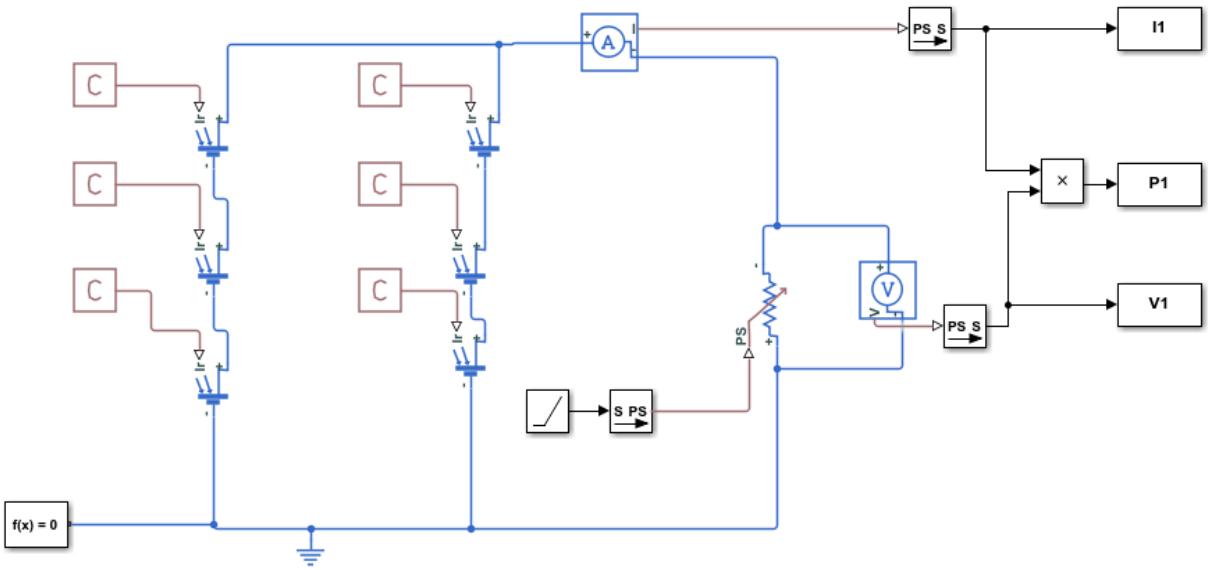

Figure 3.6: Model of solar cell in MATLAB SIMULINK

Thermal drift

In real world introducing the measured values of the thermal drift as given by several PV cells producers, The PV cell temperature, T_c, changes depending to the operating conditions; specifically, when the temperature increases, the photo-generated I_{ph} current increases

slightly, whereas the open-circuit voltage, V_{oc} decreases highly, as shown the following equation:

$$V_{oc}(T_c) = V_{oc,}STC(T_c)[1 - K_v(T_c - T_{c,}STC)] \quad (3.18)$$

Where K_v is the open-circuit voltage thermal coefficient, given in $C^{\circ -1}$, which is depends on the technology. The expectation of PV module performance in terms of electrical power output in the field that is introduced by manufacturer of the module, it is modeled by using of correlations of PV power as a function of operating variables, T_c and G. The parameterization of PV power with temperature used model is given by the following equation:

$$P_p(T_c) = \eta_{STC} * A_{PV} * G[1 - K_p * (T_c - T_{STC})]$$

$$= \frac{G}{G_{STC}} * P_{STC} * [1 - k_p * (T_c - T_{STC})] \quad (3.19)$$

Where

η_{STC} : The reference module efficiency at STC,

A_{PV} : The panel surface area

k_p : The power temperature coefficient for the PV module

3.4 Environmental Impact of FPV power generation

The FPV power generation is affected by variables such as wave-height (m), wind speed (m/s), and lake fetch (km). Its structure against wave-height effect, the stress of the structure was developed with respect to the wave-height through many element analyses. The Molitor was proposed the design wave-height formula that is shown as equation (3.20). Variables under different conditions were applied to this equation [49].

$$h_w = 0.06\sqrt{VF} + 0.76 - 0.27\sqrt[4]{F} \quad (3.20)$$

Where,

h_w: Wave-height (m),

V: Wind velocity (m/s),

F: Fetch (km) (length of the surface on which wind can act)

Meteorological stations typically detect the wind at height of 10m. The station data to be corrected with Hellman formula that is expressed as follows [50]*:*

$$V_w(h) = V_{10}\left(\frac{h}{h_{10}}\right)^{\alpha_H} \quad (3.21)$$

The wind speed is starting from V_{10} at the height of 10m. The parameter α_H , the Hellman exponent, it is a number that depends on the location in a range that goes from 0.06 (unstable air above open water surface) to 0.6 (stable air above human inhabited areas).The fact that the relevant basin surface is slightly below the open land level. We assume a typical value of 0.2

and this, at height of 0.7m; it shows a reduction of 50% of the wind speed. Then we can determine the pressure of the wind on the panels using the standard formula:

$$P_v = \frac{1}{2}\rho C_d V_w^2 \quad (3.22)$$

Where;

P_v : The pressure of the wind on the panel,

V_w^2 : The module of the wind speed to the square

C_d : The coefficient of the object

ρ : The density of air

Depending on the surface S of the solar panel which can be evaluated the force acting on the solar panel and perpendicular to it. Let as active force be $F_a = P_v S$ with a factor C_d =0.5, $\rho = 1225 kg/m^3$ and with the velocity of 20m/s at the water surface (very strong gust), the pressure generated is 300Pa. In fact the forces of the buoyancy and the horizontal component sums up and tends to generate increasing forces on the connected rafts. Due to this the wind and wave forces acting on the system are small compared to the system generating force. The distribution of the forces depends on the alpha angle of the panel and the beta angles. When the sinking force increases the beta angle changes, to prevent this sinking force is always balanced by the force of Archimedes. The wave force acting on the mooring and high waves can fall onto the floating plant in open lake/seas to minimize the effects of the wave while maintaining a constant buoyant force [51].

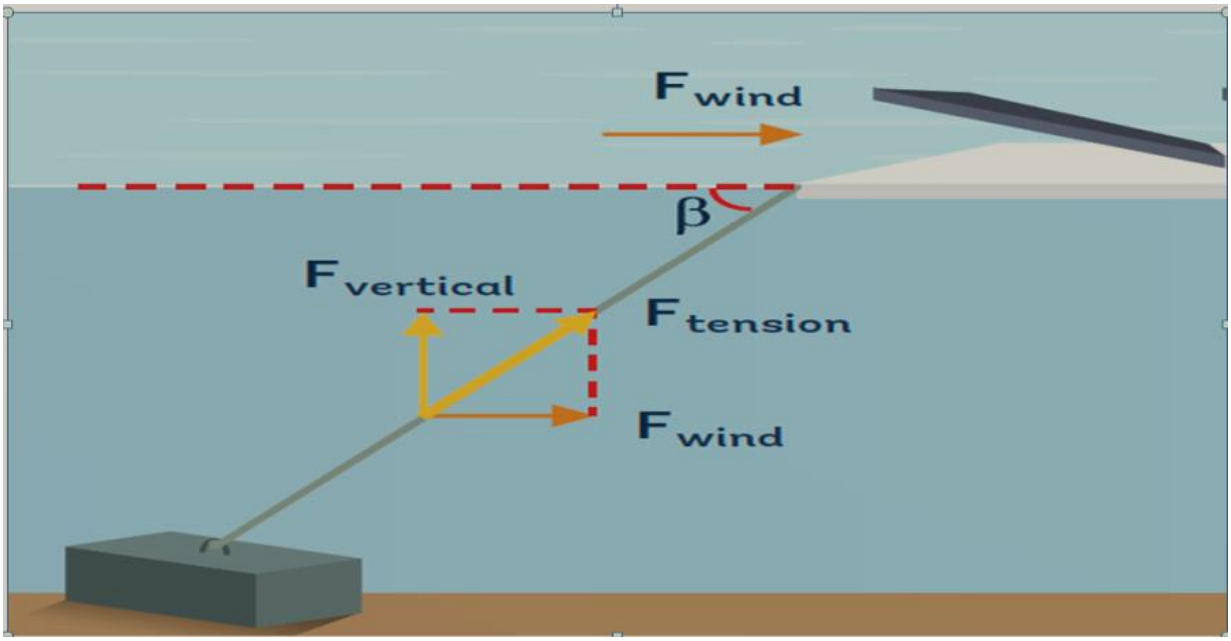

Figure 3.7: the angle of a mooring line & force exerted by wind on the floating platform

The larger tilt angles (β) will lead to higher tension for the same amount of wind load.

$$F_{tention} = \frac{F_{wind}}{cos\beta} \quad (3.23)$$

$\beta = angle\ of\ the\ mooring\ line;$

$F_{wind} = force\ of\ wind;$

$F_{vertical} = vertical\ uplift\ force$

3.5 High -Density polyethylene (HDPE pipes)

To make the structure float, HDPE cubes were considered during this paper. The enormous amount of cubes that would be needed, the floating solar PV system design uses an alternative. Long pipes that can be directly extruded on surface of the water, made with the same material, HDPE (HIGH-density polyethylene).

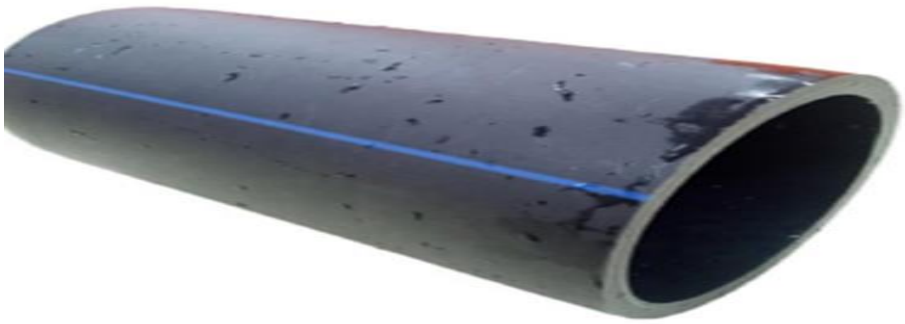

Figure 3. 8: HDPE Pipes Used in the Construction (Alibaba, 2019)

The quantity of pipe needed for one plat form is calculated using the Archimedes' principle and the buoyancy force.

$$F_B = Mg = \rho_f g V_d \quad (3.24)$$

F_B : Buoyancy force

M: Mass of element.

ρ_f : Fluid density. (Water at 4℃ has a $\rho_f = \frac{1g}{cm^3} = 10^3 kg/m^3$)

V_d : Displaced fluid volume.

An estimation of the total volume of pipe used in one of the platforms is:

$$V = A * L = \left[\pi {R_{exr}}^2 - \pi R_{int}^2\right] * \left[L_{perimeter} + L_{rows}\right] \quad (3.25)$$

$L_{perimeter} = 2\pi R$; R=radius of the pipe

$L_{row} = panel\ row\ dimenition$

$R_{ext} = extrenal\ radius\ of\ the\ pipe$

3.6 Single axis solar tracking model for floating solar PV system

The principle of floating solar tracking system developed in this thesis is shown by the following block diagram

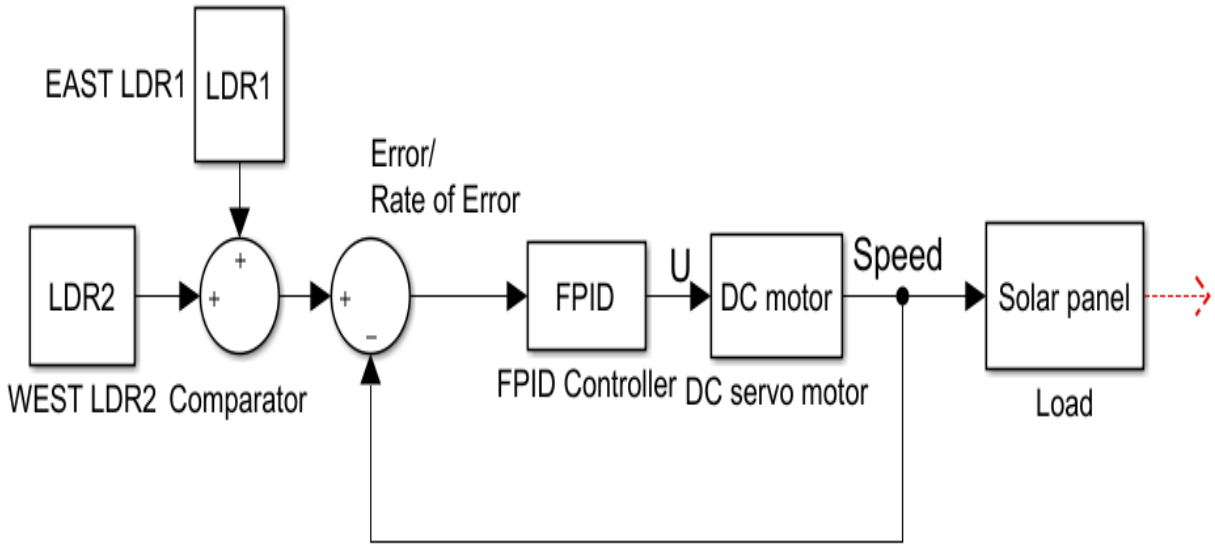

Figure 3.9: block diagram of floating solar tracking system

Figure 3.9 shows that the set point is the intensity of solar light received on the east side of the PV panel. The two LDR sensors are used to sense the position of the sun depends on the time. The two sensors are putting the east and west direction near to the floating PV panel. The sensor can detect the voltage across each LDR sensors, from the two opposite side of LDRs; voltage difference occurs due to the solar light intensity variations. The floating solar PV panel can shift the position into high voltage difference of LDR. The voltage difference of the two LDR sensors can be zero; this can be suggested that the light can be distributed equally on the whole panel. The two sensors will be adjusted east to west direction for the whole day. The DC motor is used to rotate the floating solar panel and the speed of the motor is controlled by PID controller. A fuzzy logic based controller is also used to tune the gain of PID controller [52].The controlled variable is the position of the PV panel based on differences in the intensity of solar light received by the east and west side of the PV panel. If the output voltages of the two LDR sensors are not same then it will result an error which becomes the input for the fuzzy logic controller. The controlled signal generated by Fuzzy-PID controller (PWM signal) as an input to rotate the motor a pre-determined angle or will order the DC motor to move or stop.

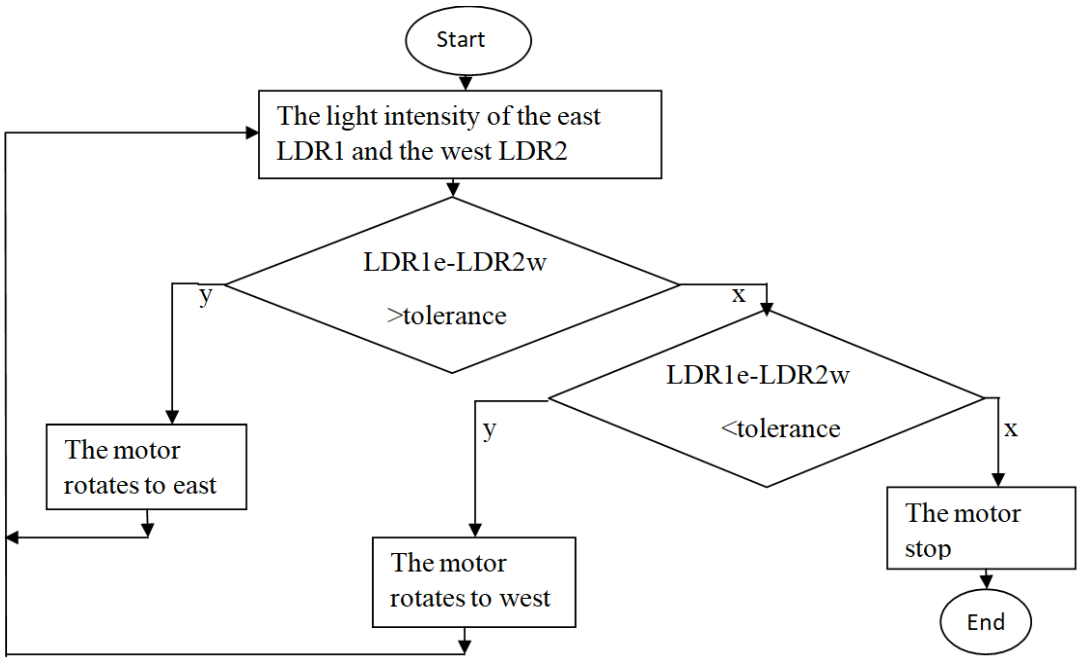

Figure3.10: the control algorithm of floating PV solar tracking system

3.7 Design and analysis of floating solar tracking PV system controller

There is different type of controllers used for position control of tracking solar PV panel among those in the following section are considered on PID and fuzzy-PID controllers with DC servo motor.

3.7.1 Hybrid Fuzzy PID controller model

The output values are, $\Delta K_p,\ \Delta K_i\ and\ \Delta K_d$, which comes from input variables that have been handled with fuzzy reasoning , fuzzy solution and quantification. Then they are added with the initial PID parameters to get new PID parameters and implement the online adjustment of PID parameters. In the end the values are getting from PID controller. The fig3.12 shows the structure of Fuzzy -PID controller. Using the fuzzy controller rule on- line, PID parameters, $K_p, K_i\ , K_d$ are adjusted. The block diagram of a self-tuning Fuzzy-PID controller is shown in figure below.

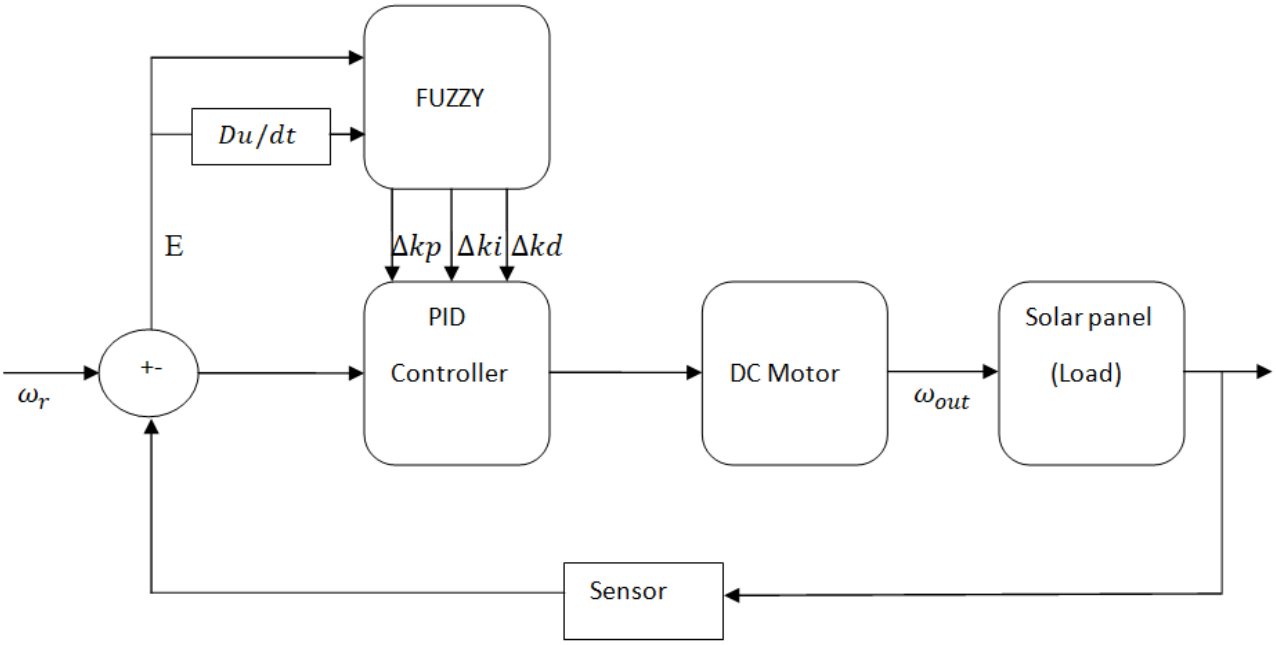

Figure 3.11: self tuning Fuzzy-PID controller model

PID parameters fuzzy self-tuning is to find the fuzzy relation between the three parameters of PID and "e" and "de", and depending to the principle of fuzzy control, to modify the three parameters in order to meet different requirements for control parameters when "e" and "de" are different, and to do the control strategy a good dynamic and static performance [53].

3.7.2 Design and analysis of PID controller

A PID controller combines proportional gain, integral gain/reset and derivative gain/rate modes to calculate the output based on error between a measured variable and a desired set point as represented in the Laplace domain Equation (3.26).

$$G_{con} = \left(K_p + \frac{K_i}{s} + K_d.s\right), \text{ and } G_{con} = K_p\left(1 + \frac{1}{T_i s} + T_d s\right) \quad (3.26)$$

Where, K_p is the proportional constant, $K_i$is the integral time and K_d is the derivative time. The proportional mode considers the present state of the error and the integral control mode looks into the past history of the error, while the derivative mode anticipates the future values of the error and acts on that prediction. The purpose of the derivative mode is to predict the errors and take corrective action in advance. The integral mode returns the controlled variable to set point after the disturbance at input and eliminates the offset, which the plain proportional controller cannot do. The reason proportional controller results in an offset are because it disregards the past history of the error; in other words, it leaves the accumulated effect of past errors uncorrected. The integral mode continuously looks at the total past history of the error by continuously integrating the area under the error curve and eliminates the offset.

3.6.2.1 Loop tuning mechanism

A. Manual tuning

The control framework must be online; one tuning strategy is to to begin with set K_i and K_d values to zero. Increment K_P until the yield of the circle wavers, and after that K_P ought to be set to around half of that for a "quarter sufficiency decay" sort reaction.

At that point increment K_i until any balanced is corrected in adequate time for the method, In any case; as well much K_i will cause precariousness.

At long last, increment K_d, on the off chance that required, until the circle is worthy fast to reach its reference after a stack unsettling influence. In any case, as well much K_d will cause intemperate reaction and overshoot. A fast PID loop tuning usually overshoot slightly to reach the set point more quickly; however, some systems cannot accept overshoot, an over damped closed – loop system is required, which will require a K_p setting significantly less than half that of the k_p setting that was causing oscillation. The PID parameters can be determined by using manual loop tuning mechanism. Thus are K_p = 30; Ki = 9100 and K_d = 110. The MATLAB/SIMULINK model is shown in figure 3.12 and the PID controller transfer function is given in equation (3.27).

$$G(s) = 30 + \frac{9100}{s} + 110s \qquad (3.27)$$

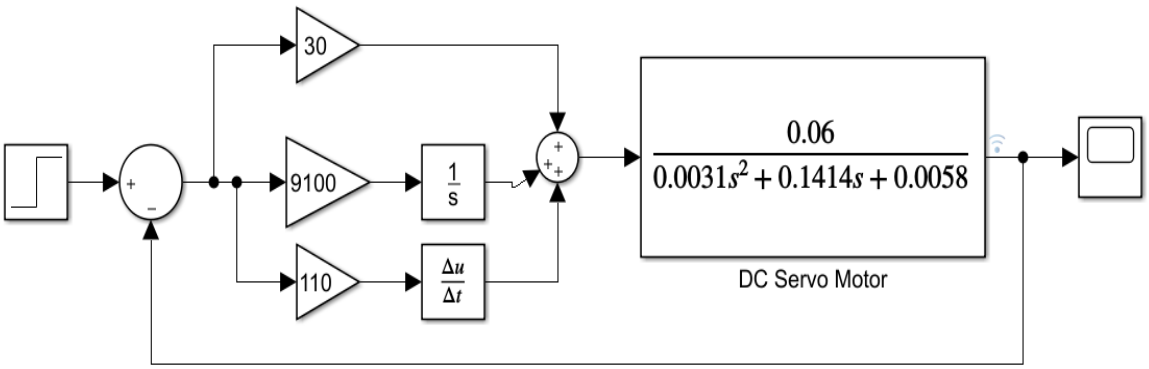

Figure 3.12: Manual loop tuning of SIMULINK model

The PID parameters affect the system dynamics which are:

Four major characteristics of the closed –loop step response

1. Rise Time: the time it takes for the plant output y to rise beyond 90% of the desired level for the first time.
2. Overshoot: the peak level is higher than the steady state, normalized against the steady state.
3. Settling Time: the time it takes for the system to converge to its steady state.

4. Steady- state Error: the difference between the steady-state output and the desired output.

Table 3.3: Tuning effect of independent P, I and D in closed-loop system response [54]

Closed loop response	Rise Time	overshoot	Settling time	Steady state error	stability
Increasing K_p	Decrease	Increase	Small increase	decrease	degrade
Increasing K_i	Small decrease	increase	increase	Large decrease	degrade
Increasing K_d	Small decrease	decrease	decrease	Minor change	improv e

B. Convectional PID tunings methods

The system models may be determined using system identification techniques, such measuring output for an impulse or step input. Most PID controllers are tuned on-line due to machine and process variations. The theoretical calculations for an initial setting of PID parameters can be by-passed using a few tuning rules. There are different tuning methods used in convectional PID tunings.

1. The Ziegler-Nichols tuning rule for open loop system

Ziegler and Nichols conducted various tests and proposed rules for deciding esteem of K_P, K_i, K_d based on the temporal step reaction of a plant.

It is proposed more than one strategy. The open circle framework bend can be characterized two constants, delay time (L) and time steady (T) which are decided by drawing a digression line at the enunciation point of the bend and finding the crossing points of the digression line which the time pivot and the steady-state level line. The exchange work of such a plant may be approximated by a to begin with – arrange framework with transport delay.

$$G(s) = \frac{ke^{-Ls}}{Ts+1} \qquad (3.28)$$

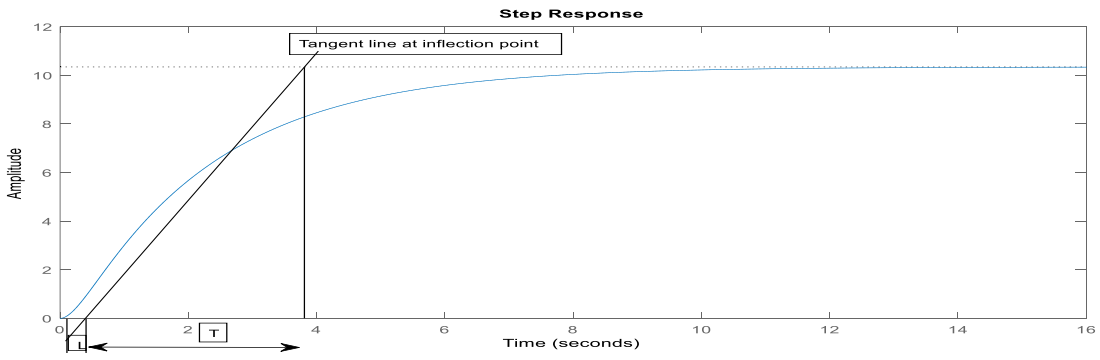

Figure 3.13: S-shaped step input response curve

Table 3.4: ZN tuning step input response of plant

Types of controller	k_p	T_i	T_D
P	$\frac{T}{L}$	∞	0
PI	$\frac{0.9T}{L}$	$\frac{L}{0.3}$	0
PID	1.2T/L	2L	0.5L

From the figure 3.13 the approximation value of delay time L and time constant T is 0.25sec and 3.85sec respectively. The transfer function of PID controller tuned using step response is:

$G(s) = K_p\left(1 + \frac{1}{T_i s} + T_D s\right)$;

$k_p = 1.2\frac{T}{L} = \frac{1.2*3.85}{0.25} = 1.2 * 15.4 = 18.48$;

$T_i = 2L = 2 * 0.25 = 0.5\ and\ T_d = 0.5L = 0.125$

$$G(s) = 18.48\left(1 + \frac{2}{s} + 0.125s\right) = 18.48 + \frac{36.96}{s} + 2.31s \quad (3.29)$$

2. Z-N Closed Loop Tuning Method

This closed Circle tuning strategy was moreover made by Ziegler and Nichols almost the same time as their open loop strategy was created and it is additionally utilized to as the recurrence reaction strategy, this strategy is based on certain characteristics of the method elements. Their plan of the strategy was based on knowing the point where the Nyquist bend of the method exchange work G(s) converges the negative genuine hub. They characterized two parameters, $K_u\ and\ T_u$, based on this point, which can be determined ultimate gain using Routh-hurwitz criteria method and ultimate period. The method for determining these parameters is as follows. Connect the controller to the plant, turn off the integral control, i.e. set $T_i = \infty$, and turn of the derivative control by setting$T_d = 0$. Increase the gain K until the process starts to oscillate. The ultimate gain where this occurs is $K_u = 0.2645$ and the period of the oscillations will be $T_u = 0.69$ which is obtained from appendix d. Again Ziegler and Nichols came with simple formulas that relate $K_u\ and\ T_u$ to K, $T_i\ and\ T_d$ for P, Pi, and PID controller from table 3.5 [54].

After determination of the ultimate gain and period, we can use the Ziegler–Nichols tuning rules (Table 3.5) to establish the PID tuning constants. This design method is based on increase k_p from 0 to a critical value K_{cr} at which the output first exhibits sustained

oscillations. To do that, first set $T_i = \infty$ and$T_d = 0$, then the critical gain K_{cr} and the corresponding period P_{cr} can be determined from simulation. The Ziegler-Nichols formula used to set the values of the PID parameters is shown in table 3.5.

Table 3.5: Ziegler-Nichols PID tuning rules

Type of controller	K_p	K_i	K_d
P	$0.5K_{cr}$		
PI	$0.45K_{cr}$	$\frac{T_u}{1.2}$	
PID	$0.6K_{cr}$	$\frac{T_u}{2}$	$0.125T_u$

To determine the values of $K_p, K_i, and\ K_d$ can be substituting the value of K_u, T_u using the above table 3.5.The Transfer function of PID controller tuned using frequency method

$$G(s) = k_p\left(1 + \frac{1}{T_i s} + T_D s\right)$$

$$= 0.6K_{cr}\left(1 + \frac{1}{0.5p_{cr}s} + 0.125p_{cr}\right)$$

$$= \frac{0.075K_{cr}p_{cr}\left(s+\frac{4}{P_{cr}}\right)^2}{s}$$

$$G(s) = 0.1587\left(1 + \frac{1}{0.3450s} + 0.0863s\right) \quad (3.30$$

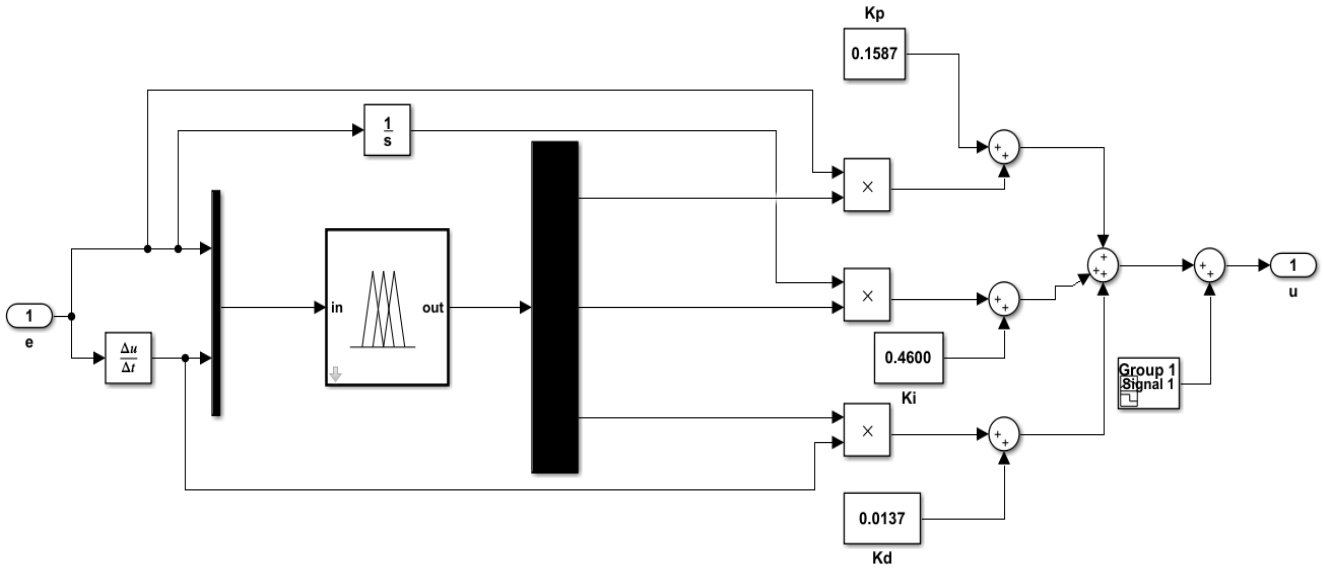

Figure 3.14: Model components of Fuzzy-PID controller block

3.7.3 Design of Fuzzy controller for floating solar PV system

3.7.3.1 Fuzzy logic controller design

The input to the Fuzzy controller are light intensity error "$e(t)$" of LDR sensor and change-in-light intensity error "$d(t)$" . The input of the fuzzy logic controller is expressed in the figure below.

$$e(t) = LDRG_r(t) - LDRG_{out}(t) \quad (3.31)$$

$$d(t) = e(t) - e(t-1) \quad (3.32)$$

Steps in fuzzy system design

- Identify the inputs with their ranges and name them
- Identify the outputs with ranges and name them
- Create the degree of fuzzy membership function for each input and output
- Construct the rule base that the system will operate
- Decide how the action will be executed by assigning strengths to the rules

The fuzzy logic controller having the following stages [55].

Fuzzification: - it implies the process of the transforming the crisp values of inputs of a controller domain.

Knowledge Base: - the knowledge base of FLC consists of data base and rule base

i. Data base:-it is used to provide necessary information for functioning of fuzzification module, rule base and defuzzification module
ii. Rule base: - the function of rule base is to represent in a structured way the control policy.

Fuzzy interface system

Fuzzy interface system has a simple input-output relationship. Input data from the external world is processed by the fuzzy interface system to produce the data the events having place in this these process are referred as the basic fuzzy interface algorithm. Mamdani fuzzy is of the fuzzy interface system.

Defuzzification

The control output derived from the combination of input, output membership functions and fuzzy rules is a fuzzy element and this process is called fuzzy interface. To do the fuzzy output available to real application, a defuzzification process is needed. The defuzzification process is meant to convert the fuzzy output back to the crisp or classical output to the control objective. The output is still a linguistic variable, and this linguistic variable needs to be

converted to the crisp variable through the defuzzification process. Three defuzzification techniques are commonly used, which are [56]:

I. Mean of Maximum Method,
II. Center of Gravity and
III. The Height method.

I. Mean of Maximum Method

The mean of Maximum (MOM) defuzzification method computes the average of those fuzzy conclusions or outputs that have the highest degree. If the servo motor x is rotated FAST. By using the MOM method, this defuzzification can be expressed as

$$MOM(FAST) = \sum_{\frac{X \in T}{T}} X' \ , T = \{X' \ 1 \ \mu FAST(X') = Support \ \mu FAST(X)\} \quad (3.33)$$

Where; T is the set of output x that has the highest degrees in the FAST. The graphical representation of the MOM method is shown in figure x. MOM method is that it does not consider the entire shape of the output membership function, and it only takes care of the points that have the highest degrees in that function. For those membership functions that have different shapes but the same highest degrees, this method will produce the same result.

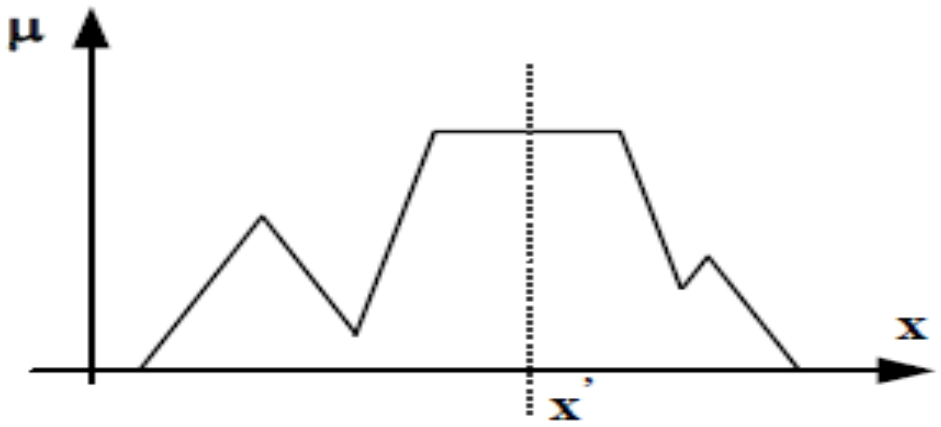

Figure 3.15: Graphical representation of defuzzification of MOM method

II. Center of Gravity (COG)

It is the most popular defuzzification technique and is widely utilized in actual applications. This method is similar to the formula for determine the center of gravity in physics, the weighted average of the membership function or the center of the gravity of the area bounded by the membership function curve is computed to be the crisp value of the fuzzy quantity.

$$COG(FAST) = \left(\frac{\sum_x \mu FAST(x) * x}{\sum_x \mu FAST(x)}\right)$$

If x is a continuous, this defuzzification result is

$$COG(FAST) = \frac{\int \mu FAST(x)dx}{\int \mu FAST(x)dx} \quad (3.34)$$

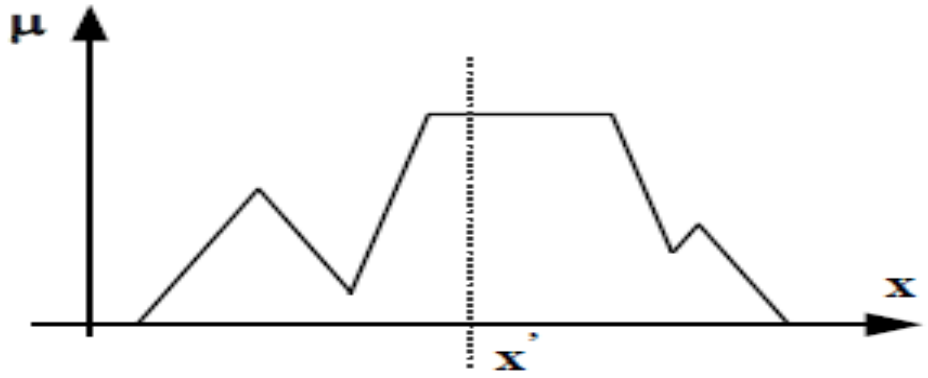

Figure 3.16: A graphical representation of the COG method

III. The Height Method (HM)

This defuzzification method is valid only for the case where the output membership function is an aggregated union of symmetrical functions. This method can be divided into two steps. First the consequent membership function F_i can be converted into a crisp consequent $x = F_i$ where F_i the center of gravity of is F_i. Then the COG method is applies to the rules with crisp consequents, which can be expressed as

$$x = \frac{\sum_{i=1}^{M} w_i F_i}{\sum_{i=1}^{m} w_i} \quad (3.35)$$

Where; w_i is the degree which the i^{th} rule matches the input data; the advantage of this method is its simplicity.

Adjusting fuzzy membership functions and rules

In order to improve the performance of FLC, the rules and membership functions are adjusted. The membership functions are adjusted by making the area of membership functions near ZE region narrower to produce finer control resolution. On the other hand, making the area far from ZE region wider gives faster control response. Also the performance can be improved by changing the severity of rules [57]. To study the effect of rise time (T_r), maximum overshoot (M_p) and steady-state error (SSE) when varying $K_p, K_i \; and \; K_d$.

Design of Membership Function (MF)

A. Input variable

Fuzzy sets of intensity RDR1 error (LDR1e) variable

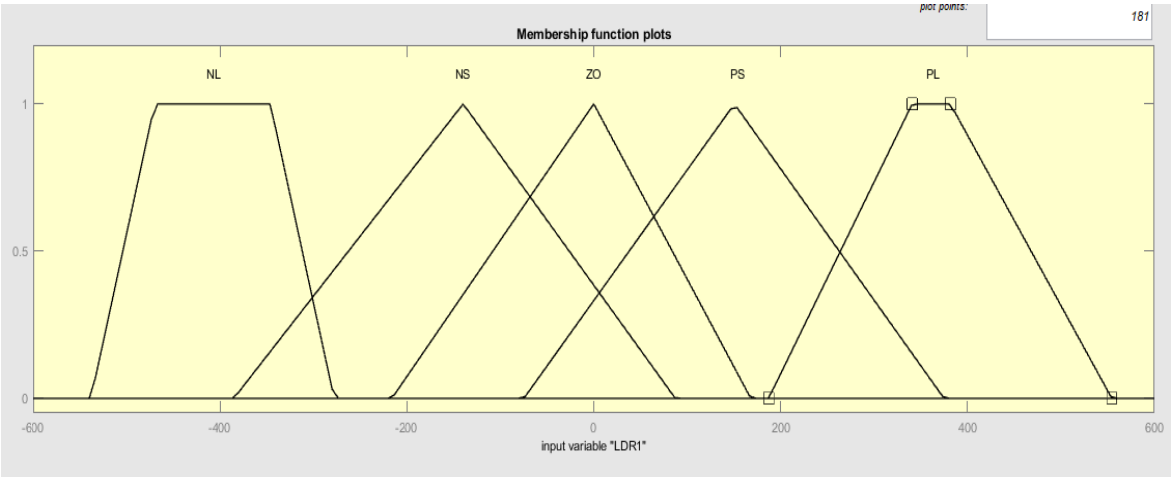

Figure 3.17: Membership Function of Intensity LDR1 Error

Table 3.6: Membership Function of Intensity LDR1 Error

Fuzzy set (linguistic variables)	description	Numerical range	Shape of membership function
Negative Large (NL)	Large intensity difference in negative direction	-600 to 200	Trapezoidal
Negative small (NS)	Small intensity difference in negative direction	385.2 to 87.23	Triangular
Zero (ZO)	The intensity difference is zero	-200 to 200	Triangular
Positive small (PS)	Small intensity difference in positive direction	-74.77 to 374.8	Triangular
Positive large (PL)	Large intensity difference in positive direction	168 to 576	Trapezoidal

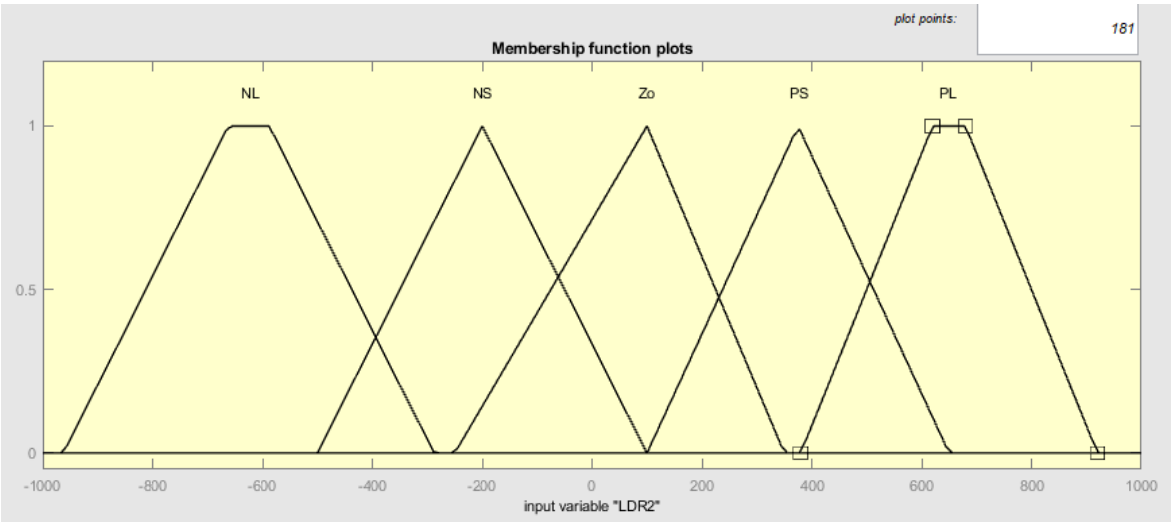

Figure 3.18: Membership Function change of Intensity LDR2 Error

Table 3.7: Membership Function change of Intensity LDR2 Error

Fuzzy set (linguistic variables)	description	Numerical range	Shape of membership function
Negative Large (NL)	Large intensity difference in negative direction	-1000 to -250	Trapezoidal
Negative small (NS)	Small intensity difference in negative direction	-500 to 100	Triangular
Zero (ZO)	The intensity difference is zero	-250 to 250	Triangular
Positive small (PS)	Small intensity difference in positive direction	100 to 650	Triangular
Positive large (PL)	Large intensity difference in positive direction	350 to 950	Trapezoidal

B. Output Variables

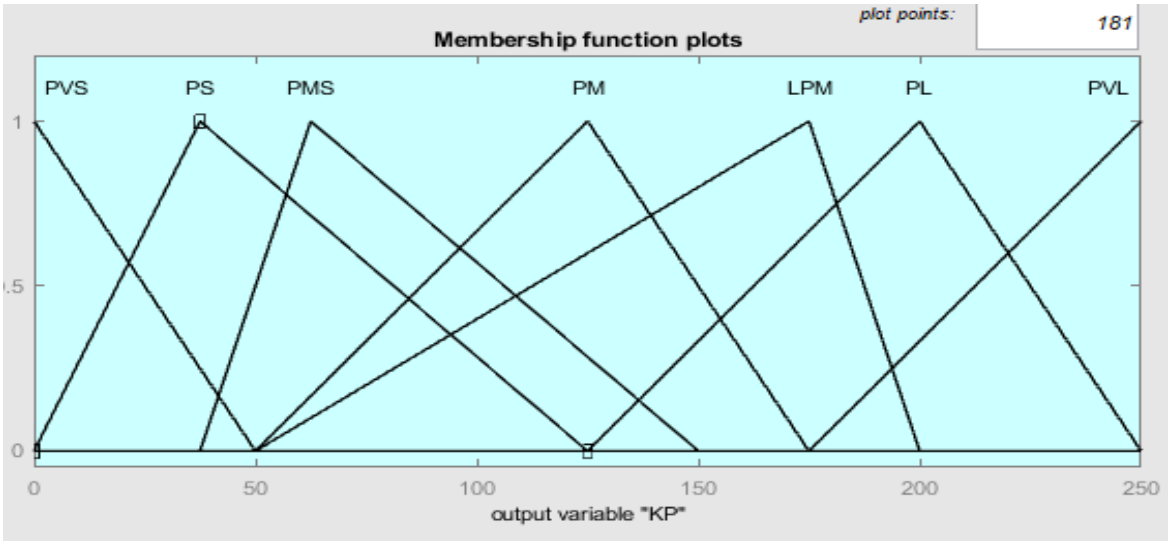

Figure 3.19: proportional gain kp membership function

Table 3.8: proportional gain kp membership function

Fuzzy set (linguistic variables)	Numerical range	Shape of membership function
Positive very small (PVS)	0 to 0, 0 to 50	Triangular
Positive small (PS)	0 to 37.5, 37.5 to 125	Triangular
Positive medium small (PMS)	37.5 to 62.5, 62.5 to 150	Triangular
Positive medium (PM)	50 to 125, 125 to 175	Triangular
Large Positive medium (LPM)	50 to 175, 175 to 200	Triangular
Positive large (PL)	125 to 200, 200 to 250	Triangular
Positive very large (PVL)	175 to 250, 250 to 250	Triangular

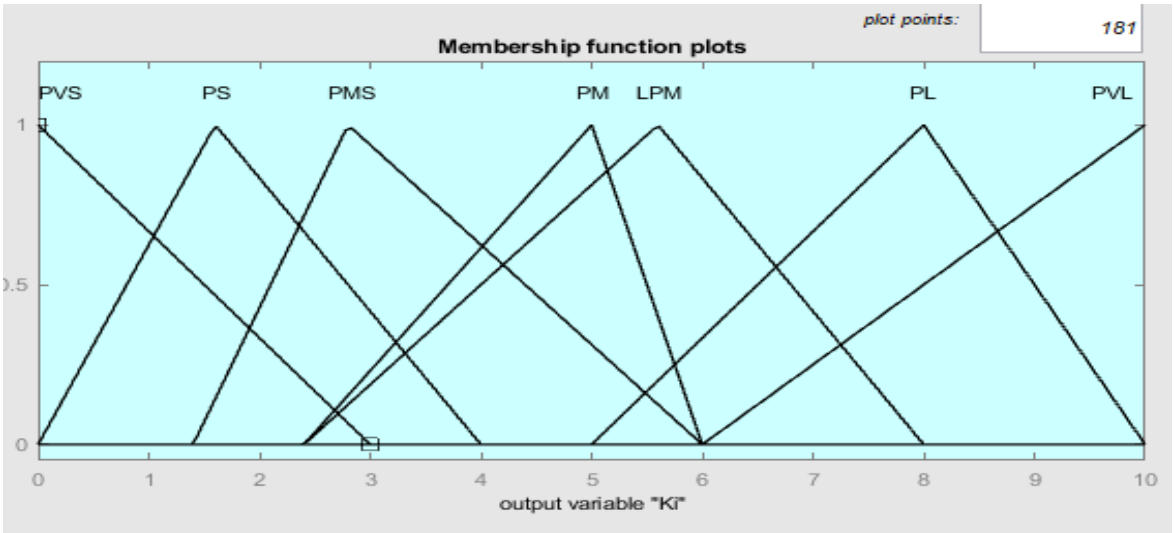

Figure 3.20: Integral gain Ki of membership function

Table 3.9: integral gain Ki of membership function

Fuzzy set (linguistic variables)	Numerical range	Shape of membership function
Positive very small (PVS)	0 to 0, 0 to 3	Triangular
Positive small (PS)	0 to 1.6, 1.6 to 4	Triangular
Positive medium small (PMS)	1.4 to 2.8, 2.8 to 8.6	Triangular
Positive medium (PM)	2.4 to 5, 5 to 6	Triangular
Large positive medium (LPM)	2.4 to 5.6, 5.6 to 8	Triangular
Positive large (PL)	5 to 8, 8 to 10	Triangular
Positive very large (PVL)	6 to 10, 10 to 10	Triangular

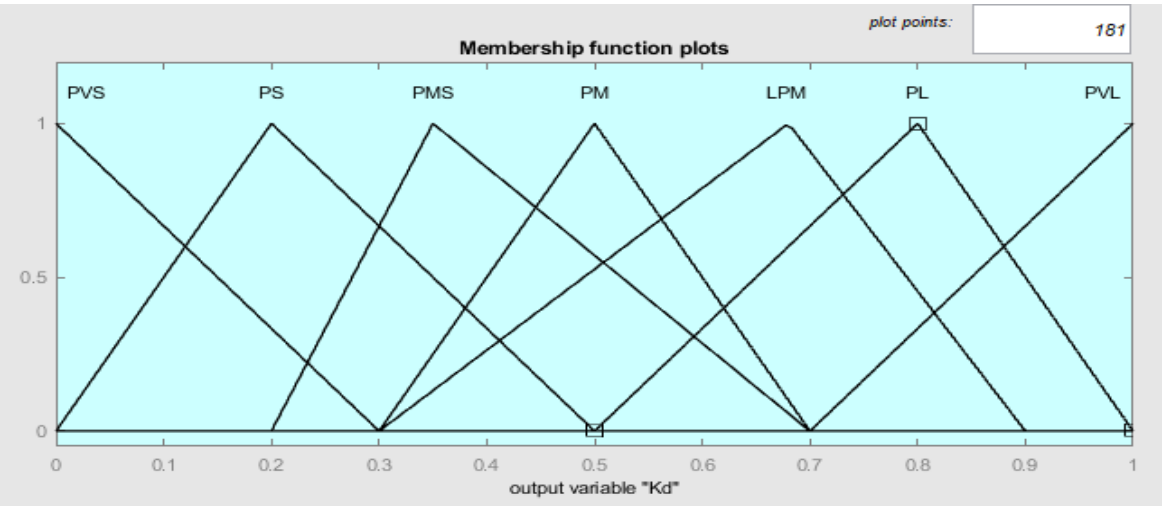

Figure 3.21: Derivative gain kd of membership function

Table 3.10: Derivative gain kd of membership function

Fuzzy set (linguistic variables)	Numerical range	Shape of membership function
Positive very small (PVS)	0 to 0,0 to 0.3	Triangular
Positive small (PS)	0 to 0.2, 0.2 to 0.5	Triangular
Positive medium small (PMS)	0.2 to 0.35, 0.35 to 0.7	Triangular
Positive medium (PM)	0.3 to 0.5, 0.5 to 0.7	Triangular
Large Positive medium (LPM)	0.3 to 0.68, 0.68 to 0.9	Triangular
Positive large (PL)	0.5 to 0.8, 0.8 to 1	Triangular
Positive very large (PVL)	0.7 to 1, 1 to 1	Triangular

Fuzzy rule table design of intensity error for LDR1 and LDR2

One –axis solar tracking system generally uses two sensors. LDR sensors measuring light density are placed on solar tracking system by indicating in east and west. The main idea is to read the value from LDR1 and compare it with the value of light density from LDR2. Then, depending on the difference between the two values, the controllers will decide and send commands to the motor and change its angle in order to make the difference equal the tolerance value (LDR1-LDR2=tolerance**).**

Table 3.11: Error for LDR1 and change of error for LDR2

$dLDR2e/LDR1e$	NL	NS	ZO	PS	PL
NL	ZO	PS	PL	PL	PL
NS	NS	ZO	PS	PL	PL
ZO	NL	NS	ZO	PL	PL
PS	NL	NL	NS	ZO	PL
PL	NL	NL	NL	NL	ZO

Fuzzy rules design for output variable of K_p , K_i and K_d

Table3.12: fuzzy rule base design of Kp

$dLDR2e/LDR1e$	NL	NS	NO	PS	PL
NL	PVL	PVL	PVL	PVL	PVL
NS	LPM	LPM	LPM	PL	PVL
NO	PVS	PVS	PS	PMS	PMS
PS	LPM	LPM	LPM	PL	PVL
PL	PVL	PVL	PVL	PVL	PVL

Table 3.13: fuzzy rule base design of Ki

$dLDR2e/LDR1e$	NL	NS	NO	PS	PL
NL	PM	PM	PM	PM	PM
NS	PMS	PMS	PMS	PMS	PMS
NO	PS	PS	PVS	PS	PS
PS	PMS	PMS	PMS	PMS	PMS
PL	PM	PM	PM	PM	PM

Table 3.14: Fuzzy rule base design of Kd

$dLDR2e/LDR1e$	NL	NS	NO	PS	PL
NL	PVS	PMS	PM	PL	PVL
NS	PMS	LPM	PL	PVL	PVL
NO	PM	PL	PL	PVL	PVL
PS	LPM	PVL	PVL	PVL	PVL
PL	PVL	PVL	PVL	PVL	PVL

3.7.3.2 Fuzzy control system design assumptions

The fuzzy control deign that can be contained six main assumptions commonly build whenever a fuzzy rule-based control policy is selected [58]. The plant is observable and controllable: input and output variables are usually available for observation and measurement or computation.

- There exists a body of knowledge compromising a set of linguistic rules, engineering common sense, intuition, or a set of input-output measurements data from which rules can be extracted.
- A solution exists.
- The control engineering is looking for a "good enough" solution, not necessarily the optimum one.
- The controller will be designed within an acceptable range of precision.
- The problems of stability and optimality are not addressed explicitly; such issues are still open problems in fuzzy controller design.

3.7.3.3 Fuzzy interface system

First we defined on E in domain of e linguistic variables for LDR1 and defined on the EC in domain of ec linguistic variables for LDR2. Set the deviation e basic domain {el, eh} = {-600,600}, error change rate (ec) basic domain {ecl, ech} = {-1000, 1000}, Δk_p and Δk_I basic domain {0, 250}, {0, 10} and Δk_D basic domain {0, 1}.

The typical FIS inputs are the signals of error E and change of CE in light intensity sensor. The FIS output is the control action inferred from the fuzzy rules. The configuration of FIS for our fuzzy controller is given the below figure.

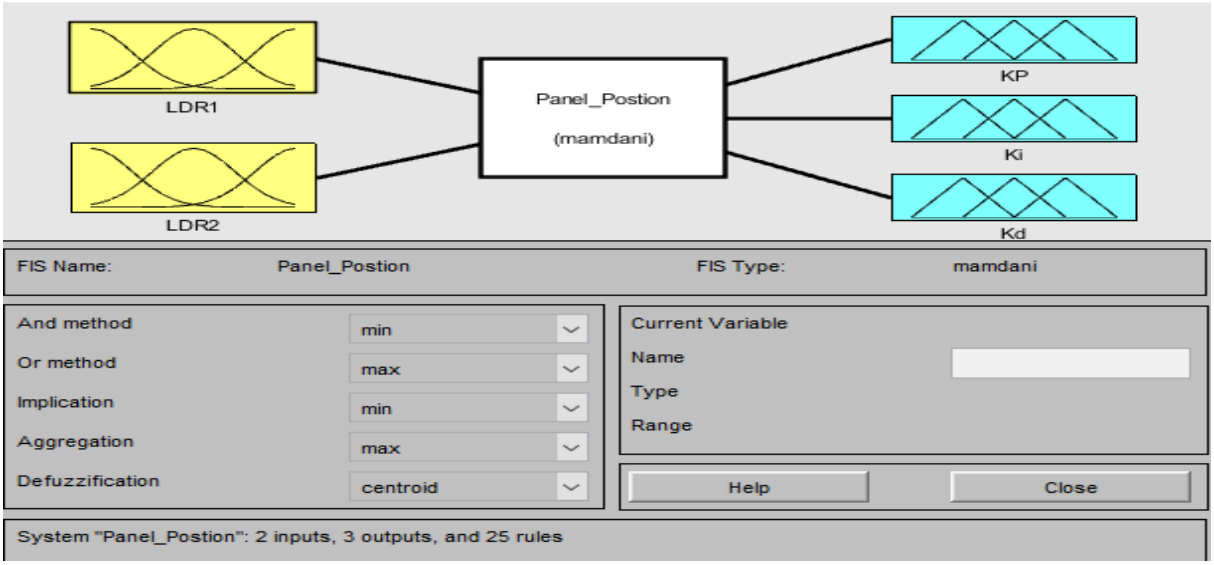

Figure3.22: Fuzzy interface block

Figure 3.22 (a), (b), (c) shows the surface viewer of KP, KI and KD with the E of LDR1 and CE of LDR2 respectively and shows the rule viewer of fuzzy interface system. Where, the rule viewer of fuzzy interface system and the IF THEN rule is given in appendix A and B respectively.

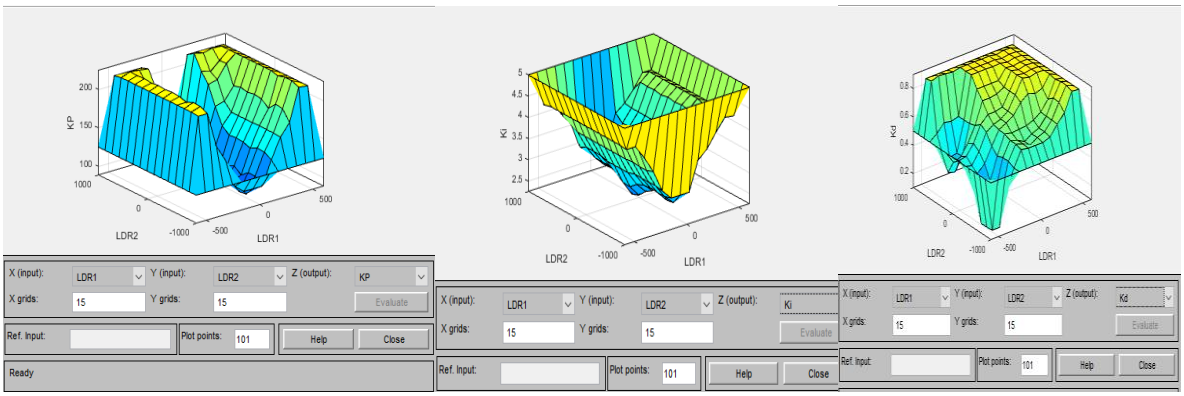

(a) (b) (c)

Figure3.23: surface viewers of KP, KI and KD

3.7.3.4 Fuzzier Design

Figure 3.23 is a graph of the intensity error of LDR1 and change in intensity error of LDR2 fuzzy membership functions. It assigns a crisp value's degree of membership to five fuzzy linguistic values NL, NS, ZO, PS, and PL. the fuzzy input membership functions used for error in intensity of LDR1 and change of error in intensity of LDR2 are triangular type. The universe of discourse of each membership function is shown in table 3.15 with degree of membership.

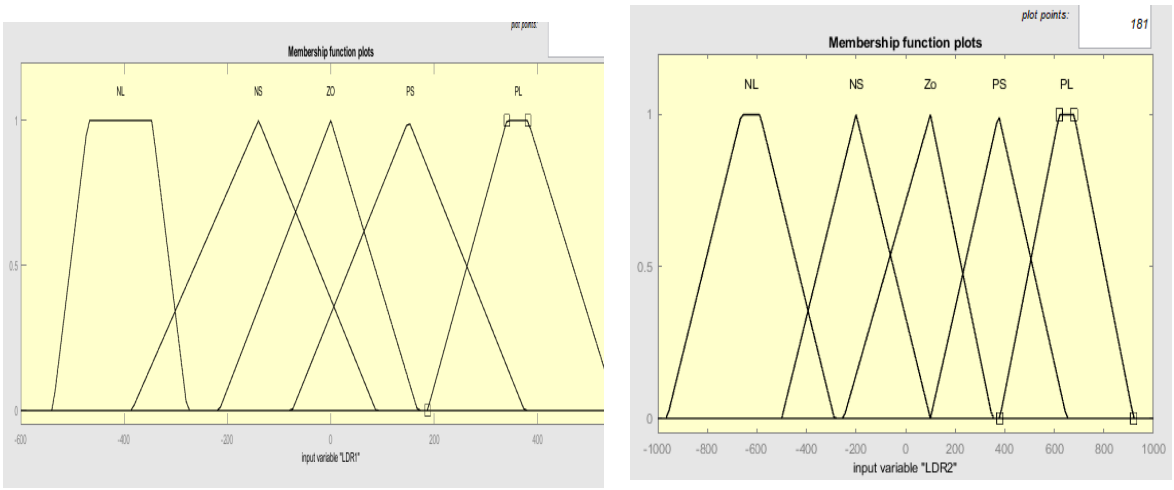

Figure 3.24: membership function for error and change of error in intensity of sensor LDR

Table 3.15: membership function universe of discourse of error and change of error in intensity of LDR

E(LDR1)	EC(LDR2)	Degree of Membership				
		NL	NS	ZO	PS	PL
-600 to -400	-1000 to -600	0 to 1	0	0	0	0
-400 to -200	-500 to -200	1 to 0	0 to 1	0	0	0
-200 to -74.77	-200 to 100	0	1 to 0	0 to 1	0	0
-74.77 to 100	100 to 400	0	0 to 1	1 to 0	1 to 0	0
100 to 200	400 to 700	0	0	1 to 0	0 to 1	0 to 1
200 to 400	700 to 1000	0	0	0	1 to 0	0 to 1

3.8 DC servo motor modeling

A common actuator in control systems is the DC motor. It directly provides rotary motion and coupled with wheals or drums and cables provide translational motion. DC motors are widely used in industrial applications, robot manipulators, speed and position control of motors are required. Consider a DC motor, whose electric circuit of the armature and free-body diagram of the rotor is shown in figure 3.24.

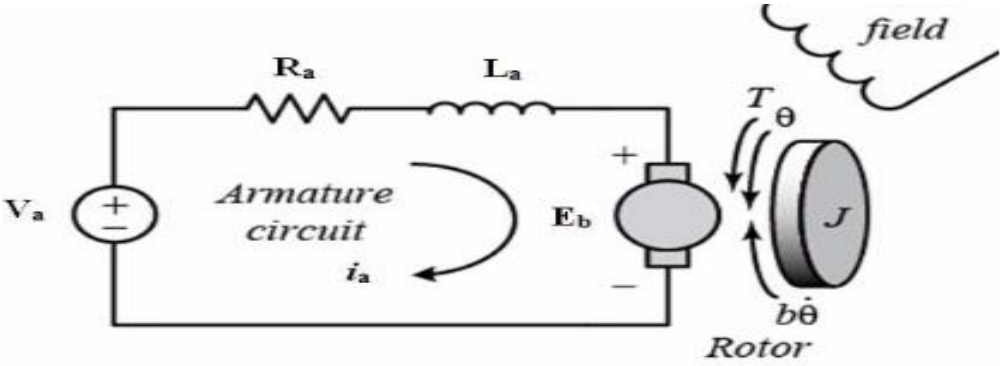

Figure 3.25: Schematic diagram of DC motor

The input is the armature voltage V in volts (driven by a voltage source). Measured variables are angular velocity of the shaft ω in radian per second and the shaft angle θ in radian.

Where:

V_a=armature voltage (V)

R_a=armature resistance (Ω)

L_a=armature inductance (H)

i_a=armature current (A)

E_b=back emf (V)

θ=angular position of rotor shaft (rad)

3.8.1 System modeling

In armature control of DC motor, the voltage applied to the armature of the motor is adjusted without changing the voltage applied to the field where the output voltage and motor torque is related the equation below.

$$V_a(t) = R_a i_a(t) + \frac{L_a di_a(t)}{dt} + E_b(\text{t}) \quad (3.36)$$

The motor torque T; is related to the armature current I, by constant factor k:

$$T = ki \quad (3.37)$$

The back electromotive force (emf), E_b is related to the angular velocity by

$$E_b = K\omega = \frac{Kd\theta}{dt} \quad (3.38)$$

In the figure above the following equation based on the Newton's law combined with the Kirchhoff's law cab be expressed as:

$$\frac{Jd^2\theta}{dt^2} + \frac{bd\theta}{dt} = Ki \quad (3.39)$$

$$\frac{Ldi}{dt} + Ri - V + \frac{kd\theta}{dt} = 0 \quad (3.40)$$

Table 3.16: Parameters of the servo DC motor parameter values

parameter	value	unit
Armature resistance (R_a)	2.2	Ω
Armature inductance (L_a)	0.5	H
Torque constant(K_t)	0.06	Nm/A
Back emf constant (K_b)	0.06	Nm/A
Inertia of motor rotor (J)	0.0062	Kgm^2/rad
Friction coefficient (b)	0.00l	Nm

3.8.2 Transfer function of DC motor

Using the Laplace transform equation (3.41) and (3.40) can be expressed as:

$$Js^2\theta(s) + bs\theta(s) + ki(s) \quad (3.41)$$

$$LsI(s) + RI(s) = V(s) - KS\theta(s) \quad (3.42)$$

From the equation (3.36), $I(s)$ can be expressed as:

$$I(s) = \frac{V(s)-Ks\theta(s)}{R+Ls} \quad (3.43)$$

Equation (3.43) substitutes from equation (3.41) to obtain:

$$Js^2\theta(s) + bs\theta(s) = (\frac{K(V(s)-ks\theta(s))}{R+Ls} \quad (3.44)$$

The equation for the DC motor is shown in the following block diagram in the figure 3.20.

From the equation (3.44), the transfer function from the input voltage $V(s)$, to the output angleθ, directly follows:

$$G(s) = \frac{\theta(s)}{V(s)} = \frac{K}{S[(R+Ls)(Js+b)+K^2)]} \quad (3.45)$$

$$G(s) = \frac{\omega(s)}{V(s)} = \frac{k}{[(R+Ls)(Js+b)+k^2]} \quad (3.46)$$

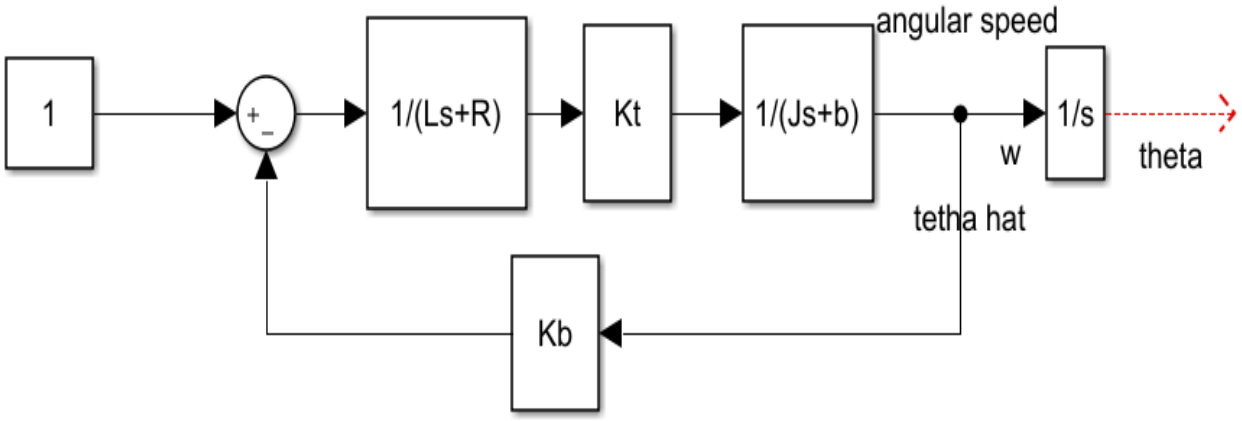

Figure3.26: MATLAB SIMULINK model for DC servo motor

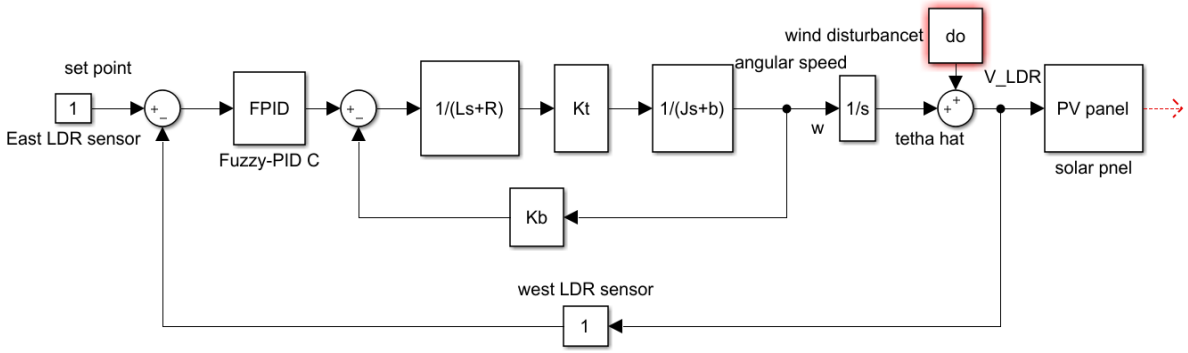

Figure 3.27: model of floating solar tracker system

The transfer function from the input voltage,$V(s)$, to the angular velocity, ω is:

$$G(s) = \frac{\omega(s)}{V_a(s)} = \frac{k_t}{[(R+Ls)(Js+b)+k_t k_b]} = \frac{0.06}{0.003s^2+0.1414s+0.0058}$$

Motion equation of floating PV solar panel:

$$\frac{d^2\theta}{Jdt^2} + Kb\frac{d\theta}{dt} = T; \qquad (3.47)$$

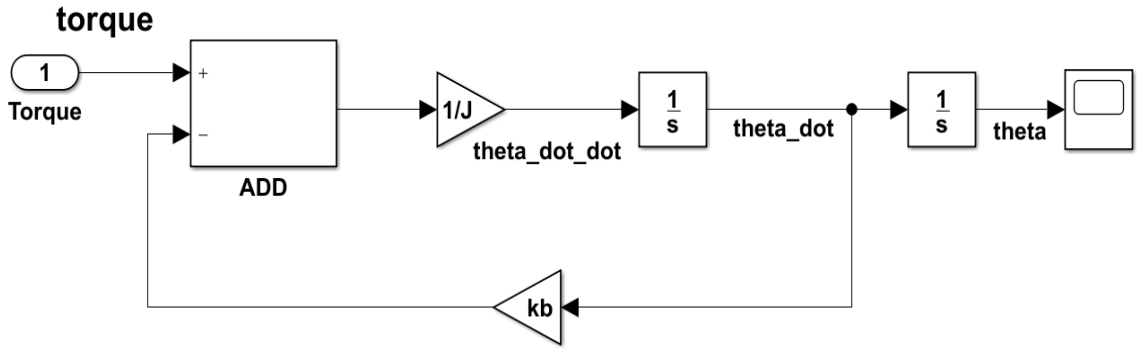

Figure3.28: MATLAB SIMULINK model for solar panel motion

3.9 LDR sensor model

The LDR sensor could be a variable resistor that changes the resistance concurring to the escalated of occurrence beam lit up on to it. As the escalated of daylight changes, the resistance and the voltage of LDR sensors alter.

The resistance diminishes with expanding occurrence light intensity. The LDR sensor unit consists of two sensors. These are utilized for measuring light escalated and creating analog voltage signals to be sent to control modules. They sense the position of the sun in vertical pivot i.e. east and west side.

Sensors are introduced on the sun powered board and found around a walled in area; the LDRs are isolated by dark surface or it is called balancer. The design of the plant is to calculate the moment of inertia of the solar panels in order to determine the location of the axis or rotary axis appropriately. In this case there are two possibilities; in the middle of the horizontal side (l) or in the middle of the vertical side (W) of solar panels. The output voltage across the resistor is the input of the controller. Based on the input, the servo motor rotates clockwise (CW) or anticlockwise (CCW).

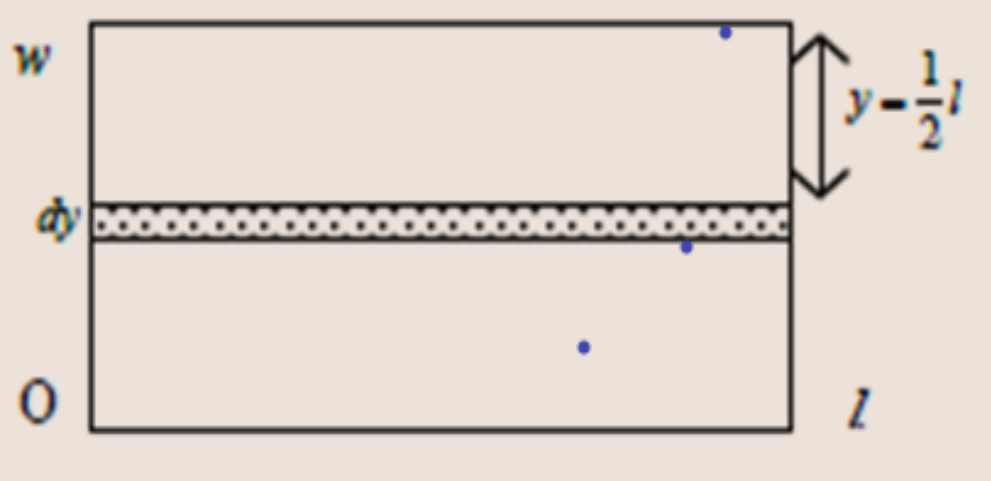

Figure 3.29: the rotary axis of solar panels

Hypothetically, the littler the minute of idleness of a protest at that point it'll be simpler to move. Based on calculations, the most excellent position of the rotating pivot is set within the center of vertical side of sun powered boards since it has moment of inertia littler than others. To determine the torque needed to move solar panels, in order to obtain the suitable characteristics of dc motors. Based; on the specifications of the PV panel that the value of the minimum torque is required to derive the PV panel position [59].

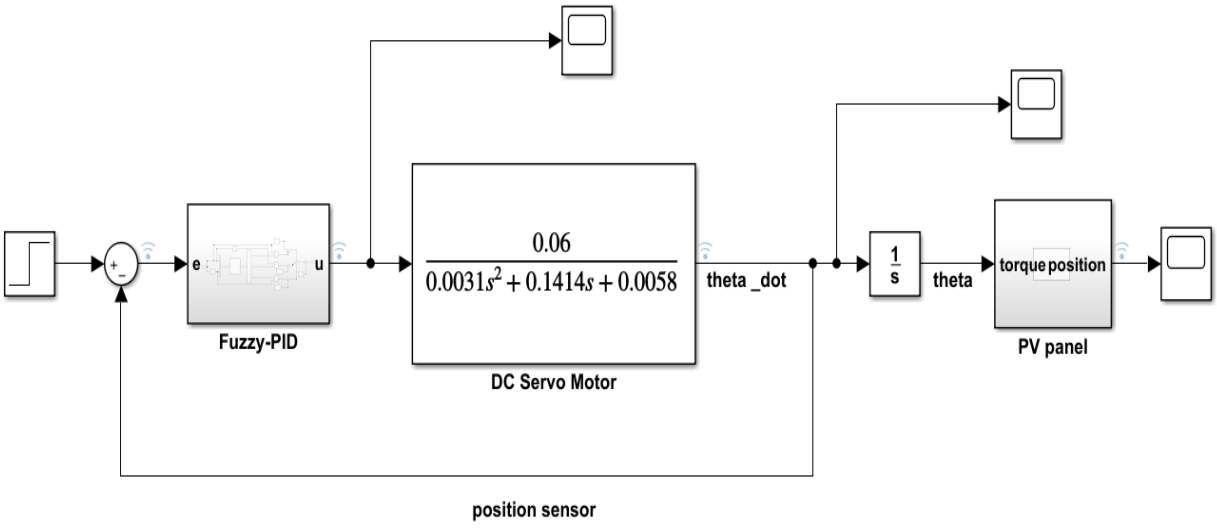

Figure 3.30: General SAST MATLAB/SIMULINK model of floating solar PV system

3.10 Number of panels and energy production

Lake Tana is the largest lake in Ethiopia and the source of Abay (Nile). The lake is around 84 Kilometers long and 66 Kilometers wide, with most extreme profundity of 15 meters and rise of 1,788 meters [60]. Surface area of Lake Tana is $5544km^2$. For the most part 9x9 modules/arrays are proposed to induce the FPV control that utilized to produce 210.762kW. The area of the sunrise module/panel SR-660260 is 1640mmx1992mm=3,266,880mm^2 = $3.26688m^2 \approx 3.3m^2$. The proposed array value of power is equals $3.3m^2 * \frac{210.762KW}{0.26KW} = 2675.056m^2$ $(0.2675 * 10^{-4}km^2)$.

The sun based board to be secured is 0.1% of the surface range of Lake Tana which can be assessed the control and the number of boards.

Estimation of 0.1% area= $5544km^2 * 0.001 = 5.544km^2$;

The drifting PV sun powered boards range to be secured is 0.1% to appraise its range that has been creating the taking after powers.

$0.2675 * 10^{-4}Km^2 \cong 210.762kw; 5.544Km^2?; 210.762kW * \frac{5.544Km^2}{0.2675*10^{-4}Km^2} \cong 207.25 * 10^3Kw = 207.25MW$.

The required PV board is SR-p660260 /60, 260w. The maximum electric power supplied by a PV system when it receives a solar irradiance of $1kW/m^2$ at the cell temperature of $25°C$.

One PV panel or SR-p660260/60 has 260w; then the total number of boards can be communicated as:

$3.3m^2 = 260W; 3.3km^2 = 260W;\ 5.544km^2?;$

$5.544km^2 * \frac{260\text{W}}{3.3*10^{-6}\text{km}^2} = 436.8 * 10^6\text{W} = 436.8\text{MW};$

$number\ of\ Pv\ panels = one\ pv\ panel * 436.8 * \frac{MW}{260W}$

$= 1680 * 10^3 panels \qquad \cong 1680 * 10^3 panels$

The 1080MW power and the area to be covered is $13.707km^2$ (0.635%).

The coasting sun based PV framework of hourly vitality era can be assessed as takes after:

$$W = I * A * \eta \tag{3.48}$$

Where, I is mean hourly parameter and A is the area of the lake covered by floating solar PV panels. η is the proficiency of the chosen PV panel's which is decided as

$$\eta = \eta_{module} * \eta_{tem} * \eta_{module} \tag{3.49}$$

η_{module} , the degree of efficiency of a module η_{tem} is the PV conversion efficiency and $\eta_{inverter}$ is the effectiveness of inverter. In this proposal based on the chosen PV board (polycrystalline 157 x157 mm cell with peak power of 260wp and module dimensions of 1640 x 992 x 35) $\eta_{module}\ and\ \eta_{inverter}$ were determined from PVSystem software thus were 0.160 and 0.96 respectively.

η_{tem} is expressed as:

$$\eta_{tem} = \eta_{stc}[1 - 0.0047 * (T_{panel} - 25℃)] \quad (3.50)$$

Where η_{stc} is an efficiency defined as a floating solar PV panel standard condition (STC) and 0.47% is the floating PV panel temperature coefficient.

T_{panel} is the temperature of a coasting PV board which is evaluated as takes after:

$$T_{panel} = T_{amb} * \frac{(NOCT - 20℃)}{0.8} * I \quad (3.51)$$

Where, T_{amb} is the encompassing discussing temperature which is expected break even with to the temperature of lake range, NOCT is the operation cell Temperature of selected PV panel.

3.11 Mathematical estimation of FSPV plant evaporation rate

Anticipating evaporation by the FSPV plant is secured by them. The water evaporation reduction had been two reasons: - (1) the decrease in water and air interaction from the covered area which directly affects the evaporation reduction.

(2) The alter in warm adjust of the lake after the control plant being built which causes the lake to be colder and hence decreases the overall vanishing all through the whole lakes surface. The mathematical relations and equations have been developed incorporating temperature, solar day hours, and solar radiation.

Penman's method is one of the foremost utilized mathematical methods for estimation of evaporation in a simplified way using routine weather data as follows:

$$E_1 \approx 0.051(1 - \alpha) * R_s * \sqrt{T + 9.5} - 2.4\left(\frac{R_s}{R_a}\right)^2 + 0.052 * (T + 20)\left(1 - \frac{R_h}{100}\right) * (a_u - 0.38) + 0.54u \quad (3.52)$$

E : Normal every day water surface evaporation (mm/day at sea level, z=0).

R_s : Average sunny hours per day

$n\ and\ N$: observed average number of sunny days

R_a : The sun powered irradiance on the surface of the environment

T: Average extreme temperature

$T = (T_{max} + T_{min})/2$; For analyze month (℃)

u : Normal esteem of wind speed (m/s) at an altitude 2m above water surface

R_h : Average air humidity in daily mean percentage

$$R_s = R_a + (0.5 + 0.25\frac{n}{N}) \quad (3.53)$$

G_w: Having geographical width

j : Selected month

The maximum possible number of sunny days for selected month can be expressed as follows:

$$N \approx 4 * G_w * \sin(0.53j - 1.65) + 12 \quad (3.54)$$

$$R_a = 3N \sin(0.131N - 0.95G_w)\,; G_w > \frac{23.5\pi}{180} \quad (3.55)$$

$$R_a = 118N^{0.2} \sin(0.131N - 0.2G_w)\,; G_w < \frac{23.5\pi}{180}$$

From eq.3.52 is adjusted empirically for higher altitude h (m);

$$E = E_1 + 0.00012 * h \quad (3.56)$$

The every day volume of water dissipation can be communicated as takes after:

$$V\left(\frac{m^3}{day}\right) = E\left(\frac{m}{day}\right) * A \quad (3.57)$$

E : Amount of evaporation

A : Surface area of the lake

The water can be saved by installing the FSPV pant system thus can be expressed as follows

$$\Delta V\left(\frac{m^3}{day}\right) = K * E\left(\frac{m}{day}\right) * A_{ca} \quad (3.58)$$

Where K is reduction factor determined by the type and platform's reflective functionality, its coverage level with panels, and panel's performance and this coefficient decreases evaporation volume due to the fact that a portion of solar irradiance passes through panels and reaches the water surface.

CHAPTER FOUR

MATLAB SIMULATION STUDIES AND ANALYSIS OF RESULTS

This chapter describes how the MATLAB/SIMULINK models of the proposed drifting sun based PV frameworks are implemented to test and identify the functionality of the proposed following controllers. The PV system position is simulated in MATLAB. The execution of the proposed counterfeit insights controller based on sun light coordinate to the surface of the sun powered PV boards.

4.1 Photovoltaic system modeling using SIMULINK

The design is modeled and simulated using 2018a/SIMULINK. The system modeled consists of PV array model, DC/DC boost converter model used to interface PV output to the inverter to track the most extreme control of the PV cluster using the solar tracker, DC/AC three phase PWM inverter model used to interface with AC grid. LCL low pass filter to the supply a pure sinusoidal yield voltage to the grid. The PV cluster used in the simulation is a 260W power that nine strings with nine modules of 260W power. 9x9 elements are combined to produce the desired power at standard condition specified at irradiation of ($G = 1000kW/m^2$) and temperature of ($T = 25℃$).

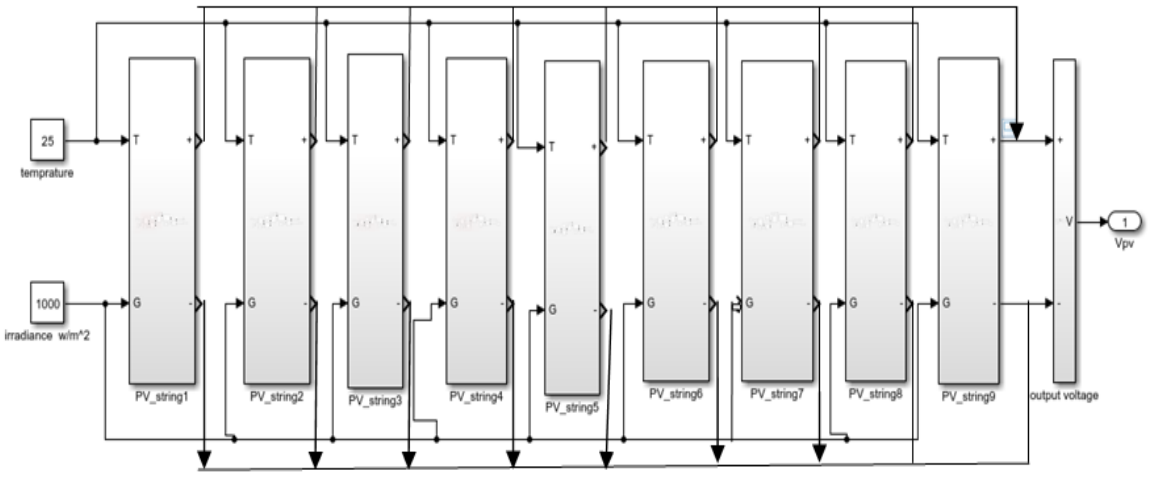

Figure 4.1: Connection of nine PV strings in parallel

In figure 4.1 series parallel connections are applied, first a 260W PV module are designed to create a strings which consists nine series modules, then sun powered PV panel connecting 9 PV strings in parallel as the designed calculated values.

Generally 9x9 modules are implemented to get the FPV power that utilized to produce 210.762kW.

Table 4.1: proposed module and array values (SR-P660260)

Parameters of SR-P660260	Modeled module values (SR-P660260)	Proposed array value (SR-P660260)
Open circuit- voltage (V_{OV})	37.89V	3069.09V
Short circuit current (I_{SC})	9.08A	735.48A
Current at maximum power point (I_{mpp})	8.5A	688.5A
Voltage at maximum power point (V_{mpp})	30.61V	2479.41V
Number of cells in series Ns	60	4860
Power at maximum power point (p_{mpp})	260W	210.76kW

Table 4.2: Estimating generating power and number of panels

Area	Number of panels	Generating power
$1m^2$	1	$78.78w$
$3.3m^2$	1	260w
$2675m^2$	$810.6 \cong 811$	210.762kw
$5.544km^2$	$1680 * 10^3$	$207.25MW$

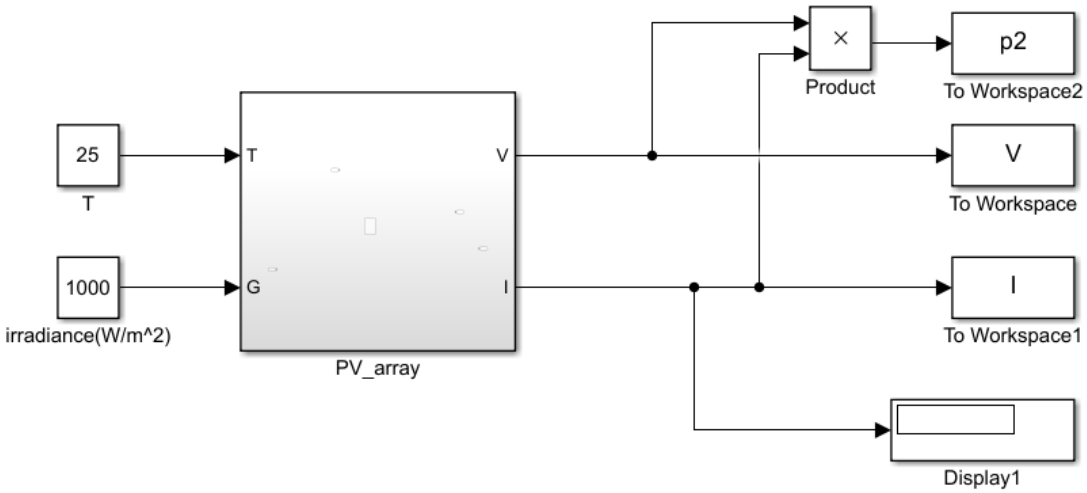

Figure 4.2: SIMULINK model for floating solar system of PV array

The Voltage to power, current to voltage and current to power curve of the simulated solar PV model is used to analysis the influence of the light intensity of radiation (irradiance) and temperature variation on the output characteristics of the floating PV panel.

The output of the PV array is recorded in different level of solar irradiation (1200, 1000, 800, 600, 400 and 200) w/m^2 at different environmental temperature (80, 60, 45, 25, 17 and -10) at standard irradiation values or random value of temperature and irradiation level and the SIMULINK result of the model of PV - array the current and power of characteristics are shown in table below.

Table 4.3: SIMULINK result at standard irradiation (G) for different temperature

Temperature (℃)	@ $1000w/m^2$	
	Current (A)	Power (W)
10	1308	1.438e+04
18.8	1268	1.395e+04
25	1240	1.364e+04
45	1150	1.265e+04
60	1083	1.191e+04
80	993	1.092e+04

Table 4.4: SIMULINK result at 25℃ temperature for different intensity of light

Intensity of light (W/m^2)	@ 25℃	
	Current (A)	Power (W)
1400	1736	1.91e+04
1200	1488	1.637e+04
1000	1240	1.364e+04
800	992.1	1.091e+04
600	744.1	8185
400	496	5456
200	248	2728

Table 4.5: SIMULINK result at 45℃ temperature for different intensity of light

Intensity of light (W/m^2)	@ 45℃	
	Current (A)	Power (W)
1400	1610	1.771e+04
1200	1380	1.518e+04
1000	1150	1.265e+04
800	920.2	1.012e+04
600	690.2	7592
400	460.1	5061
200	230	2530

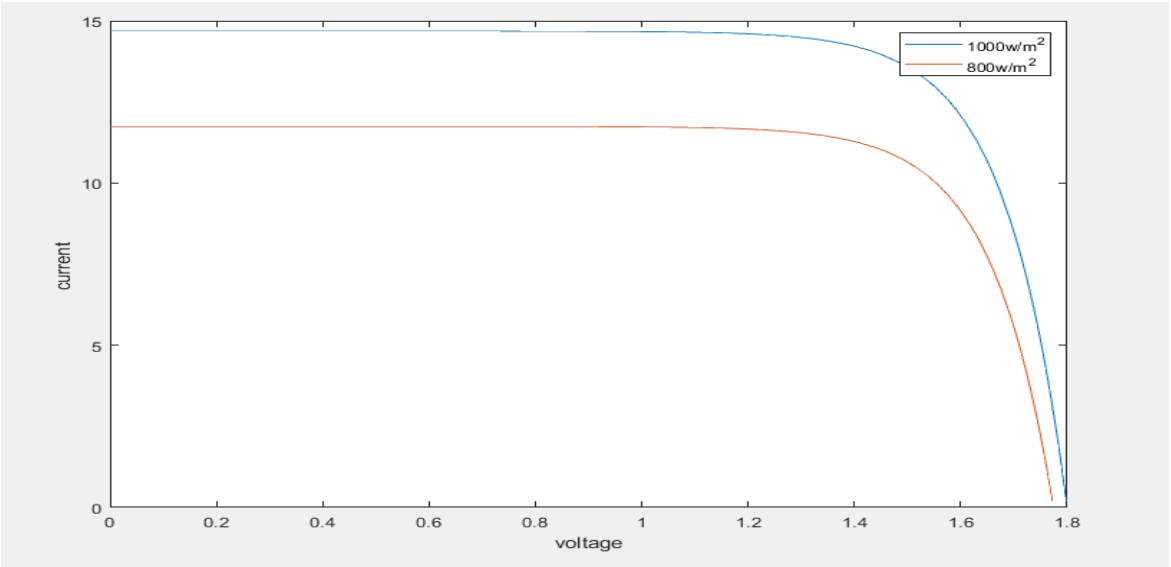

Figure 4.3 : V-I characteristics of PV module

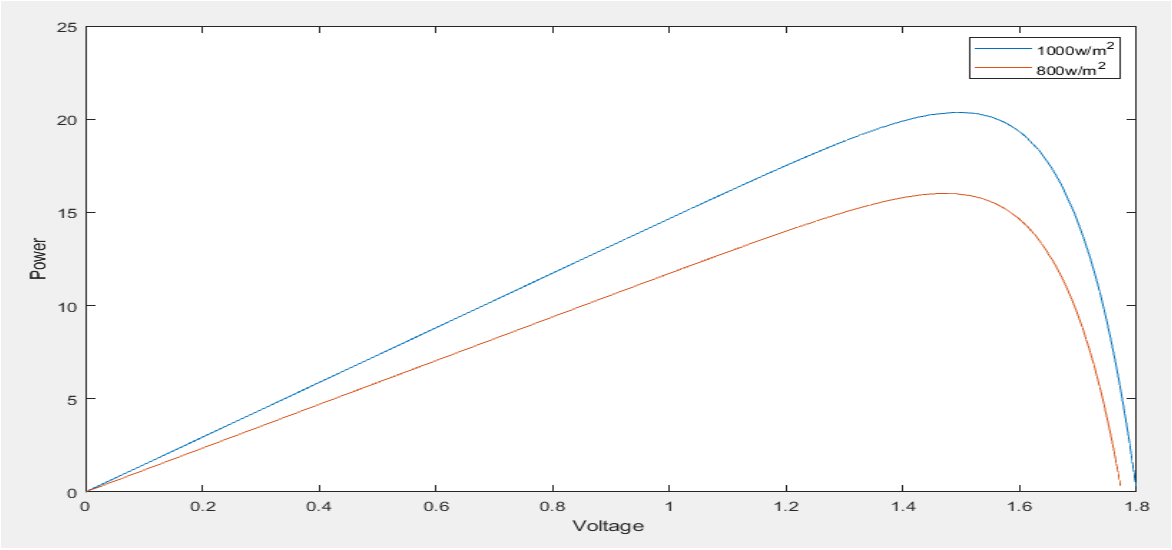

Figure4.4: P-V characteristics of PV module

4.2 Meteorological data

For the design of FPV system meteorological data like latitude, longitude (sun angle), solar irradiation of the location and temperature are crucial for the consideration of output power from PV module. The details information is obtained from Lake Tana meteorological data using NASA-SSE satellite data 1983-2005 (PVST software).

Latitude: $11°36'$ north

Longitude: $37.333°$ east

Altitude: $1776m$

Elevation: 1788m

4.3 Tilt angle

Intended the irradiation obtainable at tilt and the power output needed, the PV module can be sized using module specifications provided by manufacturers. Lake Tana is located at latitude of $11°36'N, 37°23'E$ from horizontal and vertical respectively. Since the PV module sized to achieve the demand of energy at the average light intensity, the PV module will face at angle of $15 + 11°36'N$ degree north from horizontal due to maximize light intensity (irradiance) received. In the winter season the PV module may at angle $15 - 11°36'N$ and in spring the PV module will be faced to the same angle of latitude.

Table 4.6: Seasonal irradiation and ambient temperature of Lake Tana [PVSYST software]

Month	Irradiation (W/m^2) or global horizontal irradiation	Horizontal diffuse irradiation (w/m^2)	Temperature (℃)
January	258.3	45.0	19.8
February	272.1	56.3	20.9
March	271.7	73.7	21.6
April	278.8	80.8	20.8
May	263.3	83.3	19.9
June	237.9	87.9	17.6
July	215.0	92.5	16.3
August	215.8	95.0	16.4
September	242.1	85.8	17.3
October	244.2	71.7	18.0
November	250.4	52.5	18.4
December	247.9	43.8	18.7
Year	**249.6**	**72.4**	**18.8**

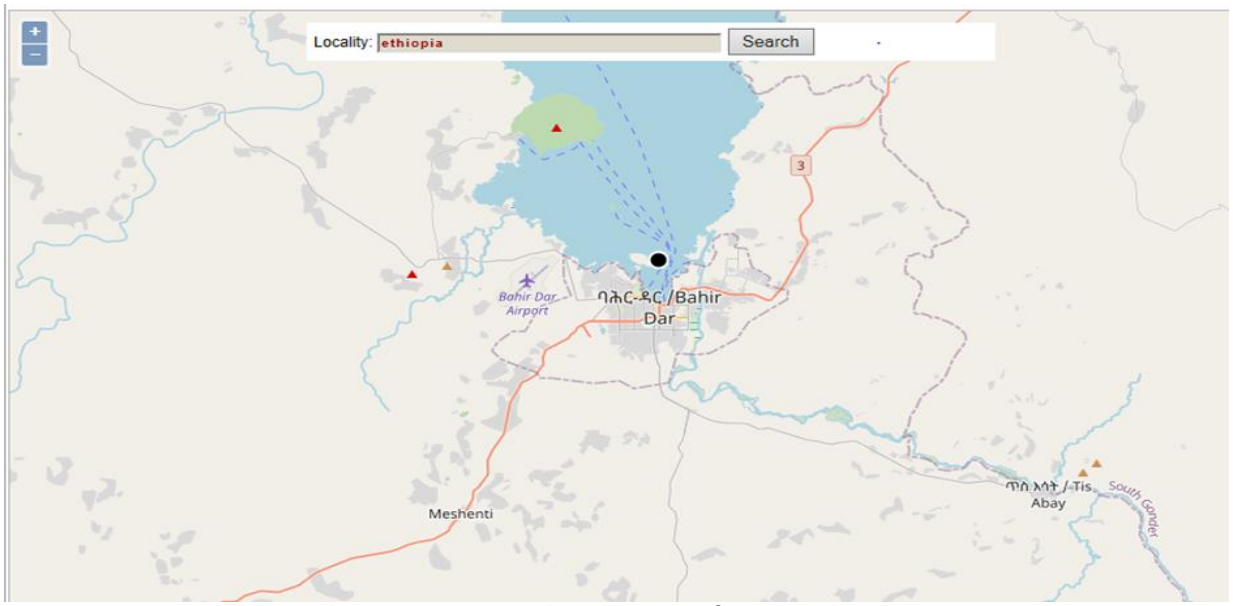

Figure4.5: Lake Tana location on map [PVSYST software online]

The transfer function of the DC motor is expressed as follows

$$G(s) = \frac{0.06}{0.0031s^2+0.1414s+0.0058}$$

Calculate the critical gain or ultimate gain by using routh-hurwitz criteria can be shown as:

Assume that $K_i, K_d = 0$

$$T.F = \frac{KG(s)}{1+KG(s)H(s)}$$

$$= k_p * \frac{0.06}{\frac{0.003s^2+0.1414s+0.0058}{1+K_P*\frac{0.06}{0.0031s^2+0.1414s+0.0058}}} = \frac{K_p}{0.0031S^3+0.1414s^2+0.0058s+K_p}$$

To determine K critical point using characteristics equation of the transfer function:

Characteristics equation is $0.0031s^3 + 0.1414s^2 + 0.0058s + K_p$.

$$0.0031s^3 + 0.1414s^2 + 0.0058s + K_p = 0$$

s^3	0.0031	0.0058
s^2	0.1414	K_p
s^1	$\frac{0.1414*0.0058-0.0031*k_P}{0.1414}$	$0 < K_p < 0.2645$
s^0	K_p	$K_p > 0$

The critical point is 0.2645. This critical point is ultimate gain. DC servo motor is used for the movement of the floating solar PV panels and the speed of the motor is controlled by using PID controller. PID controller was tested the controller gains which can be tuned manually. $K_p = 30, K_i = 9100\ and\ k_d = 110$. The response of the system graph is shown in figure 4.5. It has been seen that the speed is varying with time and it is not stabilized with manual gains.

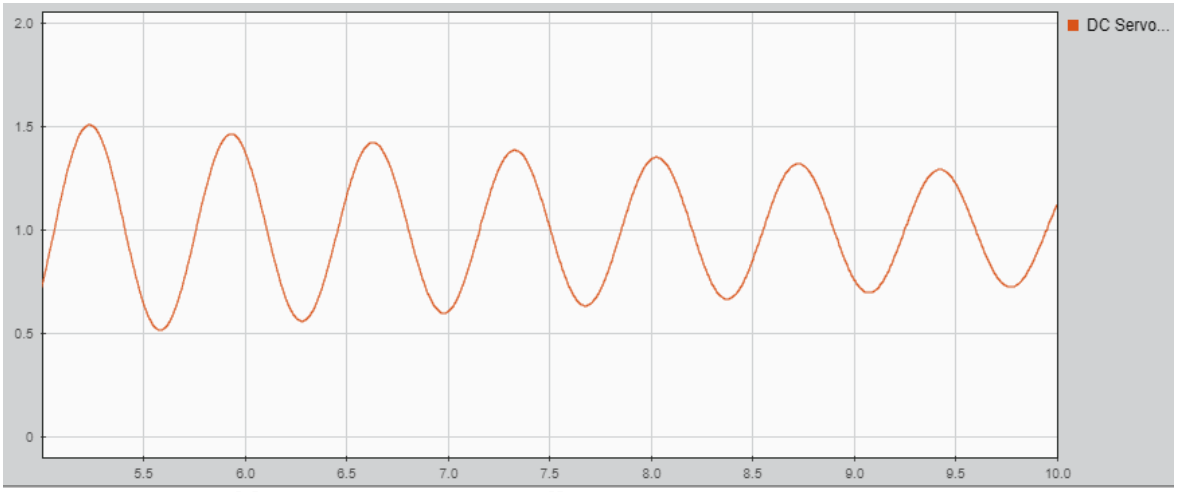

Figure 4.6: manual loop tuning PID controller response

The Ziegler-Nichols –Tuned closed loop response method which has been determined automatically the gains of PID controller in mat lab environment. In this system, gain parameters are; $k_p = 0.1587; k_i = 0.4600;\ k_d = 0.0137$. The derivative time (T_d) and integral time (T_i) is $0.0863;\ 0.3450$ respectively. The transfer function was used to control the east-west movement of the solar panels that is Continuous-time transfer function given in equation 4.1 and mat lab function is shown in Appendix C. Simulation results for ZN-Tuned PID controller is shown in figure 4.6.

sys_G =

0.0008213 s^2 + 0.009522 s + 0.0276

---------- (4.1)

0.003 s^3 + 0.01496 s^2 + 0.01532 s + 0.0276

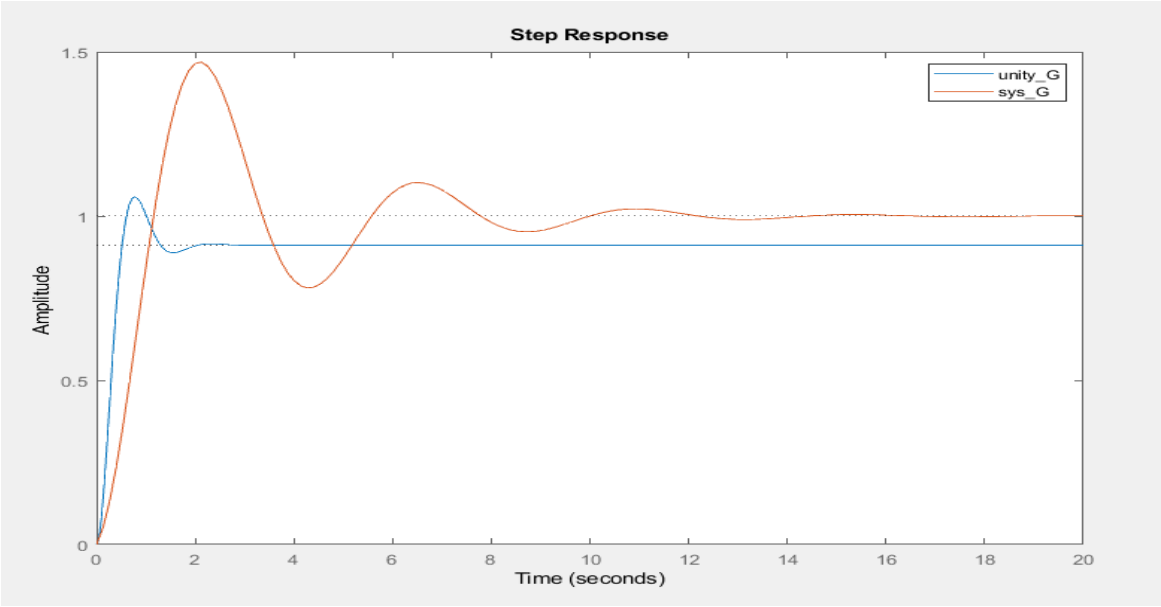

Figure 4.7: Response of the system using ZN – Tuned PID Controller

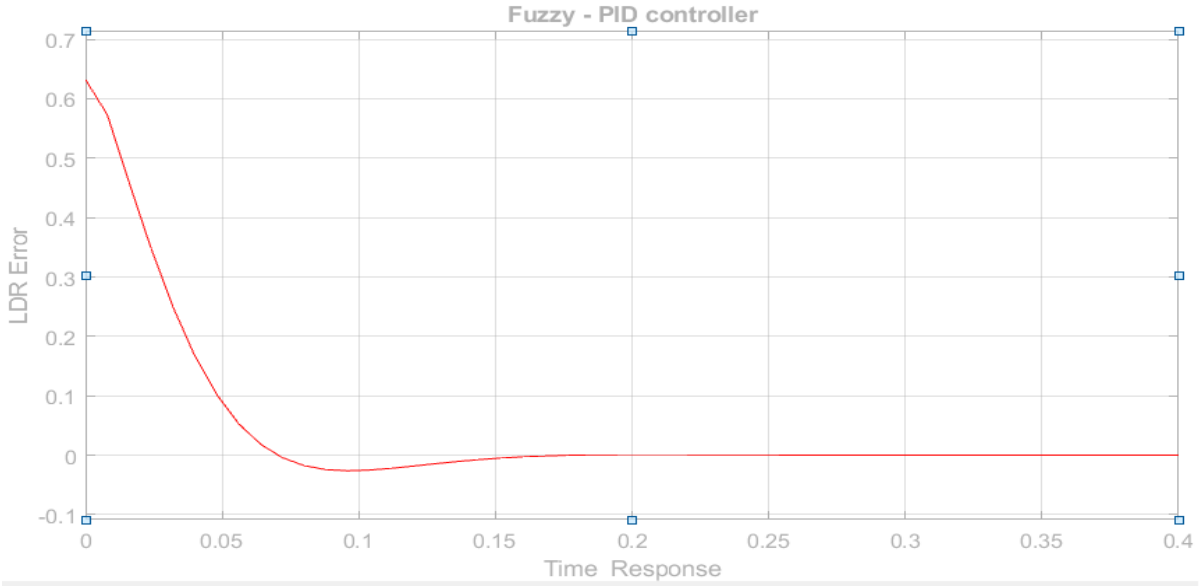

Figure 4.8: LDR error Vs Time response of fuzzy tuned PID controller servo motor

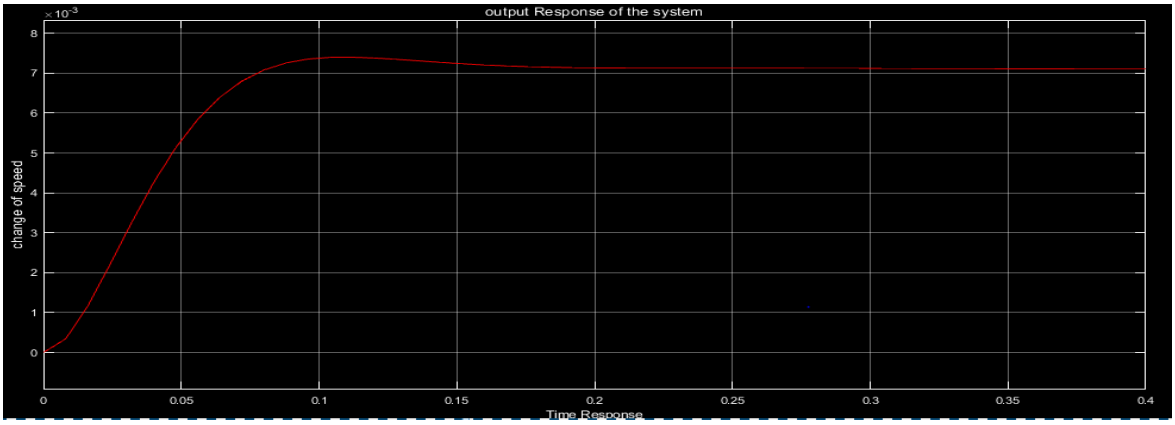

Figure 4.9: Change of speed Vs Time Response of SAST with Fuzzy tuned PID controlled DC servo motor

4.4 Comparison of PID controller and FPID controller methods

The transient parameters comparison is shown in table

Table 4.7: Comparison of PID and FPID controller

Transient parameters	PID controller	FPID controller
Choose time	2.13s	0.112
Rise time	0.842s	0.0527s
Settling time	11.2s	-
Peak overshoot	46.8%	3.646%

CHAPTER FIVE

CONCLUSION AND RECOMMENDATION

5.1 CONCLUSION

The thesis; "performances optimization of generating power on a floating solar power plant" is mostly studied to design and perform a solar tracking systems which go along with the sun direction for generating maximum output energy for electrical powered utilization. This thesis contains of sensors and DC servo motor mechanism for alternating the panel in the direction of sun. Fuzzy – PID controller situation /based control system takes care of sensing sunlight and controlling DC servo motor mechanism. The dominant controlling device of the thesis is fuzzy-PID controller of which LDR's and DC servo motor with panel structure to its shafts are interfaced. The Fuzzy-PID controller obtains from LDR sensors with regard to the direction of sun and the controller action and controls the rotation of floating solar panels depend on DC servo motor derive. The average temperature of Lake Tana is 18.8℃ and temperature 25℃. The figure4.10 SIMULINK model of output power is 1.268e+04w and 1.24e+04w at $\frac{1000w}{m^2}$ in both conditions. A model that shows the single axis floating solar PV system tracking was developed. The performance optimization of the proposed PID and fuzzy-PID controller is checked through simulation conceders using MATLAB/SIMULINK. It is analyzed that from Ziegler-Nichols closed loop PID controller tuning method simulation results that the overshoot is 46.8%, rising time is 0.842 seconds, pick time is 2.13seconds and the settling time is 11.2 seconds with the proposed fuzzy-PID controller while overshoot is 3.646%, rising time is 0.0527seconds; pick time is 0.112second and the sampling time is taken as 0.4seconds. In this thesis, a single axis floating solar tracking system is planned to extend the execution of a coasting sun based energy; which is a most efficient renewable energy source for the future. Fuzzy logic controller is maintained to the vibration of floating solar panel systems.

5.2 Recommendation

Given to the limitation of this study, it is recommended that further research should be done regarding that have more technical aspects of fuzzy-PID controller based single axis solar PV tracking system design. Since this thesis is designed on fuzzy-PID controller based single axis solar tracking to harvest electrical energy for irrigation purpose and other electrifications. Further research should be done by the coordination of mechanical experts, civil experts and electrical experts can be designed and implemented with the involvement of government.

6. REFERENCE

[1] D.T. Cotfas and P. A. Cotfas. Multi concept Methods to Enhance Photovoltaic System Efficiency, International Journal of Photo energy, November 2019

[2] Youssef Mallal et al.High-Performance Emulator for Fixed Photovoltaic Panel, international journal Volume 2019, or https://doi.org/10.1155/2019/3951841.

[3] Ethiopian Journal of Environmental Studies and Management Vol. 4 No.1 2011.

[4] S. Ozcelika*, H. Prakashb, R. Challooc; Two-Axis Solar Tracker Analysis and Control for Maximum Power Generation, 2011.

[5] Prof.Jadhav Pallavi S, FLOATING SOLAR PLANT, 7th International conference on emerging Trends in engineering, Technology, science and Management on October 2017.

[6] Professor (Dr.) D P Kothari, Floating Solar PV Potential in Large Reservoirs in India,International Journal for Innovative Research in Science & Technology, Volume 2, April 2016.

[7] Mohammad Fereshtehpour, Reza Javidi Sabbaghian, Ali Farrokhi, EhsanBahrami Jovein, Elham Ebrahimi Sarindizaj; Evaluation of Factors Governing the Use of Floating Solar System: A Study on Iran's Important Water Infrastructures, 2020.

[8] Mohsen Taherbaneh , Maximizing Output Power of a Solar Panel via Combination of Sun Tracking and Maximum Power Point Tracking by Fuzzy Controllers, International Journal of Photo energy Volume 2010,

[9] A. Zeroual, M. Raoufi **,** M. Ankrim and A.J. Wilkinson,"Design and construction of a Closed loop Sun Tracker with Microprocessor Management", International Journal on Solar Energy, Vol. 19, 1998, Page(s): 263-274.

[10] Brito, M., Galotto, L., Sampaio, L., Melo, G., &Canesin, C;(2013, March). Evaluation of the main MPPT techniques for photovoltaic applications, IEEE Transactions on Industrial Electronics, 60(3), 1156–1167

[11] Algazar, M. M., Monier, H., Halim, H., & Salem, M. (2012) Maximum power point tracking using fuzzy logic control Elsevere Journal on Electrical Power and Energy Systems,39, 21–28.

[12] Patil (Desai) Sujay S., Wagh M. M., Shinde N. N. , A Review on Floating Solar Photovoltaic Power Plants, International Journal of Scientific & Engineering Research Volume 8, Issue 6, June-2017 789 ISSN 2229-5518

[13] Minor M. Arturo, High–Precision Solar Tracking System, Proceedings of the World Congress on Engineering 2010 Vol II ,WCE 2010, June 30 - July 2, 2010, London, U.K.

[14] Tonui J, Tripanagnostopoulos Y. Improved PV/T solar collectors with heat extraction by forced or natural air circulation. Renewable Energy, 2007;32:623-37.

[15] Swimsol "Solar Sea" – the world´s first floating solar power plant for the sea -Scheuch Foundation,https://www.scheuch-foundation.org/en/swimsol-solarsea-the-worlds-first-floating-solar-power-plant-for-the-sea/

[16] Kim Trapani1 and Miguel RedónSantafé; A review of floating photovoltaic installations: 2007–2013 - Trapani - 2015 - Progress in Photovoltaic's: Research and Applications-WileyOnlineLibrary; https://onlinelibrary.wiley.com/doi/abs/10.1002/pip.2466

[17] R. Babour, solar tracking: analysis & optimization, 2019

[18] Rosa-Clot, M. R. C., & Tina, G. M. T. (2018) [Bild/Grafik], The Floating PV Plant, Submerged and Floating Photovoltaic Systems, 89–136. https://doi.org/10.1016/b978-0-12-812149-8.00005-3

[19] Siecker J., Kusakana K., Numbi B. P., (November 2017), *"A review of solar photovoltaic systems cooling technologies,"* ELSEVIER. PDF document

[20] JamiluYa'u Muhammad, Mohammed Tajudeen Jimoh, Ibrahim Baba Kyari, Mohammed Abdullahi Gele, Ibrahim Musa. A Review on Solar Tracking System: A Technique of Solar Power Output Enhancement. Engineering Science.Vol.4,No.1, 2019, pp. 1-11. doi: 10.11648/j.es.20190401.11

[21] Marco Rosa-Clot, Giuseppe Marco Tina, in Submerged and Floating Photovoltaic Systems,

[22] R. Babour, solar tracking: analysis & optimization, 2019

[23] Jamilu,Ya'u Muhammad, Mohammed Tajudeen Jimoh, Ibrahim Baba Kyari, Mohammed Abdullahi Gele, Ibrahim Musa, A Review on Solar Tracking System: A Technique of Solar Power Output Enhancement. Engineering Science.Vol.4, No.1, 2019, pp.1-11.doi: 10.11648/j.es.20190401.11

[24]https://www.semanticscholar.org/paper/Comparison-of-Efficiencies-of-Solar-Tracker-systems-Bharathi, Ranjitha/d106ef3b1e8aec14581ed8de507e590c40e02562/figure/0

[25] A.Z. Hafez, A.M. Yousef, A comprehensive review for solar tracking systems design in Photovoltaic cell, module, panel, array, and systems applications, Conference Paper**,** June 2018 DOI: 10.1109/PVSC.2018.8547901

[26] Dola Sinha, Fuzzy Logic-based Dual Axis Solar Tracking System**,** *International Journal of Computer Applications (0975 – 8887) Volume 155 – No 12, December 2016*

[27]https://www.semanticscholar.org/paper/Design%2C-implementation-and performance-analysisof-Munna-Bhuyan/d143c1d713073ec0ada345f7b28ebdc7428b7c71/figure/0.

[28] S.Aksungur and T. Koca: Solar tracking system with PID control of solar energy panels using servo motor, International Journal of Energy Applications and Technologies 5(3) [2018] 127-130

[29] Karl Johan Astrom. “PID Control” controls system design, 2002.

[30] L.A.Zadeh, "Toward a theory of fuzzy information granulation and its centrality in human reasoning and fuzzy logic," *Fuzzy Sets and System*, vol. 90, pp. 111-127, 1007

[31] J. H.Lilly, Fuzzy Control and Identification, Hoboken, New Jersey: John Whily & Sons Inc, 2010

[32] C.C.Lee, ""Fuzzy Logic in Control Systems: Fuzzy Logic Controller, Part II"," *IEEE Trans. on Sys, Man amd Cybernetics*, vol. 20, no. 2, pp. 419-435, 1990

[33] S. D. Kaehler, Fuzzy Logic- An Introduction.

[34] J. H.Lilly, Fuzzy Control and Identification, Hoboken, New Jersey: John Whily & Sons Inc, 2010.

[35] D. S.ouil, "Effect of Different Membership Functions on Fuzzy Power System Stability for Synchronous Machine Connected to Infinite Bus," *International Journal of Computer Application*, vol. 71, no. 7, pp. 0975-8872, 2013

[36] J. Jamtzen, Foundations of Fuzzy Control, Sussex: Wiley and Sons, 2007

[37] Guanrong Chen, Trung Tat Pham., and Introduction to fuzzy sets, fuzzy logic, and fuzzy control systems, New York: CRC Press, 2000

[38] E.H.Mamdani, "Application of Fuzzy Logic to Approximate Reasoning using Linguistic Synthesis," Department of Electrical Engineering, Queen MAry's College of Engineering, London, 1974

[39] D. K. Chaturvedi, Modeling and Simulation of System using Matlab and Simulink, U.S: Taylor & Francis Group, 2010.

[40] A.Hareno, J.Julve, S.Silvisturem, L Castaner, "A Fuzzy Logic Controller for Standalone PV System," *IEEE Trans.*, pp. 1618-1621, 2000.

[41] Z.W. Woo, H.Y. Chung, J.J. Lin “A PID type fuzzy controller with self tuning scaling factors”, Fuzzy Sets and Systems, vol. 115, Issue 2, pp.321–326, October 2000.

[42] Wang Xiao-kan, Sun Zhong-liang, Wanglei, Feng Dong-qing, "Design and Research Based on Fuzzy PID-Parameters Self-Tuning Controller with MATLAB," Advanced Computer Theory and Engineering, International Conference on, pp. 996-999, 2008 International Conference on Advanced Computer Theory and Engineering, 2008.

[43] Said, S., Massoud, A., Benammar, M. and Ahmed, S., 2012. "A Matlab/Simulink-based photovoltaic array model employing Sim Power Systems toolbox", Journal of Energy and Power Engineering, 6(12), p.1965

[44] Marcelo, M. G., Gazoli, J., & Filho, E. (2009). Comprehensive approach to modeling and simulation of photovoltaic arrays IEEE Transactions on Power Electronics, 24, 1198–1208.

[45] Zhou, W., Yang, H., & Fang, Z. (2007), "A novel model for photovoltaic array performance prediction". *Journal of Applied Energy, 84*, 1187–1198.

[46] Luis, C., & Sivestre, S. (2002). *Modeling photovoltaic systems using PSpice*. Chichester: John Wiley & Sons Ltd. Mahammad, A. K., Saon, S., & Chee,W. S. (2013). Development

[47] Dyk, V. (2002) Long-term monitoring of photovoltaic devices, *Renewable Energy, 22*, 183–197.

[48] Green, M. A. (1992), *PV modules-operating principles, technology and system applications*. Kensington, Australia: Prentice-Hall

[49] Sun-Hee Kim, Seung-Cheol Baek , Ki-Bong Choi and Sung-Jin Park, Design and Installation of 500-kW Floating Photovoltaic Structures Using High-Durability Steel, Published: 23 September 2020

[50] Y. Liu, D. Chen, Q. Yi, S. Li, Wind profiles and wave spectra for potential wind farms in south China Sea. Part I: wind speed profile model, Energies 10 (2017) 125–149.

[51] Y.J. Wang, Free-surface wave interaction with a very large floating structure, J. Shanghai Jiaotong Univ. (Sci.) 19 (6) (2014) 728–735

[52] Durković, V.; Đurišić, Ž. Analysis of the Potential for Use of Floating PV Power Plant on the Skadar Lake for Electricity Supply of Aluminium Plant in Montenegro. *Energies* 2017, *10*, 1505, https://doi.org/10.3390/en10101505

[53] Ang, K.H. and Chong, G.C.Y. and Li, Y. (2005) PID control system analysis, design, and technology. IEEE Transactions on Control Systems Technology 13(4):pp. 559-576

[54] Youney, Justin, "A Comparison and Evaluation of common PID Tuning Methods" (2007). Or https://stars.library.ucf.edu/etd/3423

[55] Priyanka Singh, Hasanganj, design of tuning methods of PID controller using fuzzy logic, International Journal of Emerging trends in Engineering and Development Issue 3, Vol.5 (September 2013), ISSN 2249-614

[56] Ying Bai and Dali Wang, on 20 May 2014, Fundamentals of Fuzzy Logic Control – Fuzzy Sets, Fuzzy Rules and Defuzzification

[57] M.Chow and A. Menozzi,"on the comparison of emerging and conventional techniques for DC motor control" proc.IECON , PP.1008-1013,1992

[58] Timothy J. Ross; Fuzzy Logic with Engineering Applications third edition.

Durković, V.; Đurišić, Ž. Analysis of the Potential for Use of Floating PV Power Plant on the Skadar Lake for Electricity Supply of Aluminium Plant in Montenegro. *Energies* 2017, *10*, 1505 https://doi.org/10.3390/en10101505

[59] C.S.Chin, Model-based simulation of an intelligent microprocessor-based standalone solar tracking system

[60] Lake Tana – Wikipedia https://en.wikipedia.org/wiki/Lake_Tana

7. APPENDIX

APPENDIX A

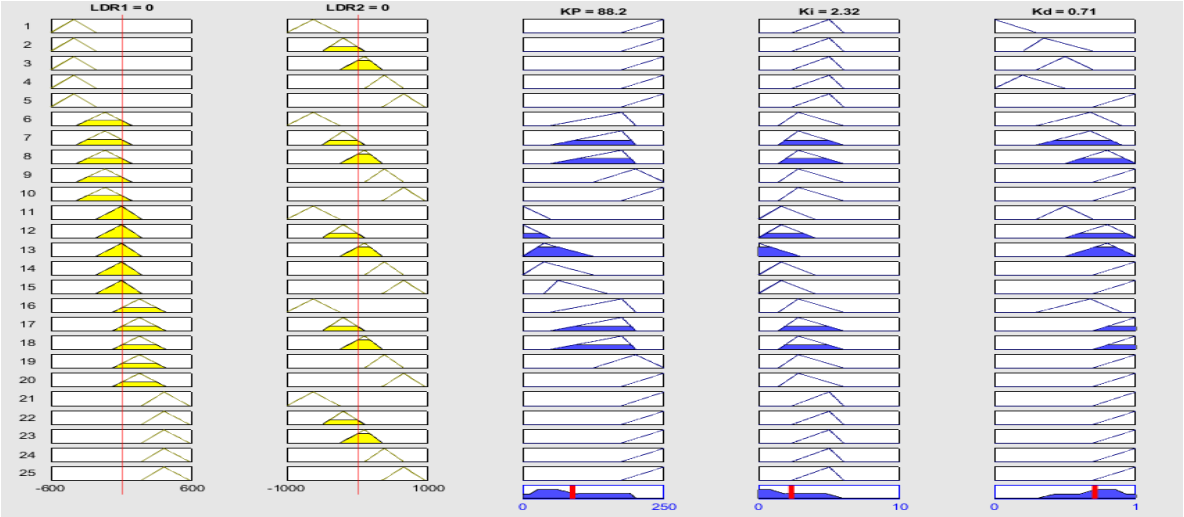

Appendix B

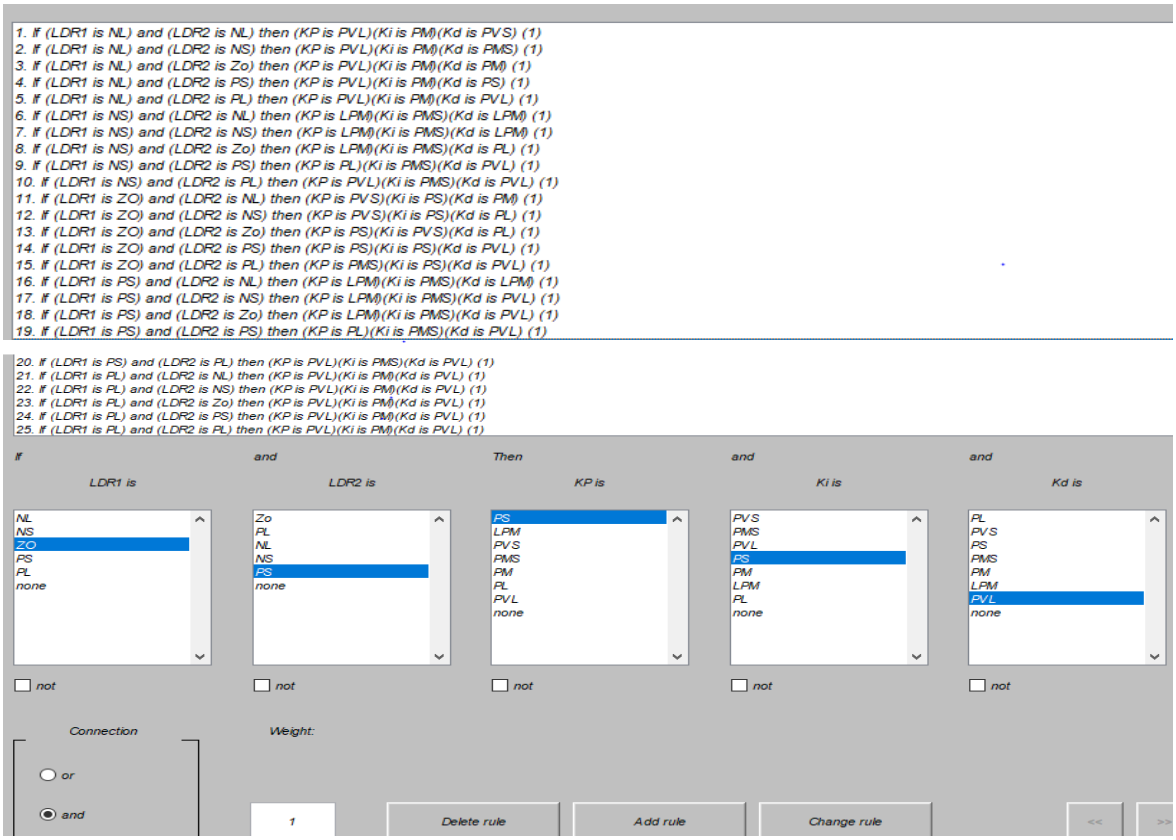

Appendix C

```
%Ziegler _ Nichols Tuning Method
close all; clear all;
s = tf('s');
G = 0.06/((0.003*s^2)+(0.01414*s)+0.0058);
rlocus(G);
```

```
 step(G);
unity_G=feedback(G,1)
step(unity_G)
hold on
Ku = 0.2645;
Pu = 0.69;
Kp = 0.6*Ku;
Ti = 0.5*Pu;
Td = 0.125*Pu;
Ki = Kp/Ti;
Kd = Kp*Td;
C = pid(Kp,Ki,Kd)
sys_G=feedback(C*G,1)
step(sys_G)
```

Appendix D